**Western Australian School of Mines**
**Department of Metallurgical and Minerals Engineering**

# Development of an Electrostatically Assisted Solvent Extraction Column

**Marc J Steffens**

**This thesis is presented for the Degree of**
**Doctor of Philosophy**
**of**
**Curtin University**

**September 2011**

## DECLARATION

To the best of my knowledge and belief this thesis contains no material previously published by any other person except where due acknowledgment has been made.

This thesis contains no material which has been accepted for the award of any other degree or diploma in any university.

_____

Marc J Steffens

September 2011

# ABSTRACT

Solvent extraction (SX) is the only commercially viable hydrometallurgical separation and purification technique for a range of metals that allows high product throughput and consistently high recoveries. After over 50 years of commercial application, however, limitations inherent to the mechanical agitation used within the most widely used commercial SX contactor – the mixer-settler – have become apparent. It is now generally accepted that mechanical agitation results in regions of high shear within the mixer, which favours the formation of crud, non-uniform droplet sizes and the formation of numerous ultra-fine droplets. The other commercially used contactor, the pulse column, does not suffer from as many problems as the mixer-settler but it is not suitable for systems with slow kinetics.

A promising alternative to these mechanically agitated solvent extraction contactors are electrostatically agitated solvent extraction (ESX) contactors. Bench-scale studies indicate that these contactors allow higher rates of mass transfer, excellent control of droplet size, and lower shear agitation than mechanically agitated contactors. There are also suggestions that the technique requires only a fraction of the power relative to that of mechanical agitation. Despite these promising attributes, a commercial application has not been achieved. This may be attributed to a poor understanding of electrostatically-assisted droplet dispersion over a range of commercially applicable solution properties, the designs of ESX contactors already proposed being unsuitable for scale-up and the performance of an ESX contactor never having been evaluated on a pilot-scale.

To better understand electrostatically-assisted droplet dispersion, a dispersion study that allowed the measurement of dispersed droplet sizes was carried out over a range of commercially applicable solution properties. To develop an ESX contactor suitable for scale-up and industrial application, various types of electrostatic field conditions were evaluated and numerous electrode designs were developed and evaluated. Finally, to evaluate the performance of the ESX contactor on a pilot-scale, a pilot-scale ESX column was constructed and its performance was compared to that of a sieve-plate pulse column, which was refurbished for this purpose.

In pursuing the first objective it was found that:

- The viscosity of both the solvent and the PLS, and the interfacial tension affect the droplet size distribution generated by electrostatic dispersion largely by affecting the number of ultra-fine droplets that form. The solvent conductivity affects droplet dispersion by affecting the degree of interfacial polarisation of the droplet.
- Electrostatic droplet dispersion occurs either via a necking or jetting dispersion mechanism. In ESX, droplet dispersion by necking is favourable as it impedes the formation of ultra-fine droplets. The predominance of one mechanism over the other is influenced by the viscosity of the PLS and solvent.

In pursuing the second objective it was found that:

- An individual electrostatic PLS disperser is not appropriate for an industrially applicable ESX column.
- Droplet motion within an electrostatic field is influenced by the electric charge that droplets carry and also by the strength and frequency of the electrostatic field. Increases in the charge of the droplet favours droplet motion and agitation; increases in the frequency of the electrostatic field favours droplet oscillation; decreases in the frequency of the electrostatic field favours droplet zigzagging.
- A horizontal rod electrode arrangement within a column type contactor was found to be the most appropriate design for scale-up because it allowed (1) good droplet dispersion and agitation, (2) adequate aqueous fluxes to be achieved, and (3) coalescence of any ultra-fine droplets that form.

In pursuing the third objective it was found that:

- An electrostatic field strength of 6.5 kV/cm and electrostatic field frequency of 40 Hz yielded the highest extraction of nickel metal from sulphate/chloride solution. Under these conditions, the fluxes achieved within the ESX column were comparable to those used in pulsed columns. This is particularly significant as it disproves the commonly perceived main limitation of electrostatic dispersion.
- Concurrent operation of the ESX and sieve-plate columns, each with an aqueous flux of 37 $m^3/h/m^2$, revealed that the metal extraction achieved within each column was comparable, with a height equivalent to a theoretical stage (HETS) of 3.30 m. This demonstrates that ESX columns can handle industrially applicable aqueous fluxes. Further improvements in the ESX column design promise enhanced results.

# ACKNOWLEDGEMENTS

I am indebted to, and would like to acknowledge several people who have helped me to complete this work. Without them this work would not be what it has become.

- My supervisor, Prof. Don Ibana for his assistance and support throughout this work, as well as for the long hours spent developing and polishing my professional skills. Mostly I am appreciative of his supervisory style that allowed me to pursue my research interests. I also wish to thank my associate supervisor, Prof. Erkki Paatero for his ideas and input into this work, as well as his assistance with some challenging analytical procedures.
- The Australian Postgraduate Award (APA) for my scholarship throughout this work and the Parker Centre for Integrated Hydrometallurgy Solutions for my top-up scholarship and for supporting some sections of this work.
- Joel Collard, my fellow PhD student. Without the many discussions we had and the time spent together developing solutions to our technical problems, this work would not have become what it is. Also Tom Waters, honours student, for his great assistance with the pilot-scale study in this work.
- The academic staff of the Minerals Engineering and Extractive Metallurgy Department. Prof. Eric Grimsey, for support, encouragement and guidance, particularly in times when the work appeared overwhelming, and Prof. Richard Browner, for advice and opinions throughout this work.
- WASM Technicians, Lewis Pannell and Martin Willigen. Lewis, for his advice and troubleshooting skills with my electrical contraptions and Martin for his advice during the construction of the pilot-scale column and also his patience as I gradually consumed his carpentry workshop.
- Peter Haig of Shell Chemicals for supplying the ShellSol® 2046 and Versatic 10 used throughout this work, and Simon Donegan, formerly of Minara Resources, for supplying nickel solution used in the piloting work.
- Lastly, but not least, my partner Kate and my family. Thank you for all of your support, encouragement and understanding throughout the course of this work.

# TABLE OF CONTENTS

# LIST OF FIGURES

# LIST OF TABLES

## Chapter 1

# General Introduction

## 1.1 Solvent Extraction in the Metallurgical Industry

Solvent extraction (SX) is a metal separation and purification technique that exploits the differences in solubility of metal species in an organic solvent phase. SX typically involves an aqueous pregnant liquor stream (PLS) bearing metal ions (M) being intimately contacted with an insoluble solvent containing an extractant (E) which, when conditions are favourable, will lead to the formation of an extracted species (ME) that is stable in the solvent phase (Eqn. 1).

$$M_{(aq)} + E_{(org)} \leftrightarrow ME_{(org)} \qquad \text{Eqn. 1}$$

Once this reaction has been allowed to occur, the "loaded" solvent and the barren PLS bearing other ions, generally impurity ions are allowed to separate. The loaded solvent is then intimately contacted with a clean aqueous "stripping" solution, which affects the transfer of metals from the solvent to the stripping solution. This solution can then be refined to produce high grade metal by processes such as electrowinning or hydrogen reduction.

Since the inception of SX for hydrometallurgical application in the 1950s, its use has significantly increased in terms of both the number of SX plants operating commercially and the number of metals being treated. Ritcey (2006a) has stated that the technique is now used for the separation and recovery of alkaline metals, alkali earths, transition metals, rare metals, precious metals, actinides and lanthanides. This increased application of SX may be attributed to the technique (1) being the only commercially viable separation technique for a range of metals, (2) being required for separating metals from highly contaminated PLSs generated by leaching ores of complex mineralogy that do not respond to traditional processing techniques and (3) producing high product recoveries relative to other separation techniques.

After almost 50 years of commercial application, several intrinsic limitations of current SX practice have become evident. Both industry practitioners and researchers agree that

one of the main drawbacks of SX is inherent to the mechanical agitation used in the current standard contactor – the mixer-settler (Proceedings of the 3rd International SX Workshop 2003). A review of commercially used contactors is appropriate for an understanding of these limitations.

## 1.2 Solvent Extraction Contactors

Of the variety of solvent extraction contactors proposed, the mixer-settler and the pulsed column have received almost exclusive use in the metallurgical industry, with others having received only specialty application.

### 1.2.1 The Mixer-Settler

As the name suggests, a mixer-settler consist of a mechanically stirred mixing tank where the solvent and the PLS are intimately mixed, and a settling tank into which the mixture overflows and is allowed to disengage. Figure 1-1 depicts a diagram of a mixer-settler. The mixer-settler remains the most commonly used contactor today which has been suggested to be a result of it being (1) a proven technology, (2) simple to construct, operate and maintain, (3) able to process high throughput volumes and (4) its performance being simple to assess (Thunaes and Colborne 1969; Hanson 1982). Nevertheless a number of inherent problems have become evident, which may be directly attributed to the mechanical agitation used. Generally mechanical agitation results in regions of high shear within the mixer vessel, which has undesirable consequences.

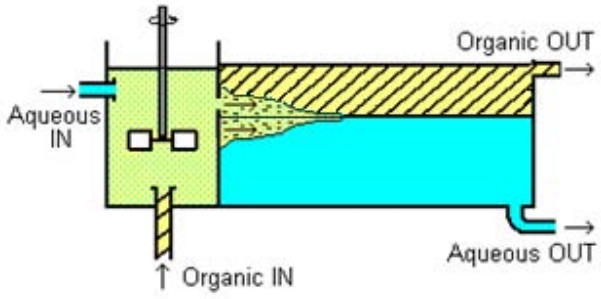


Figure 1-1. A mixer-settler contactor.

Firstly, it has been suggested that the higher shear mixing and the presence of impurities such as suspended solids, flocculants and colloidal and dissolved silica, leads to the formation of crud (Ritcey 1980; Ritcey 2006b). Crud formation represents expensive solvent and metal losses, as well as plant down-time for crud removal.

Secondly, the droplet dispersion produced by mechanical mixing is generally non-uniform in size, with a significant proportion of the droplets produced being ultra-fine (i.e. <20 μm). These ultra-fine droplets require a longer time to disengage resulting in the requirement of larger settlers and thus, an increased solvent inventory and solvent cost (Ritcey 1980; Godfrey 1994, 399). If the settler is too small, the ultra-fine droplets have insufficient time to disengage and consequently become entrained (Ritcey 2004, 312) resulting in solvent and metal losses. In addition these ultra-fine droplets act as rigid spheres, thereby inhibiting internal mixing, and therefore also mass transfer (Jeffreys 1987).

### 1.2.2 The Pulsed Column

The other main contactor used for metallurgical application, although to a much lesser extent, is the pulsed column. The pulsed column is basically an enclosed vertical column containing either perforated plates, in the case of a sieve-plate pulsed column or a series of rings and donuts in the case of the proprietary Bateman pulsed column, and also a pulsing mechanism which is often a piston pump at the bottom of the column. Figure 1-2 shows a diagram of a sieve-plate pulsed column.

The light solvent phase is fed at the bottom of the column and the heavier PLS is fed at the top; owing to the difference in density between the solvent and the PLS the PLS will settle to the bottom and the solvent rise to the top. The counter-current flow of these fluids together with the applied pulsating action creates turbulence within the column resulting in intimate contact between the two phases.

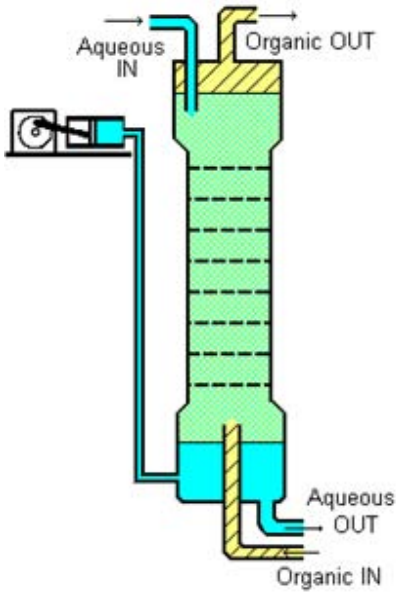


Figure 1-2. A sieve-plate pulsed column contactor.

The pulsed column does not suffer many of the problems inherent to mixer-settlers. The hydrodynamic mixing in pulsed columns is lower in shear and therefore crud formation may be significantly reduced (Vancas 2003), and the droplet size distribution can easily be confined to within narrow limits with little formation of ultra-fine droplets (Slater 1978, 134; Vancas 2003). In addition, as the column is enclosed, solvent contamination and evaporation is virtually eliminated and the solvent inventory is also lower (Smoot, et al. 1959; Ritcey 2006c, 389).

The main drawback of the pulsed column is that it is deemed unsuitable for chemical systems with slow kinetics. Owing to the lower-shear mixing within pulsed columns, mass transfer performance is generally poorer (Slater 1978, 134), which for kinetically slow systems such as copper extraction with chelating reagents, means that an excessively tall and therefore expensive pulsed column would be required (Vancas 2003). Clearly, there is a need for an SX contactor that circumvents these limitations.

A promising alternative to these commercially used mechanically agitated contactors are electrostatically agitated contactors. Studies suggest that electrostatic agitation is low shear (Scott and Wham 1989; Heckley 2002), allows higher mass transfer rates (Hund and Lancelot 1986; Scott and Wham 1989; Heckley 2002; Wildberger and Bart 2002)

and allows excellent control of droplet sizes, (Yoshida et al. 1988a; Sato 1990) while using only a fraction of the power of mechanical contactors (Scott et al. 1994; He et al. 1997).

## 1.3 Electrostatically Assisted Solvent Extraction

Since the first work that proposed the use of electrostatic fields for droplet dispersion and agitation in solvent extraction (Thornton and Brown 1966), numerous studies have indicated that electrostatically assisted solvent extraction (ESX) has unique advantages over conventional techniques particularly in that electrostatic mixing is low shear but still allows high mass transfer rates.

Despite ESX offering such highly desired attributes, a commercial application of the technique is yet to be realised. This may be attributed to: (1) a general lack of understanding of the technique, (2) previous designs of the electrostatic contactors being limited to bench-scale prototypes that are unsuitable for scale-up and industrial implementation, and (3) ESX contactors remaining unproven in treating PLS on a pilot scale.

## 1.4 Aims of the Investigation

The aim of this study was to develop an electrostatically assisted solvent extraction (ESX) contactor that is suitable for industrial application in process metallurgy. Specifically, it was aimed to:

- explore the factors that could influence electrostatic dispersion in an industrially applicable ESX column,
- develop an ESX column that is suitable for industrial application in process metallurgy,
- construct and commission the pilot-scale ESX column, and
- compare the performance of the column with a conventional pulsed column.

## 1.5 Project Scope and Limitations

The scope of this study was to investigate the effect of various solution properties on electrostatically assisted droplet dispersion, develop an ESX contactor suitable for scale-up and application in the metallurgical industry – particularly in regard to the fluxes achievable, and finally assess the performance of the developed ESX contactor on a piloting scale.

This work was based on the commercial nickel/Versatic 10 extraction system due to the growing interest in solvent extraction of nickel from laterite leach solutions, the required reagents being readily available and also sufficient technical data on the system being available. A synthetic PLS that replicates the Bulong Nickel Operations (BNO)[1] nickel-SX feed was used where possible given that BNO was located near the WA School of Mines in Kalgoorlie, WA and that sufficient plant operating data was readily available. Further, this work is limited to the development of an ESX contactor that operates with a continuous organic phase; ESX contactors that operate in aqueous-continuous mode operate by different principles and consequently their design is markedly different.

In droplet dispersion studies, droplet size distributions were measured by manually defining the size of the dispersed droplets in photographs. This approach was taken owing to the high cost of laser sizing instrumentation. Given the long times required for manual droplet definition, only selected photographs in which the droplet dispersion was deemed representative of dispersion under the given set of conditions were analysed. Further, investigation into the effect of various solution properties on the size distribution of droplets required some solution properties to be changed as independently as possible. Owing to interactive effects, altering one solution property always resulted in some associated changes in other properties. Generally these associated changes were small but where they were significant they were considered in analysis of the data.

For the pilot-scale studies within this work, the performance of the ESX column was only compared to a sieve-plate pulsed column because it is structurally similar to the ESX column, a majority of the equipment was already available in the WA School of

[1] Bulong Nickel Operations ceased operation in 2003 and is currently owned by Norilsk Nickel. The plant has been renamed Avalon Nickel Project and is being modified to process nickel sulphide concentrates.

Mines hydrometallurgy laboratory, and also data on sieve-plate pulsed columns were readily available.

## 1.6 Summary

After 50 years of commercial use of solvent extraction for the recovery of metals, it is apparent that inherent limitations in the technique exist. These limitations may be attributed to the mechanical agitation used in the most common contactor, the mixer-settler, which leads to the formation of stable emulsions and cruds, and non-uniformly sized droplets and ultra-fine droplet sizes. Pulsed columns do not suffer these problems to the same extent as mixer-settlers; however they are not applicable to extraction systems with slow kinetics.

A promising alternative to mechanical agitation is electrostatic agitation. Studies have shown that electrostatically-agitated solvent extraction (ESX) contactors allow lower shear in mixing, higher mass transfer rates, excellent control of droplet agitation and droplet sizes, while consuming only a fraction of the power of mechanically agitated contactors. The aim of this work is to progress ESX toward industrial application.

Chapter 2

# Review of Studies on Electrostatic Dispersion and Electrostatically Assisted Solvent Extraction

## 2.1 Electrostatic Dispersion

When an isolated droplet of conducting liquid that is suspended in a mass of relatively non-conducting liquid is subjected to an electrostatic field, the droplet becomes polarised and elongates in the direction of the applied field (Taylor 1964) (Figure 2-1). As the field strength is increased, the droplet will further elongate. That is, for a given field strength, the droplet will achieve its own equilibrium shape.

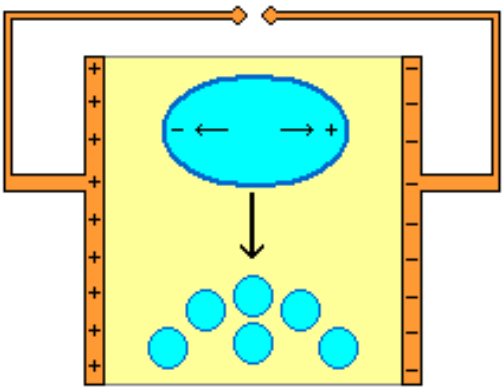

Figure 2-1. Diagram showing the deformation and dispersion of an aqueous droplet in a continuous organic phase.

The net effect of this droplet elongation is to increase the surface pressure of the droplet. That is, the elongation causes the droplet surface area per droplet volume to increase and thereby increasing the pressure acting on the droplet surface. Further increases in the field strength result in further droplet elongation, until the pressure acting on the droplet surface exceeds the interfacial tension holding the droplet together, consequently resulting in the dispersion of the droplet into numerous smaller so-called daughter droplets.

The mechanism by which droplets polarise is dependent on the charge they carry. Uncharged droplets polarise predominantly by orientational polarisation, where polar

molecules, such as water, align with the external electrostatic field and, in doing so, apply pressure to the droplet surface. Charged droplets too will polarise by orientational polarisation, but they are also polarised by a stronger interfacial polarisation. Interfacial polarisation arises when the charge contained within the droplet, which is also influenced by the electrostatic field, tends toward the droplet interface closest to the oppositely charge electrode. Given that the medium is largely non-conducting, the charge is unable to progress across the interface and thus, applies a pressure directly to the droplet surface (Melcher and Taylor 1969; Pohl 1973, 343) resulting in the polarisation of the droplet. The pressure applied to the droplet surface by interfacial polarisation is significantly larger than that applied by molecular polarisation. Therefore, in any attempt to make use of electrostatic dispersion, care must be taken to consider the amount of charge within droplets.

Numerous works on the modelling of electrostatic dispersion have been reported; some, such as those of Taylor (1964), Rosenkilde (1969) and Sherwood (1991) are purely theoretical while others, such as those of Zeleny (1917), Allan and Mason (1962); Garton and Krasucki (1964), Taylor (1966), McEwan and deJong (1966), Torza et al. (1971), Brazier-Smith (1971), and Scott and Wham (1987) include some experimental parts. The most frequently cited of these models is that developed by Rosenkilde (1969). This model states that for a dispersion to occur, the electrostatic Weber number (Eqn. 2), which is the ratio of the inertial and surface forces about the droplet, must reach 0.409 and the major-to-minor axis ratio of the droplet must reach 1.838.

$$We_E = \frac{\varepsilon\varepsilon_0 E_0^{\,2} d}{\gamma} = \frac{F_{inertial}}{F_{surface}} \qquad \text{Eqn. 2}$$

where:

| | | | |
|---|---|---|---|
| $W_e$ | = | Weber electrostatic number |
| d | = | droplet diameter (m) |
| $E_0$ | = | field intensity (kV/m) |
| $\gamma$ | = | interfacial tension (N/m) |
| $\varepsilon$ | = | permittivity of a vacuum |
| $\varepsilon_0$ | = | permittivity of continuous phase |
| $F_i$ | = | inertial force acting on the droplet |
| $F_s$ | = | surface force acting on the droplet |

Given reports that imparting a charge to droplets can influence droplet dispersion (Bailes 1981; Basaran and Scriven 1982), and that droplet charging occurs explicitly in most ESX contactors developed to date, the Rosenkilde model is fundamentally not suitable to predict the onset of droplet dispersion in such applications as the model does not consider interfacial polarisation.

To incorporate interfacial polarisation effects in a mathematical model, the conductivity as well as the permittivity of the continuous phase needs to be considered in the analysis. This was attempted by incorporating the electrical relaxation time, the ratio of the permittivity and the conductivity of the continuous phase, as well as the quantity of charge that is being carried by the droplet into the model (Melcher 1976; Scott 1989). However, for these models to be quantitatively applied to ESX, the quantity of charge being carried by the droplets throughout an ESX contactor needs to be known. This is difficult to achieve and thus, these models remain an approximate "yardstick" to predict the onset of dispersion. Therefore, the best method to establish the resulting droplet dispersion achievable under specified a set of conditions is to conduct dispersion studies.

Throughout some of the aforementioned modelling studies (Allan and Mason 1962; Garton and Krasucki 1964; Torza et al. 1971), two mechanisms for droplet dispersion were identified and the factors that influence which mechanism is predominant were explored. The mechanism by which a droplet disperses is an important consideration in the design of ESX contactors.

## 2.2 Droplet Dispersion Mechanisms

Two distinctly different droplet dispersion mechanisms have been reported: necking and jetting. Figure 2-2 shows droplet breakage by the necking and jetting mechanisms. Droplet necking is where the droplet elongates to form an oblate spheroid which gradually stretches and necks in the middle of the droplet to form several smaller sized droplets. Droplet jetting is where the droplet forms conical ends as the droplet elongates, from which numerous small droplets are ejected.

Researchers have shown that the droplet charge (Allan and Mason 1962), the uniformity of the electrostatic field (Garton and Krasucki 1964), the nature and applied frequency of the electrostatic field, the ratio of viscosity of the droplet and surrounding medium and the size of the droplet (Torza et al. 1971), as well as the electrostatic field strength (Basaran and Scriven 1982) affect the mechanism by which the droplet breaks.

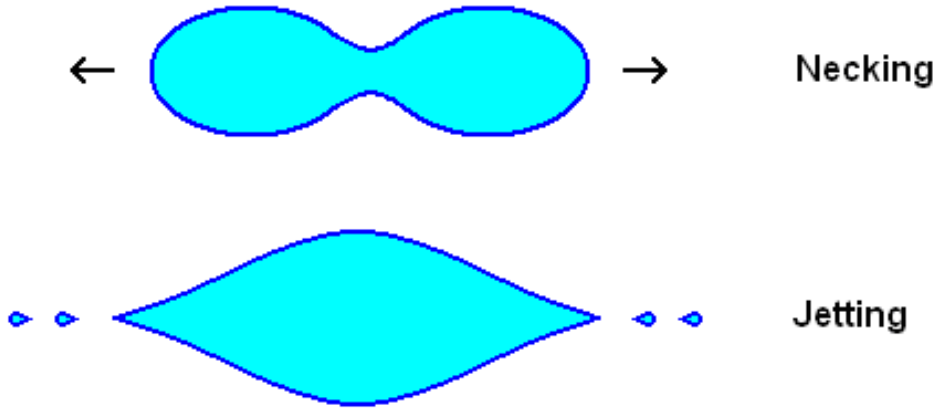


Figure 2-2. Diagram showing droplet breakage by the (1) necking and (2) jetting mechanisms.

While these studies have shown that the abovementioned variables influence the dispersion mechanism by which a droplet breaks, they made no attempt to measure the resulting droplet sizes and their distribution in relation to these variables, which is an important measurement in the design of an ESX contactor. Thus, the factors that influence the mechanism of droplet dispersion and the resulting droplet sizes had to be explored in the present study.

## 2.3 Effect of the Physical Properties of the Solution on Electrostatically Generated Droplet Size Distributions

The physical properties of the solutions in SX systems, such as the ionic strength of the PLS, the conductivity of the solvent, the viscosity of both the PLS and solvent and also the interfacial tension vary widely. Given the preceding discussion, it is reasonable to suggest that at least some of these properties will affect the droplet dispersion mechanism and therefore the resulting droplet size distribution. Consequently, the

knowledge of the effect of various solution properties on the resulting droplet size distribution is important to the design of a commercially applicable ESX contactor.

In ESX applications, the effect of these properties on the droplet size distribution generated by electrostatic dispersion remains largely unexplored and has been limited to a mere few observations. Heckley (2002) reported only that decreases in interfacial tension resulted in a decrease in the average droplet diameter. Usami et al. (1993) reported that increases in the solvent conductivity resulted in increases in the average droplet diameter, and eventually resulted in the cessation of droplet dispersion. To address this gap in the knowledge, the effect of various solution properties on the dispersed droplet size distribution will be investigated in this study.

## 2.4 Electrostatic Agitation

Apart from effecting droplet dispersion, electrostatic fields can promote mass transfer by inducing motion within and around the droplet. In theory, if an electrostatic field of a transient nature is applied, such as that from a pulsed-DC or AC power source, the droplet shape oscillates between spherical and ellipsoidal in response to the continual polarisation and depolarisation of the droplet as the current cycles (Figure 2-3). This induced oscillation facilitates internal mixing within the droplet (Taylor 1966; McEwan and DeJong 1966; Torza et al. 1971; Brazier-Smith et al. 1971; Scott et al. 1990), which in the case of extracting metal from the aqueous droplets, has been suggested to continually replenish the internal droplet surface with fresh metal ions (Yamaguchi 1995).

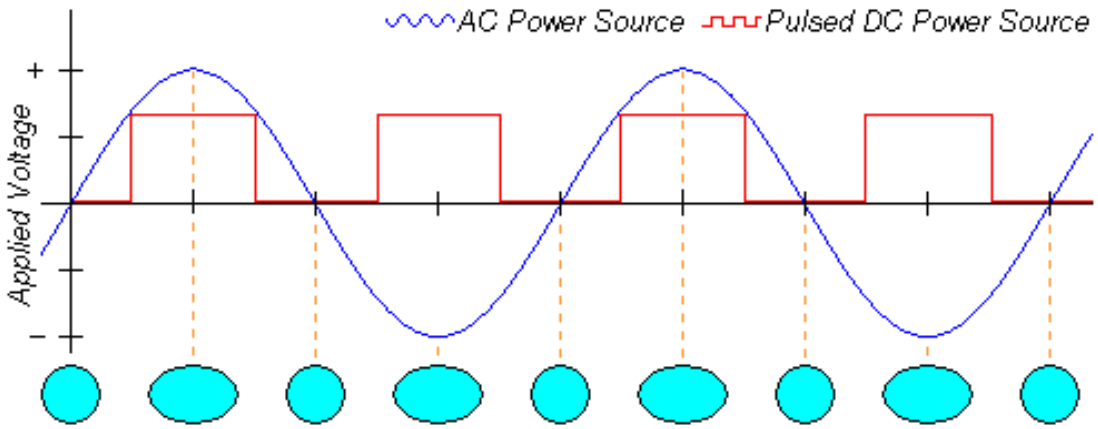


Figure 2-3. Droplet oscillation during cycling of AC and Pulsed-DC generated fields.

In addition to droplet oscillation, a transient field also induces lateral motion to the droplets, provided that the droplets are charged, such that the droplets zigzag back and forth in phase with the cycling electrostatic field (Yamaguchi et al. 1988), as is shown in Figure 2-4. This increases the slip velocity of the droplet, which is the velocity of the droplet with respect to the continuous solvent phase, results in enhancement of the film mass transfer rate around the droplet (Weatherley et al. 1990).

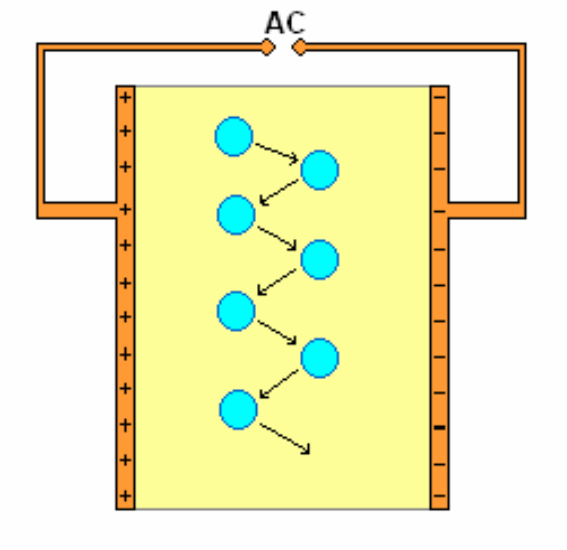


Figure 2-4. Diagram showing the droplet zigzag motion induced by a transient electrostatic field.

The uniformity of the electrostatic field to which a droplet is subjected also affects droplet motion by dielectrophoresis (Pohl 1973, 340). Dielectrophoresis is the force subjected onto a droplet when it is located in a non-uniform electrostatic field, as shown in Figure 2-5. Here, the large uncharged conducting droplet located in the non-uniform field becomes polarised, with positive dipoles forming on the side closest to the negatively charged electrode and negative dipoles forming on the side of the droplet closest to the positively charged electrode. Because the field is non-uniform it diverges across the droplet and produces unequal forces on each dipole which causes the droplet, in this case, to move toward the smaller positive electrode.

Given that non-uniform fields allow increased droplet movement by dielectrophoresis, and thus mass transfer, their incorporation into the design of an ESX contactor seems largely beneficial. Surprisingly, numerous ESX contactors developed by other investigators have not incorporated a non-uniform field in their contactor design.

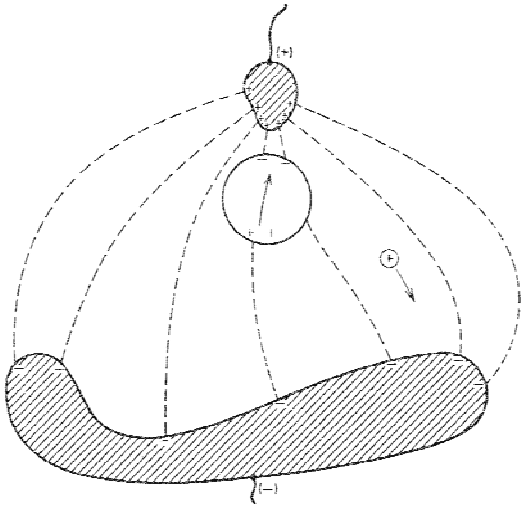

Figure 2-5. Droplet motion in a non-uniform electrostatic field (Pohl 1973, 340).

## 2.5 Interfacial Activity in the Presence of an Electrostatic Field

As well as effecting droplet dispersion and agitation, an electrostatic field has also been shown to influence interfacial activity and thus, the rate of mass transfer between phases.

Austin et al. (1971) used a Schlieren cell to investigate mass transfer in binary systems. Copper gauze electrodes were placed at the top and at the bottom of the cell with the phase interface kept equidistant (30 mm) from both electrodes. They found that, for various binary systems consisting of water and an organic solvent, increases in the applied voltage resulted in increases in the mass transfer coefficient, as shown in Figure 2-6. They suggested that the presence of electric charges at a phase interface caused local variations in surface charge density, which in turn, caused interfacial tension-induced surface flows (Marangoni flows), that convectively removed the extracted species away from the interface, allowing an increased mass transfer rate. Photographs of the Marangoni flows are shown in Figure 2-7.

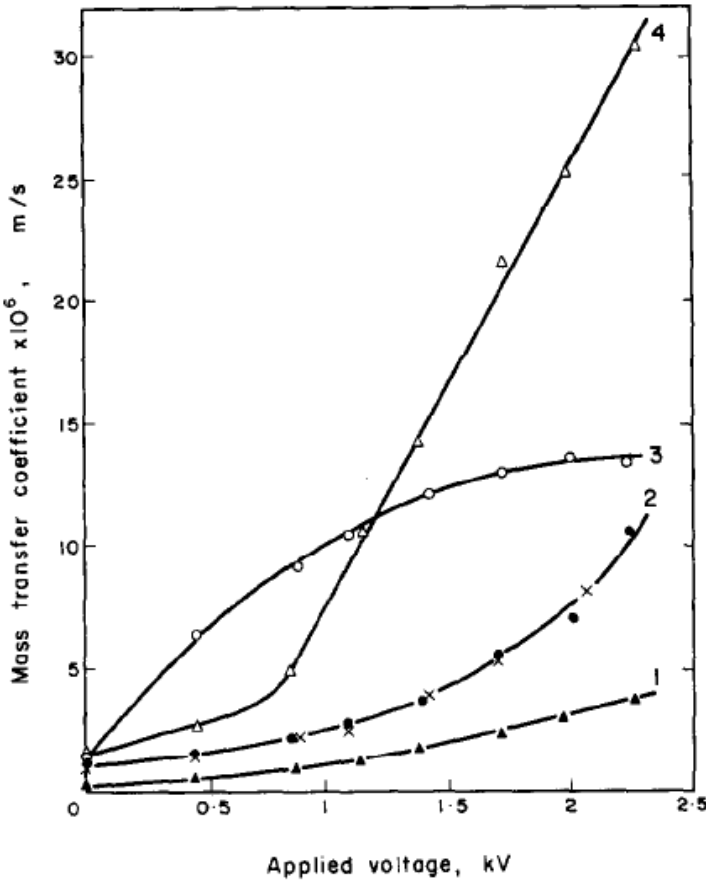


Figure 2-6. The effect of applied voltage on mass transfer coefficients of water for the systems: (1) cyclohexanol/water, (2) isobutoanol/water, (3) aniline/water and (4) ethyl acetate/water (Austin et al. 1971).

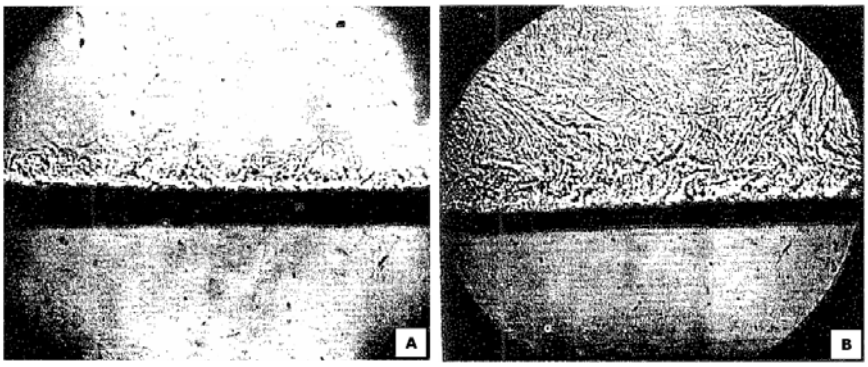


Figure 2-7. Schlieren photographs of mass transfer in isobutanol/water system at a) 0.45 kV, b) 0.85 kV. (Austin et al 1971).

In a later work, Iyer and Sawistowski (1974) extended this work using a similar experimental apparatus and reported similar results for several ternary systems. They noted that the Marangoni instabilities only occurred in the lighter organic phase and only when mass was being transferred from the aqueous to the organic phase. In addition, they found that the polarity of the charge on the lower electrode had a marked effect on the mass transfer rate. For the extraction of propionic acid from water into toluene, the mass transfer coefficient was ~2.6 x $10^6$ m/s when no potential was applied, ~3.8 x $10^6$ m/s when a negative potential was applied and ~4.4 x $10^6$ m/s when a positive potential was applied.

Martin et al. (1983) conducted experiments similar to those of Iyer and Sawistowski (1974) using a modified Lewis cell to study the extraction of copper with LIX 65N. They reported similar results and they suggested that electromigration of copper ions to the interface was modifying the metal concentration at the interface, which in turn resulted in an increased rate of mass transfer. This suggestion was supported by the findings of Wildberger and Bart (2002). Hund and Lancelot (1986) reported contradicting results to those of Martin et al. (1983) but did not provide any explanation of their data.

Bailes and Wade (1980) reported similar results to those of Martin et al. (1983) for the extraction of copper with LIX 64N and suggested that the higher mass transfer rates observed may be attributed to the orientation of the extractant molecules being favourably influenced by the charge of the droplet interface.

Collectively, the results presented by these investigators suggest that charging droplets within an ESX contactor will allow higher mass transfer rates to be achieved. This further indicates that droplet charging should be at the core of the design of an ESX contactor.

## 2.6 Electrostatic Solvent Extraction Contactors

Since the inception of the use of electrostatic fields to effect droplet dispersion, there have been several attempts to develop an electrostatically assisted solvent extraction contactor. These contactors can be classified into five main categories: (1) electrostatic spray column, (2) emulsion contactor (3) vertical electrode column, (4) plate contactor and (5) electrostatic pseudo-liquid membrane (ESPLIM).

### 2.6.1 Electrostatic Spray Columns

The first electrostatic spray column contactor, as proposed by Stewart and Thornton (1967) was a bench-scale apparatus resembling a sieve-plate column. A schematic diagram of this column is shown in Figure 2.8a. The PLS is fed into the top of the column via metallic delivery nozzles and removed from the PLS settler at the bottom. The solvent on the other hand is fed near the bottom of the column and removed from the column side immediately below the PLS delivery point. A high voltage DC power source is attached to the PLS delivery nozzles, and an earthed perforated plate is located at the bottom of the column immediately above the PLS settler. As the PLS passes through the nozzles, it becomes highly charged and, owing to electrostatic attraction, the charged droplets are accelerated toward the earthed plate.

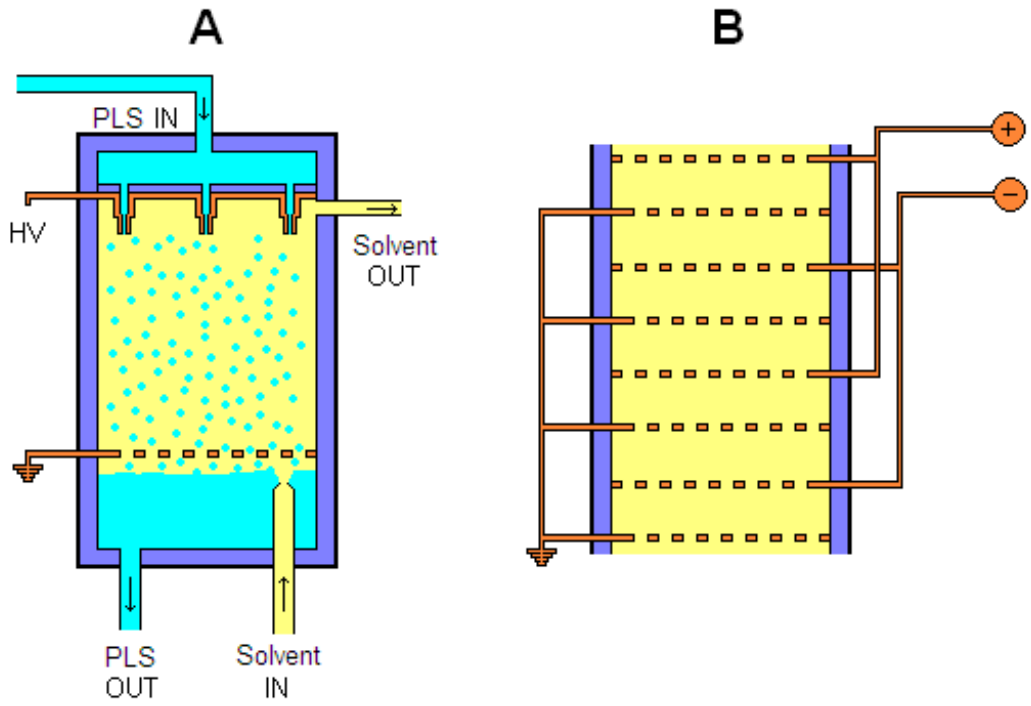


Figure 2-8. Diagrams of (A) bench-scale column and (B) section of the proposed full-scale electrostatic sieve-plate column.

This design was patented by Thornton and Brown (1966) as a quasi sieve-plate pulsed column, where alternating plates were charged and every other plate was earthed, as shown in Figure 2-8b. As the droplets enter the contactor, they are attracted to a charged sieve-plate, and thus contact the plate and become charged themselves. Consequently, they are attracted and accelerated toward the earthed sieve plate immediately below, and upon contact lose their charge. They then fall through the sieve plate and the process is repeated throughout the length of column.

This design of contactor provides excellent control of the droplet size and velocity, but the droplet size and velocity cannot be controlled independently. That is, as the applied voltage is increased, the droplet size decreases and the droplet velocity concurrently increases, resulting in somewhat inflexible operation. Also this design only allows for droplet oscillation by vortex shedding. That is, the oscillation associated with accelerating a droplet through another fluid. This occurs only at high droplet velocities where the droplet Reynolds number is above 300 (Goldburg and Florsheim 1966) and also, this is not as vigorous as the droplet oscillation imparted by applying transient

electrostatic fields. In addition to these drawbacks, it is foreseeable that when high PLS fluxes are used, significant arcing between electrodes will occur, which would result in an intermittent electrostatic field and thus, result in flooding of the column.

In a later work, Thornton (1989) presented a revised design of electrostatic spray column, a diagram of which is shown in Figure 2-9. As the PLS enters the column it falls into a charged central receptacle. As the receptacle fills with PLS, the PLS is pumped, by electrostatic means, through the nozzles on the side of the central receptacle and sprayed toward a larger surrounding earthed receptacle. The dispersed PLS droplets coalesce on the wall of this receptacle and then flow to the centre, where they fall through to the charged central receptacle immediately below. This process is repeated throughout the length of the column. The solvent is passed throughout the column counter-currently, through capped ports in each of the settler receptacles.

While this design allows somewhat more independent control of droplet size and the speed at which the dispersed phase travels through the column, it still does not allow the use of high aqueous fluxes owing to the onset of arcing between electrodes. This design therefore is unlikely to find application in process metallurgy.

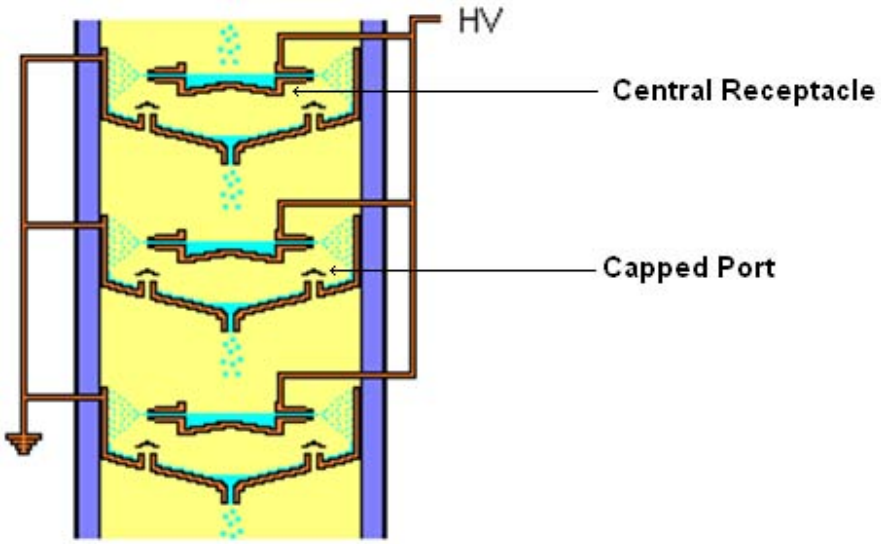


Figure 2-9. Diagram of the electrostatic spray column.

### 2.6.2 Emulsion Phase Contactor

Scott and Wham (1989) proposed an emulsion phase contactor (EPC) which emulsifies the PLS using an electrostatic field. A diagram of the EPC is shown in Figure 2-10. The contactor is a conical vessel, with the solvent feed port at the bottom and its discharge port at the top. The PLS is fed at the centre of the vessel from the top and withdrawn from the bottom. On either side of the PLS feed nozzle, are located two parallel electrodes: one is connected to earth and the other to a high voltage source. As the PLS is discharged from the nozzle, it is emulsified. When the emulsified droplets pass beyond the region of the uniform field, they are attracted to the lower points of the electrodes, by the dielectrophoretic force, where they coalesce. These coalesced droplets subsequently fall into the PLS settler.

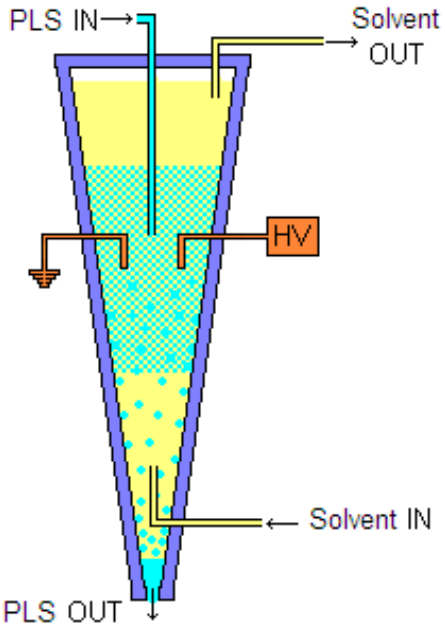


Figure 2-10. Diagram of the emulsion phase contactor.

Scott and Wham (1989) compared the performance of the EPC with a York-Schiebel column (YSC) and a Podbielniak centrifugal contactor (PCC) using a water–acetic acid–methyl isobutyl ketone (MIBK) system. They found that the EPC was 17 times more efficient than the YSC and 10 times more efficient than the PCC. Because the droplets were not agitated by the application of a transient electrostatic field, the higher mass

transfer reported may be attributed to the extremely small droplet sizes, between 1 and 10 μm, that were produced.

It seems that the EPC is not viable for commercial application in the metallurgical industry. Given that in conventional SX, emulsifying the PLS could result in the formation of a stable emulsion and crud formation (Ritcey 1980), it appears that the EPC is not suitable for industrial application particularly considering that SX feed solutions usually contain impurities such as surfactants and flocculants, which are known to contribute to the formation of stable emulsions.

### 2.6.3 Electrostatically Assisted Solvent Extraction Columns

An electrostatically assisted solvent extraction (ESX) column is, in essence, a pulsed column with agitation of the phases being effected by electrostatic instead of mechanical means. As in a pulsed column, the PLS is introduced at the top and the solvent is phase introduced at the bottom. Owing to the difference in density between the phases, the PLS settles to the bottom of the column and the solvent rises to the top of the column from where each is then withdrawn.

The main ESX column designs that have been developed to date are the corrugated plate electrode column (Warren and Prestridge 1979), vertical rod electrode column (Kowalski and Ziolkowski 1981), parallel plate electrode column (Martin et al. 1983), and parallel plate electrode column with DC disperser (Scott et al. 1994). These designs are shown in Figure 2-11.

Warren and Prestridge (1979) presented a corrugated plate electrode column design, a diagram of which is shown in Figure 2-11a. On either side of the column, corrugated electrodes are located and a DC-generated field is applied. The intermittent regions of high and low strength electrostatic field, effected by the corrugations, allow for droplet dispersion in high field strength regions and coalescence in low field strength regions and thereby minimising phase entrainment and the formation of stable emulsions. The main shortfall of this design, however, is that the electrodes are not insulated, and thus operating the column at high aqueous fluxes will undoubtedly result in arcing between electrodes, which in turn will hinder droplet dispersion and increase the power draw.

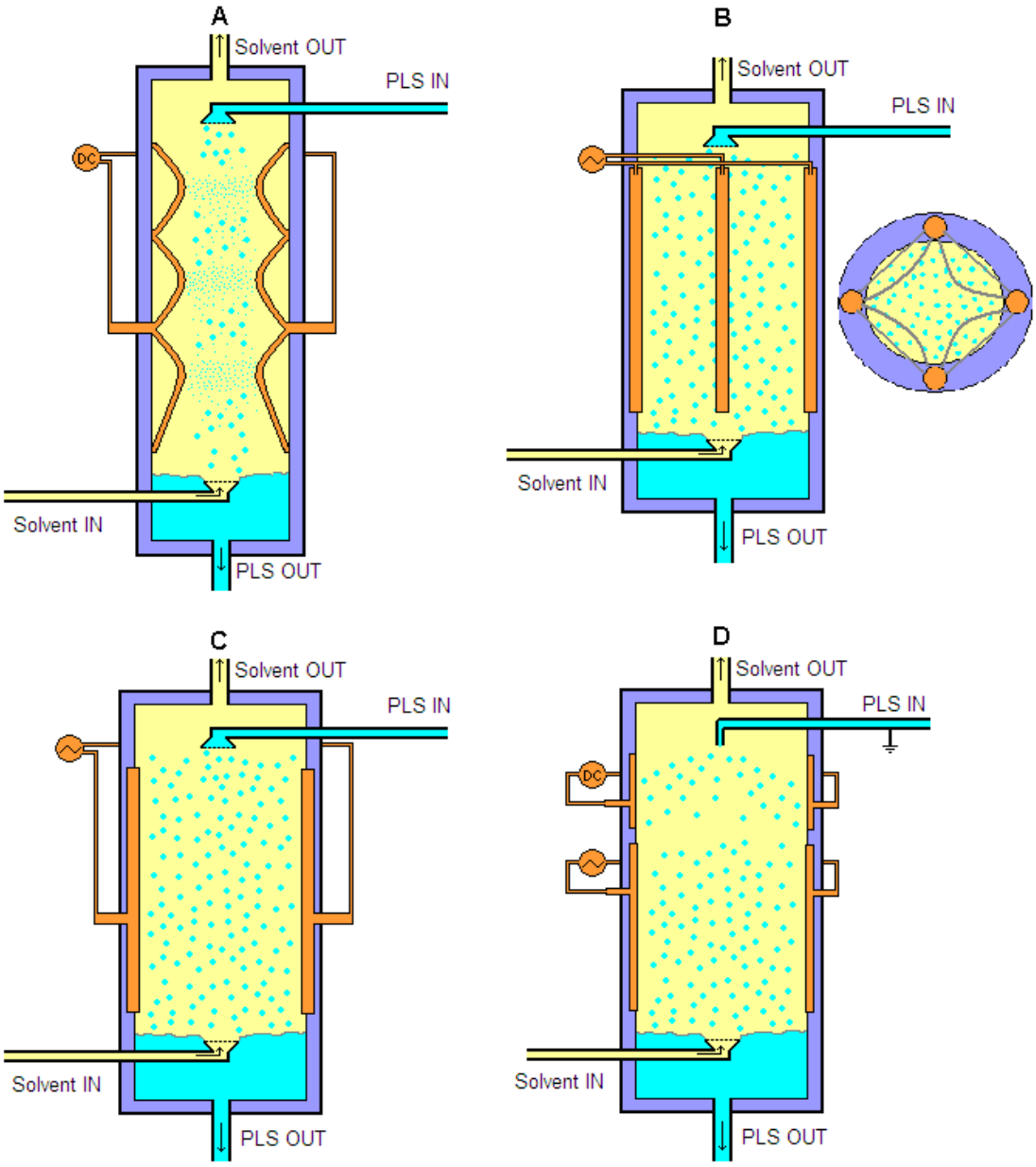


Figure 2-11. Diagrams of previously developed electrostatically assisted solvent extraction columns. (a) corrugated plate electrode column (b) vertical rod electrode column (c) parallel plate electrode column (d) parallel plate electrode column with DC disperser.

Kowalski and Ziolkowski (1981) presented a vertical rod electrode column design, a diagram of which is shown in Figure 2-11b. The column had four polyethylene-coated

vertical steel rod electrodes located equidistantly about the column, by which an AC generated electrostatic field was applied. They reported a three-fold increase in the rate of mass transfer over no-field conditions for a xylene-acetic acid-water system. Yamaguchi et al. (1988; 1989), using a comparable column but with a DC power source connected to alternate electrodes, reported a 50% increase in mass transfer for a water-iodine-cyclohexane system over that of no-field conditions. While the non-uniform field in this column design promotes lateral movement of non-charged aqueous droplets and also coalescence of fine droplets, it also allows large regions of low field strength at the centre of the column, where droplets can fall through undispersed. This represents a significant processing inefficiency and would add considerably to the height requirement of this column in an industrial application.

Martin et al. (1983) presented the parallel plate column, a diagram of which is shown in Figure 2-11c. Located on either side of the column are flat plate electrodes, by which an electrostatic field is applied to the column contents. The advantages of this design over others previously presented are that it does not allow droplets to pass through the column undispersed. The authors, however, reported arcing between electrodes at high PLS flow rates. Briggs et al. (2000) also investigated the parallel plate column, but the electrodes were insulated and spaced further apart. The insulation virtually eliminated the arcing between electrodes. The increased electrode spacing, however, required the application of a higher voltage to the electrodes for droplet dispersion to occur. For a scale-up to industrial application the voltage required for droplet dispersion would be significantly higher and arguably on the verge of practically unfeasible. In addition, this design does not facilitate the coalescence of small, slow settling droplets, which may then lead to significant entrainment of the solvent.

Scott et al. (1994) enhanced the basic design of the parallel plate column by incorporating an individual DC disperser region above the pulsed-DC agitation electrodes, as shown in Figure 2-11d. The DC disperser allows the production of uniformly sized droplets such that the frequency of the electrostatic field applied to the agitation electrodes can be optimised for the selected droplet size. The only significant weakness, which was reported by the investigators, is arcing between the electrodes and the delivery needle, and also between the lower set of agitation electrodes when high

aqueous fluxes are used. If this weakness can be resolved, the use of DC dispersers has some merit, and thus further investigation is warranted.

It seems that in developing a scale-up application of an electrostatic column, the most significant hurdle to overcome is to devise a suitable electrode arrangement. A suitable electrode arrangement must be able to (1) tolerate adequate aqueous fluxes, (2) be insulated to prevent arcing between electrodes, (3) promote coalescence of ultra-fine droplets and (4) be scaled-up to commercial size without requiring excessively high voltages to generate an electrostatic field strength sufficient to effect droplet dispersion.

### 2.6.4 Plate Contactors

Yamaguchi and co-workers (Yoshida et al. 1988a; 1988b) developed the inclined plate contactor, a diagram of which is shown in Figure 2-12. On the top and bottom, shown in orange, are electrodes by which the electrostatic field is applied; the upper electrode is connected to a high voltage source and the lower electrode is connected to earth. On the top left-hand corner the PLS is introduced and at the bottom right-hand corner the PLS is withdrawn. The solvent is circulated counter-current to the PLS flow.

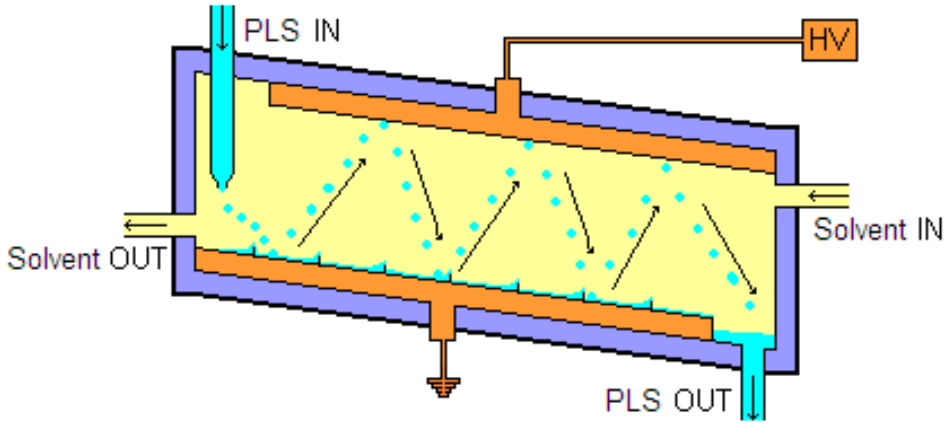


Figure 2-12. Diagram of an inclined plate contactor.

As the PLS droplets enter the contactor, they fall downward onto the lower plate and merge with the aqueous film flowing over the plate. Owing to the highly charged upper electrode, droplets are pulled from the flowing film, which is promoted by the flash boards, and are attracted toward the upper electrode. Upon touching the upper electrode,

they acquire charge and are consequently attracted to and move toward the lower electrode where they dissipate charge upon contact. This cycle is repeated until the droplets reach the aqueous discharge port.

The main advantage of this contactor is that the charged droplets coalesce instantaneously upon impact with the flowing film. This however, is outweighed by the contactor drawing high amounts of power (Yoshida et al. 1986) and also being unable to tolerate sufficient PLS fluxes required for industrial application owing to the bridging of droplets and consequent arcing between electrodes. In addition, owing to the flat design of the contactor together with the low PLS fluxes achievable, a large contactor foot print would be required to treat PLS flows typical in commercial SX operations.

To overcome the short circuiting, Yamaguchi and Kanno conceived the rod-plate contactor (Yamaguchi and Kanno 1996; Yamaguchi 1995; 1997), a diagram of which is shown in Figure 2-13. At the top of the contactor is a metallic point electrode, which is connected to a high voltage source (~60 kV) and at the bottom is a flat plate electrode that is earthed. The PLS is introduced at the bottom of the left hand side of the cell and withdrawn from the bottom right hand side. Above the PLS level in the contactor, the solvent is fed counter-currently to the PLS flow. To avoid arcing between electrodes with high dispersed-phase hold-ups, a nitrogen atmosphere between the point electrode and the solvent was incorporated.

When a relatively weak electrostatic field is applied to the contents of the contactor, the PLS-solvent interface becomes rippled. As the strength of the electrostatic field strength is increased to produce a corona discharge, the ripples at the interface become larger and PLS droplets eject from the ripple tips. These droplets migrate upward and toward the rod electrode until they reach the upper solvent level. At the interface the droplets acquire charge and are subsequently attracted downward toward the earthed PLS settler.

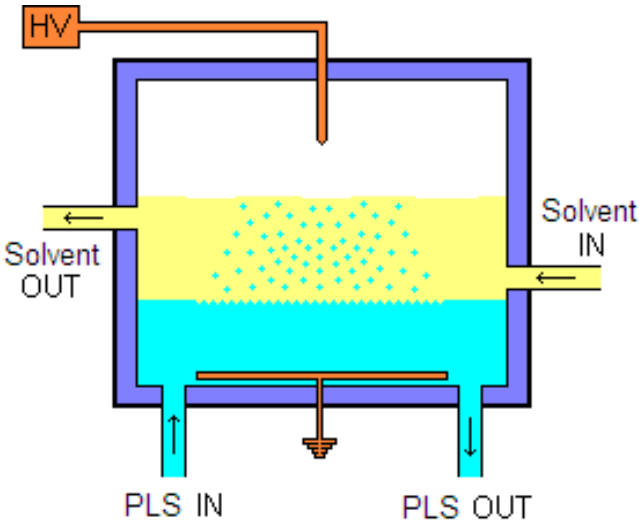


Figure 2-13. Diagram of a rod-plate contactor.

While this design eliminates bridging between electrodes and thereby reduces the power draw, this design allows more short-circuiting of PLS. That is, depending on the PLS flow through the contactor, a reasonably large proportion of the PLS can pass through the contactor without it necessarily having been dispersed in the solvent phase. This reduces the extraction efficiency achievable within the contactor. Also, similar to the inclined plate contactor, the floor space required for an industrial application would be excessively large.

### 2.6.5 Electrostatic Pseudo-Liquid Membrane (ESPLIM)

One application of electrostatic dispersion that has been the subject of considerable interest is the separation technique called electrostatic pseudo liquid membrane (ESPLIM). It involves the simultaneous extraction of the metal ions from the PLS feed to the solvent, and their stripping from the solvent with a strip solution. This eliminates the limited loading capacity of the solvent as well as the limitations imposed by equilibrium.

A diagram of the ESPLIM contactor is shown in Figure 2-14. It is essentially a rectangular cell that is divided into two compartments – extraction and stripping compartments – by a permeable baffle that allows the solvent to be continuous throughout the cell. On opposite sides of the cell, and on both sides of the baffle screen

are electrodes by which an electrostatic field is applied. To the top of the extraction compartment, the feed solution and the pH modifier are dosed, and to the top of the stripping compartment, the strip solution is dosed. Owing to the difference in density between the PLS and solvent phase, the PLS droplets formed fall through the solvent phase until they are under the influence of the electrostatic field where they disperse, and then oscillate and zigzag until they reach the settler at the bottom of the compartment.

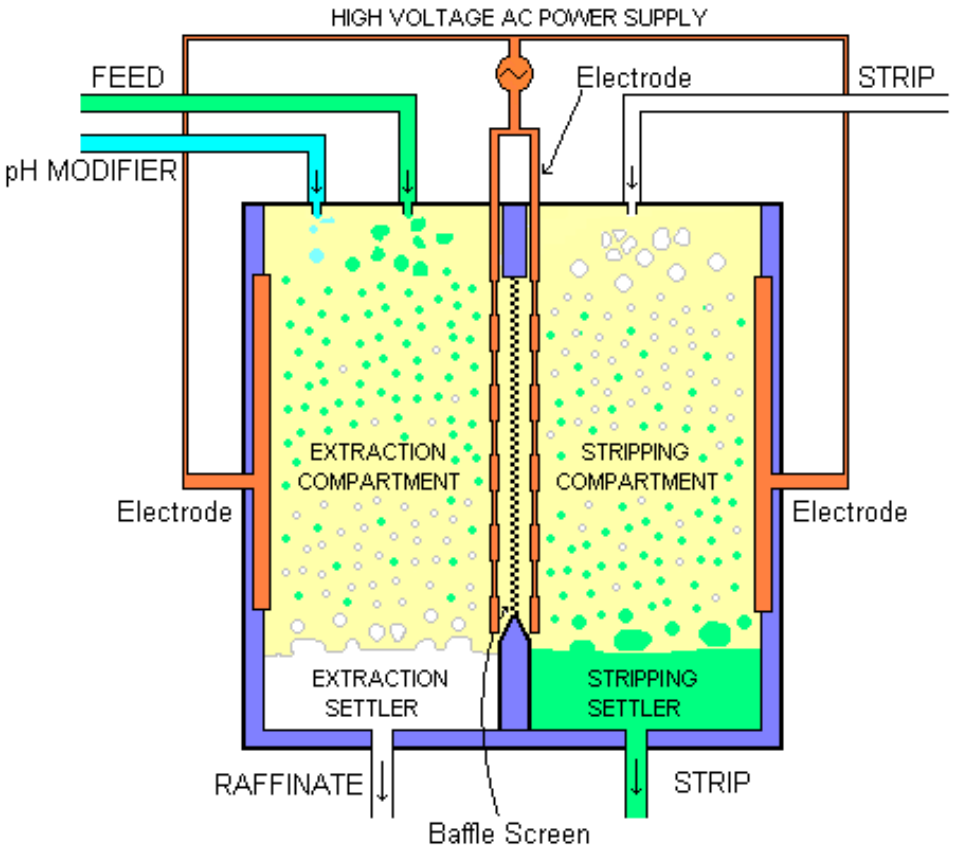


Figure 2-14. Diagram of an ESPLIM cell (Steffens and Ibana 2005).

In the extraction compartment, the extractant is first pre-neutralised with ammonia or ammonium hydroxide in the case of an acidic-type extractant which was used in this work. The pre-neutralised extractant then reacts with the metal ions in the feed stream to form the extracted species. These extracted species then migrate to the stripping compartment owing to the concentration gradient. Here, the extracted species are contacted with the acidic stripping droplets, leading to the transfer of the metal ions to

the stripping droplets and the regeneration of the extractant. As in the extraction compartment, the regeneration of the free extractant forms a concentration gradient that drives its migration back to the extraction compartment and the cycle is repeated.

Studies on the ESPLIM technique have reported many promising results, and has so far shown to separate, purify and concentrate rare earth metals (Zhou & Gu 1988; Gu et al. 1994; Yang et al. 1995; Yang et al. 1998; 1999), nickel (Gu et al. 1990; Williams et al. 1997; Steffens & Ibana 2005) and cobalt (Gu 1990; Heckley et al. 2002; Collard et al. 2005) amongst others. However, studies (Yang et al. 1998; Heckley 2002; Steffens & Ibana 2005), have found that impurities in the PLS co-extract significantly, owing to the non-equilibrium nature of the technique. In current commercial SX practice these co-extracted impurities are scrubbed, but, because metals are extracted and stripped simultaneously in ESPLIM, scrubbing of the solvent is not possible. This is a major limitation of the technique. More importantly, the aqueous fluxes that have been achieved in ESPLIM studies are significantly lower than what is required for commercial application.

### 2.6.6 Synopsis of Electrostatic Contactors

To establish which of the electrostatic solvent extraction (ESX) contactor designs is most suitable for scale-up, and thus industrial application in process metallurgy, each contactor design was assessed against specific criteria including droplet uniformity, achievable volumetric throughput, mass transfer, flexibility and control of operation, and scale up considerations. A summary of the assessment undertaken is shown in Table 2-1.

Based on these criteria, the column design appears to have the greatest industrial potential for the following reasons:

- it seems to be the most likely contactor to allow adequate volumetric throughputs (fluxes) that are required for industrial application;
- it allows for the dispersed droplets to be vigorously agitated and thus, provide high mass transfer rates;
- it allows the formation of uniformly sized droplet dispersions in which the droplets are of an appropriate size;

- it minimises short circuiting of droplets and thus higher processing efficiency;
- it offers good control of operating variables and thus, column performance; and
- its application is versatile and allows the incorporation of solvent scrubbing.

The main weakness, however, of the previously reported ESX column designs is the lack of an electrode configuration that is appropriate for industrial metallurgical application. Thus, the development of an appropriate electrode arrangement is one of the major aims of the present work.

Table 2-1. Comparison of the various electrostatic contactors developed.

| | Droplet Uniformity | Achievable Volumetric Throughput | Mass Transfer | Flexibility and Control of Operation | Scale-up Considerations | Other Considerations |
|---|---|---|---|---|---|---|
| **Spray Columns** | Excellent. Controlled by DC field. | Low. Limited by arcing between electrodes. | No data presented. Seems poor owing to drop oscillation effected only by vortex shedding. | Low. Independent control of droplet size and velocity not possible. | Requires intricate connection of plates to power supply. | High O:A ratios required to limit arcing between electrodes. |
| **Emulsion Phase Contactor** | Excellent. Droplet size between 1 - 10 μm. | Low. Limited by arcing between electrodes. | Excellent. PLS is emulsified. | Good. Dispersion can be controlled by adjusting field strength. | May require additional coalescers to lower entrainment. | Impurities in real PLS may lead to stable emulsion and crud. Potential phase disengagement issues. |
| **Corrugated Plate Electrodes Column** | Average. Droplets continually dispersing and coalescing. | Low. Limited by arcing between electrodes. | No data presented. | Good. Dispersion can be controlled by adjusting field strength. | Requires development of alternative electrode configuration. | - |
| **Vertical Rod Electrodes Column** | Low. Large droplets passing through column. | No data presented with high throughputs used. Seems to be good as electrodes insulated. | Poor. Considerable short-circuiting of PLS. | Low. Cannot ensure all droplets are dispersed. | Requires development of alternative electrode configuration. | Channel of low strength electric field in column centre allows short circuiting. |
| **Vertical Plate Electrodes Column** | No data presented. | No data presented where high throughputs used. Seems to be good as electrodes insulated. | Good. Application of AC type field enhances droplet agitation. | Good. Dispersion controlled by adjusting field strength. | Requires development of alternative electrode configuration. | Ultra fine droplets may cause flooding. Excellent control of droplet agitation. |
| **Vertical Plate Electrodes Column (with DC Disperser)** | Excellent. Controlled by disperser connected to DC power supply. | Low. Limited by arcing between electrodes. | Excellent. Applied field frequency optimal for agitation of given droplet size. | Good. Dispersion and agitation can be controlled by adjusting field strength and frequency. | Requires development of alternative electrode configuration. | Ultra fine droplets may cause flooding. Excellent control of droplet agitation. |
| **Plate Contactors** | No data presented. | No data presented. | Low. Design allows considerable PLS short-circuiting. | Low. | Large floor space required. | - |
| **ESPLIM** | No data presented. | Good. Swelling & leakage of droplets between compartments at high flows. | Good. Application of AC type field enhances droplet agitation. | Good. Dispersion and agitation can be controlled by adjusting field strength and frequency. | Difficult owing to swelling and leakage of droplets between compartments. | Design does not allow scrubbing of the solvent. |

## 2.7 Variables that Affect the Performance of an Electrostatic Solvent Extraction Column

The operation of an ESX column is largely the same as that of the conventional pulsed column except that the agitation provided is achieved by use of an electrostatic field rather than hydrodynamic pulsing. Therefore this section will focus on the aspects of the column relating only to electrostatic dispersion and agitation.

### 2.7.1 The Effect of Electrostatic Field Strength

It has been established that initially, increases in the strength of the electrostatic field result in slight increases in the average droplet diameter, but reaches a value such that further increases in the field strength result in decreases in droplet diameter (Martin et al. 1983; Gu 1990; Heckley 2002). This trend is shown in Figure 2-15. The initial increase in droplet diameter has been attributed to coalescence of droplets (Gu 1990) and also their elongation resulting in a larger droplet diameter (Heckley 2002), and the decrease in droplet diameter is owing to electrostatic dispersion. Differences in the data presented appear to be owing to the differences in the physical properties of the solutions used, and differences in electrode insulation. In addition, differences in the measurement techniques appear to have contributed to the differences in the reported data. Thus, the electrostatic field strength must be optimised in any particular system and contactor.

Martin et al. (1983) investigated the effect of the electrostatic field strength on the dispersed phase hold up over a range of dispersed phase flow-rates. Their results are shown in Figure 2-16. They found that initial increases of the applied voltage resulted in a decrease in dispersed phase hold-up, after which further increases of the applied voltage resulted in increases in the dispersed phase hold-up. This trend was attributed to the changes in droplet size with changes in the electrostatic field strength. Similar trends have been reported by subsequent investigators (Kowalski and Ziolkowski 1981; Yamaguchi et al. 1988; Briggs et al. 2000).

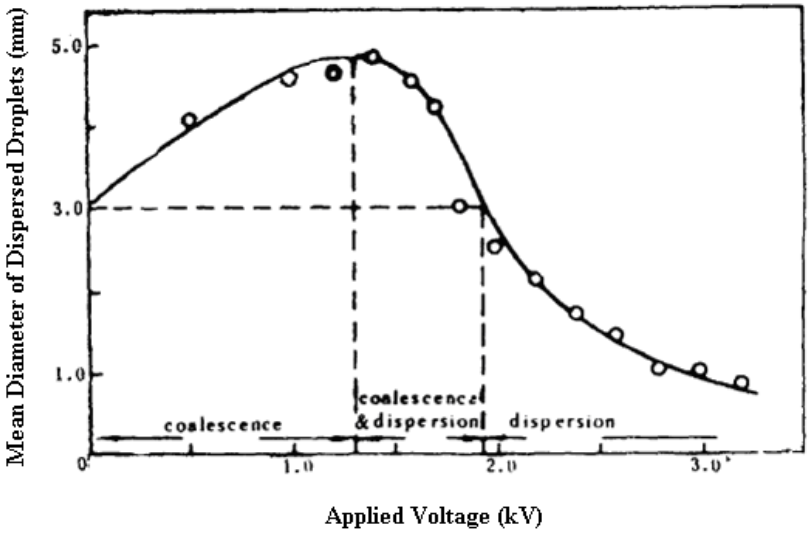


Figure 2-15. Effect of electrostatic field strength on mean droplet diameter (Gu 1990).

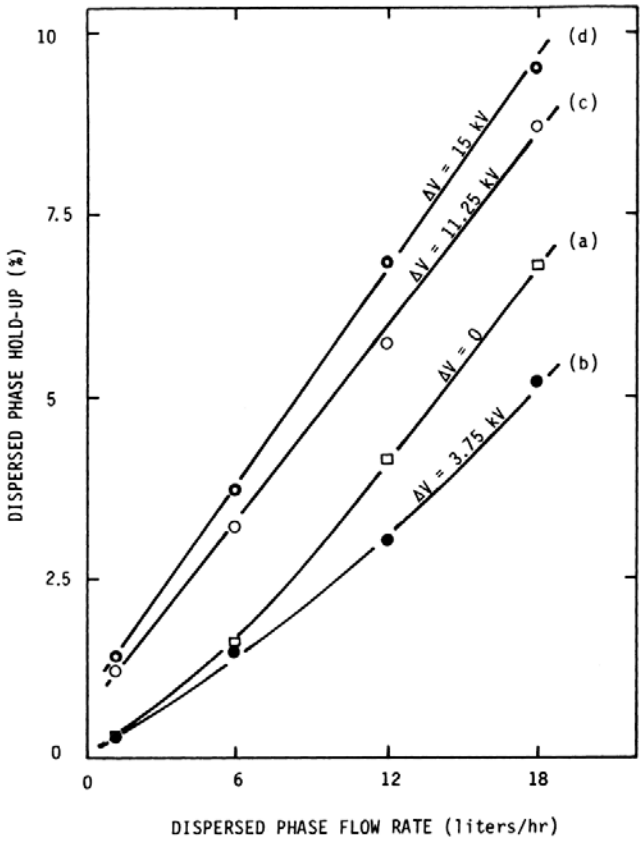


Figure 2-16. Effect of dispersed phase flow-rate on dispersed phase hold-up for a variety of electrostatic field strengths (Martin et al. 1983).

The dispersed phase hold-up values reported by these studies, however, are relatively small compared to that used in commercial-scale pulsed columns, which is a direct result of the low aqueous fluxes applied. Table 2-2 shows the aqueous flux used in electrostatic column studies to date and also those used in commercially used pulsed columns. It is apparent that the aqueous fluxes tested in electrostatic columns are significantly below those used in commercial-scale pulsed columns.

Table 2-2. Comparison of the aqueous fluxes in recent electrostatic column studies and industrial-scale pulsed columns.

| **Study** | **Column Type** | **Aqueous Flux** ($m^3/h/m^2$) |
|---|---|---|
| Martin et al. (1983) | Vertical-plate column | 3.77 |
| Suyama et al. (1993) | Vertical-plate column | 0.48 |
| Usami et al. (1993) | Vertical-plate column | 2.948 |
| Scott, et al. (1994) | Vertical-plate column | $9.15\times10^{-4}$ |
| Briggs et al. (2000) | Vertical-plate column | 2.41 |
| Lerner (2006) | Bateman pulsed column | 15-70 |
| Ritcey (2006) | Sieve-plate pulsed column (Ni-Co system) | 37 |
| Ritcey (2006) | Sieve-plate pulsed column (solids, gels) | 20 |

For an ESX column to receive commercial application, it is important that it can tolerate fluxes typical for industrial pulsed columns as larger reagent inventories and increased construction costs may offset other realisable advantages (Ritcey, pers. com. 2006). This suggests that, for an ESX application to reach industrial application, it must be able to tolerate fluxes similar to those applied in industrial columns and then tested against an already industrially proven contactor to ascertain industrial viability.

### 2.7.2 The Effect of the Applied Frequency of the Electrostatic Field

The frequency of the electrostatic field has been shown to have a significant effect on (1) droplet stability and dispersion and (2) droplet oscillation and zigzagging.

Scott (1987) investigated the effect of the applied voltage and applied frequency of an electrostatic field on droplet stability and dispersion. For selected frequencies between 20 and 120 Hz, the field strength was increased until the droplet ruptured, the results of which are shown in Figure 2-17. It is evident that initial increases in the applied frequency to 25 Hz resulted in a decrease in droplet stability, but further increases in the applied frequency to 45 Hz resulted in an increase in droplet stability. Above 45 Hz, however, further increases in the applied frequency resulted is a steady decrease in droplet stability. The peak in droplet stability observed at 45 Hz was attributed to the droplet vibrating sympathetically at its natural frequency.

In addition, this study also found that (1) as the droplet size increased, the peak in droplet stability shifted to lower applied frequencies and (2) that the applied frequency influenced the mode of droplet rupture. Accordingly, low frequencies result in the shattering of droplets into numerous smaller daughter droplets while high frequencies result in the rupturing of droplets into fewer relatively large droplets.

Other studies have also reported that the applied frequency affects droplet oscillation and zigzagging, which has been suggested to increase the rate of mass transfer owing to the continual replenishment of the droplet interface with fresh metal ions and extractant molecules (Heckley 2002; Collard 2011). Collard (2011) reported a significant increase in cobalt extraction – from 20% to 45% – by optimising the applied frequency.

Despite the little amount of research conducted on the effect of the applied frequency on droplet stability and metal extraction, it is evident that the applied frequency for optimal mass transfer will change between chemical systems and contactor type. Therefore the applied frequency needs to be optimised for any particular system and contactor.

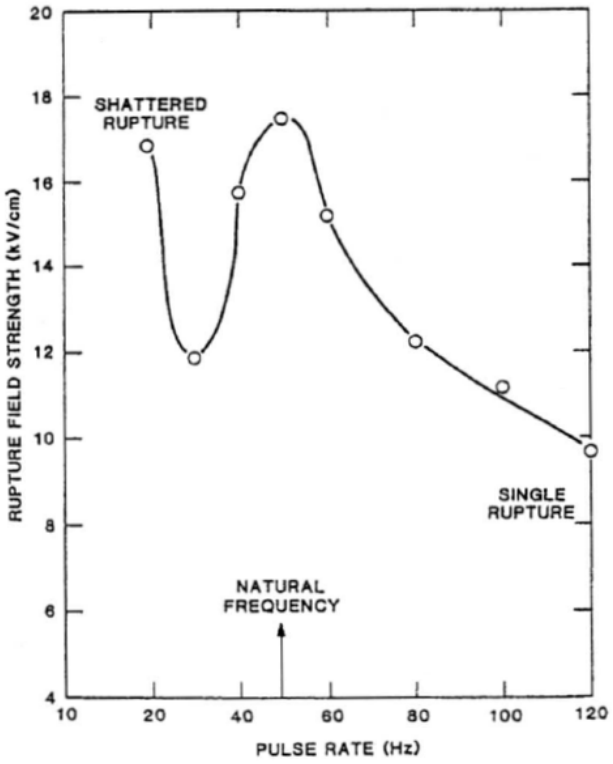


Figure 2-17. Field strength required to rupture water droplet of 1.78-mm diameter as a function of applied voltage (Scott 1987).

### 2.7.3 Electrode Insulation

Insulation of electrodes has only recently received attention, when dispersed phase hold-ups, which are sufficient for arcing to occur between electrodes, have been investigated. Arcing between electrodes must be minimised, if not eliminated, to maintain a high voltage difference between electrodes, and thereby, allow dispersion to occur.

A range of electrode insulation materials have been investigated in previous ESX studies. Martin et al. (1983) and Collard (2011) conducted investigations with spray-on Teflon® coated electrodes; Martin et al. (1983) did not report any arcing but Collard (2011) reported that arcing occurred with higher aqueous fluxes. The ESPLIM study of Gu (1985) used an electrode made of insulated copper wire wrapped around a plastic plate. Heckley (2002) attempted to replicate these results by constructing similar electrodes but found that the wire insulation was attacked by the solvent and that arcing between electrodes occurred. Scott et al. (1994) used graphite-impregnated fibreglass

electrodes and reported no arcing; this has not been verified owing presumably to the difficulty in manufacturing these novel electrodes.

Rigid plastics such as Halar® (Briggs et al. 2000) and Lexan® (Heckley 2002) have been successfully used for electrode insulation. Briggs et al. (2000) reported slightly higher applied voltages were required to achieve the same degree of metal extraction. Collard et al. (2005) and Steffens and Ibana (2005) used heat-shrink Teflon® tubing to insulate electrodes. They found that the insulation allowed high dispersed phase hold-ups without any arcing occurring.

From these reports it is apparent that an electrode within an ESX column must be (1) a good insulator, (2) capable of withstanding high voltages, (3) resistant to chemical attack and (4) have a long service life.

## 2.8 Power Consumption in ESX Contactors

Electrostatic dispersion and agitation has been shown to be extremely energy efficient in comparison to conventional mechanical methods. This was attributed to the fact that the electrostatic force acts almost exclusively on the aqueous-organic interface only to disperse and agitate the droplets rather than moving the bulk liquid that is required in mechanical agitation. (Scott 1989; Yamaguchi 1995).

Numerous investigations have reported power draws much lower than conventional contactors. Scott and co-workers compared the power requirement of an emulsion phase contactor (Scott and Sisson 1988) and a vertical plate ESX column (Scott et al. 1994) with a laboratory-scale baffled mechanical mixer. They reported power draws of 0.00238 and 0.0024 W/mL of dispersed aqueous phase for the emulsion phase contactor and vertical plate column, respectively, while the laboratory-scale mechanical mixer required about 25 W/mL to achieve a similar dispersion. This represents a power saving of around 99%.

As was also highlighted by Scott et al. (1994), the energy required for an ESX contactor is directly proportional to the electrical properties of the bulk aqueous/organic composite. This means that, as the dispersed (aqueous) phase hold-up increases, the

power draw increases. Given that industrial SX columns operate with significantly higher fluxes than those used in these studies, accurate measurement of power requirement of an ESX columns can only be achieved with a column that is operating with a dispersed phase hold up comparable to that of an industrial SX column.

Scott et al. (1994) also compared the power draw with and without aqueous flow for low and high strength electrostatic fields. The power draw when there was no aqueous flow was 2.5 W, whereas for flow with low and high strength electrostatic fields they were 2.5 W and 4.4 W, respectively. This demonstrates that a significant proportion of the power consumed is dissipated in the power delivery system, and an accurate comparison of power required by an ESX contactor and a conventional mechanical contactor can only be made when a more efficient and purpose-built industrial power supply is used.

## 2.9 Control of pH in ESX Columns

All electrostatic column studies involving metal transfer have used a salt of a weak acid to buffer the pH of the feed stream to maintain the required pH (Suyama et al. 1993; Scott et al. 1994; Briggs et al. 2000). The use of such reagents for industrial pH control is expensive; the industry uses ammonia or ammonium hydroxide.

Within an ESPLIM apparatus, the use of ammonia and ammonium hydroxide for in-situ solvent neutralisation, where solvent pre-neutralisation is impractical, has been successfully demonstrated (Collard et al. 2005; Steffens and Ibana 2005). However, the use of these reagents for solvent pre-neutralisation prior to entering an ESX column has not been attempted.

Jääskelainen and Paatero (1999) showed that pre-neutralising a solvent using ammonium hydroxide can increase the conductivity of the solvent. If the solvent is too conductive, droplet dispersion using an electrostatic field may be hindered or prevented (Usami et al. 1993). In this case, the solvent will need to be pre-equilibrated with ammonia gas. The feasibility of this approach is explored in the present study.

## 2.10 Summary

ESX contactors promises to alleviate the shortfalls of conventional solvent extraction contactors while at the same time offering distinct advantages including low shear agitation, higher mass transfer rates and significantly lower power consumption. Despite these possible advantages, an industrial ESX application has not been realised. This may be attributed first and foremost to the lack of an ESX contactor design that offers a comparable performance with that of a conventional contactor in terms of aqueous flux.

Another major shortcoming of the current understanding of ESX contactors is in regards to the effect of the physical properties of the solutions on the properties of droplet dispersion, and thus, mass transfer. The physical properties of the solutions in solvent extraction systems vary considerably and therefore it is important to consider their effects on droplet size distributions in designing an ESX contactor.

Among the ESX contactors proposed by previous investigators, the column appears to be the most suitable for industrial application in process metallurgy because (1) it seems the most likely design to allow industrially applicable fluxes, (2) it allows for the droplets to be vigorously agitated and thus provide high mass transfer rates, (3) it allows the formation of uniformly sized droplet dispersions in which the droplets are of an appropriate size, (4) it minimises short circuiting of droplets, and (5) it allows precise control of operating variables and thus, contactor performance. The main shortfall, however, of the column designs presented by previous investigators, is the difficulty of scale up.

In evaluating the performance of an ESX column, the most appropriate and optimal mode of pH control, the optimal electrostatic field strength and frequency, and also the maximum flux achievable first need to be established. Once established, the performance of the ESX column will be benchmarked against an industrially established contactor such as an SX pulsed column.

Chapter 3

# The Effect of Physical Solution Properties on Electrostatic Dispersion

## 3.1 Introduction

This chapter describes the attempt to determine the effects of the physical properties of the solution – namely the ionic strength and viscosity of the PLS, the interfacial tension as well as the viscosity and conductivity of the solvent – on the droplet size and their distribution generated by electrostatic dispersion. This knowledge is fundamental to the design of an ESX column that has wide commercial application and important to minimise subsequent modifications in column design.

Specifically, this chapter describes how a droplet dispersion cell was constructed, a droplet sizing procedure was developed, methods of independently changing the physical solution properties were investigated and the effect that the various physical solution properties have on droplet size distributions generated by electrostatic dispersion was established.

## 3.2 Materials and Methods

### 3.2.1 Reagents

The following reagents, which were all AR-grade unless specified otherwise, were used in this study: carboxyl methyl cellulose (LR, Sigma Aldrich), blue colouring (commercial, Queen), green colouring (commercial, Queen), Daelim 2400 (commercial, Jiangsu Yangzhou Chemical Co.), isotridecanol (commercial, Exxon Chemical), magnesium chloride dihydrate (UNIVAR), methyl cellulose (98%, Sigma Aldrich), octan-1-ol (Ajax), Octastat® 3000 (commercial, A.R. Harrison & Co.), potassium dichromate (LR, UNIVAR), propan-1-ol (Ajax), pentan-1-ol (Ajax), ShellSol® 2046 (commercial, Shell), sodium hydroxide (BDH), sodium hydroxide standard solution (Merck), sucrose (Ajax), sulphuric acid (98%, Ajax), sodium sulphate dihydrate (BDH),

sodium chloride (BDH) and Versatic 10 (commercial, Resolution). Seawater used was collected from the Esperance port and filtered using Whatman #1 filter paper.

The following reagents were used to construct and prepare the experimental apparatus: dichloromethylsilane (LR, Sigma Aldrich), Loctite® 349 adhesive (commercial, Loctite), and 1,1,1-trichloroethane (TR, Ajax).

### 3.2.2 Preparation of General Laboratory Reagents

A 0.10 M standard solution of potassium hydrogen phthalate (PHP) was prepared by weighing out approximately 20.423 g of PHP onto a watch-glass and placing in the oven at 110 °C overnight. The PHP was then placed in a dessicator and allowed to cool to room temperature. The PHP was then weighed again, transferred to a volumetric flask and the volume made up to 1 litre. To ensure the accuracy of this standard, 3 x 20 mL aliquots of 0.1 M PHP were titrated against a sodium hydroxide standard solution using phenolphthalein to indicate the endpoint.

A 0.1 M standard solution of sodium hydroxide was prepared by weighing out the appropriate amount of sodium hydroxide and transferring to a 1-L volumetric flask, with enough water added for total dissolution. The solution was allowed to cool overnight, after which the flask was filled to the mark. The solution was then standardised by titration against PHP.

Solutions of 1 M and 3 M sulphuric acid for pH adjustment were prepared by pouring the required amount of the concentrated solution into a 500-mL measuring cylinder, and then transferring to a 1-L volumetric flask that was partially filled with water. Upon cooling the flask was filled to the mark. Solutions of NaOH were prepared in a similar manner except that the required amount of sodium hydroxide pellets were weighed out and transferred into the flask. Chromic acid was prepared by transferring 15 g of potassium dichromate to a 1-L volumetric flask which was then filled to the mark with 9 M sulphuric acid.

A 2% solution of dichloromethylsilane in 1,1,1-trichloroethane was prepared by syringing 20 mL of dichloromethylsilane into a 1-L volumetric flask and filling the flask to the mark with 1,1,1-trichloroethane.

### 3.2.3 Analytical Procedures

All pH measurements made were with a bench-top pH meter (Orion, 3 Star) using a glass body–glass membrane electrode (Cole Parmer, 2112). Density measurements were made using a pycnometer (25-mL) and microbalance (Sartorius, GK 2200).

The viscosity of the PLS and solvent phases was measured using a Falling Ball viscometer (Gilmont, 3224-#1). The tube was filled with filtered test solution, and the stainless steel ball inserted to the top of the tube. The time taken for the ball to fall from the top line to the bottom line was recorded and the viscosity was then calculated using the relationship:

$$\text{Viscosity (cP)} = K \times (\rho_b - \rho_f) t$$

where K is a viscometer constant, $\rho_b$ is the density of the stainless steel ball, $\rho_f$ is the density of the fluid, and t is the time for the ball to fall from the top to the bottom line.

Dielectric constant measurements were made using a dielectric constant meter (Alpha TDR-5000, Zadow Electronics). The meter was calibrated for the appropriate range of dielectric constant after which the measurement probe was connected. The meter then measured the run time, i.e., the time required for a back voltage from the probe to reach the meter, which is directly proportional to the dielectric constant.

The conductivity of organic phases was measured using a pre-calibrated digital conductivity meter (model 1152, Emcee Electronics). The probe was connected to the meter, the probe inserted into the sample and the measurement recorded. The probe was then thoroughly washed with methanol and allowed to dry at room temperature before reuse. The conductivity of PLS phases was measured using a hand-held conductivity meter (Aqua-CP/A, TPS Instruments) with the appropriate k = 0.1 (122229, TPS), k = 1.0 (122216, TPS) or k=10 (122221, TPS) probe.

The interfacial tension (IFT) between PLS and solvent phases was measured using a surface tension meter (2041, Analite) with a 21-mm diameter platinum-iridium Du Nuoy ring (Custom, Scienglass UK). The tension reading was converted to interfacial tension using the correlation of presented by Huh and Mason (1975). A spreadsheet to correct surface to interfacial tension was made and then validated by testing the static interfacial

tension of the DI water/toluene, DI water/hexane, DI water/phenol and DI water/octane systems and comparing to literature values. Initial testing resulted in poor results: reworking the ring to remove sharp burrs and give a regular circular shape drastically improved the results.

Prior to using the Du Nuoy ring, the ring was bathed in chromic acid, washed with distilled water, briefly flamed and then stored in distilled water. This was carried out between each measurement to ensure that no residual organic was present on the ring and also to ensure that the ring surface was maintained hydrophilic.

An 8-cm diameter 5-cm tall petri dish was placed on the measurement platform of the tension meter and partly filled to a depth of 2 cm with the PLS phase. The Du Nouy ring was then taken from the storage container, gently dried and hung on the arm of the lifting arm of the tension meter. The ring was then carefully lowered so that it was approximately 3 mm above the PLS phase surface and the balanced was zeroed. The ring was then immersed into the PLS phase, and the solvent was delicately poured on top of the PLS phase to ensure minimal surface disturbance and prevent the formation of stable droplets at the interface. Sufficient solvent was transferred to ensure minimal disturbance of the air-solvent interface during testing. The ring was raised to the interface, and then raised incrementally with the tension measurements being recorded at each interval. The maximum force recorded was taken as the interfacial tension.

### 3.2.4 Experimental Setup

A diagram of the experimental setup is shown in Figure 3.1. It incorporates a PLS feed reservoir, from which the PLS phase gravity feeds through a polyvinyl chloride (PVC) delivery tube to the dispersion cell. Adjusting a manual valve allowed control of the PLS flow through the delivery tube and feed needle. The droplets were released immediately above two Teflon® coated electrodes located at the top of the dispersion cell; each was connected to the high voltage power supply. The dispersed droplets settle through the solvent in the cell into the settler, from which the PLS was periodically withdrawn to maintain a constant fluid level within the cell.

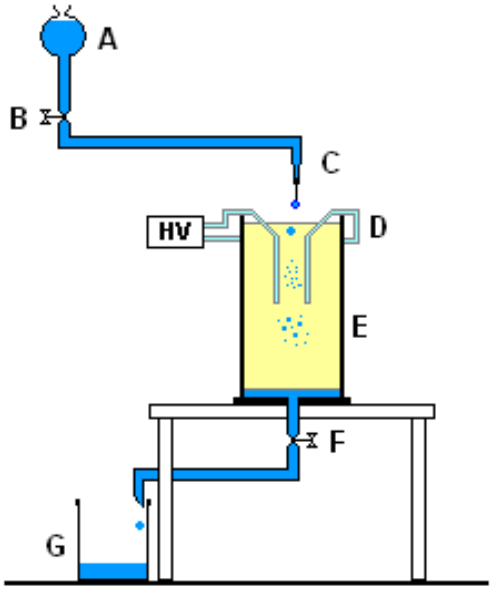


Figure 3-1. Diagram of the experimental set-up for observing droplet dispersion. (A – feed reservoir, B – feed valve, C – feed needle, D – dispersion electrodes, E – dispersion cell, F – discharge valve, G – discharge receptacle)

The PLS feed delivery needle was a 20-gauge hypodermic needle with a blunt tip (K3342-20, Becton Dickinson). The cell was constructed entirely of glass with internal dimensions 50 x 50 x 150-mm and a 12-mm diameter barbed fitting with tap inserted into the column base. The left and right side walls were 10-mm thick glass, each 50 x 200 mm in size, and the front and rear were 3-mm thick glass, each 70 x 200 mm in size. The base was made of 10-mm thick glass and was 150 x 150 mm in size. The glass sections were bonded together with Loctite® 349 adhesive.

Each of the dispersion electrodes was stainless steel plate coated with Teflon®. Each plate was 1 x 45 x 85 mm in size; a 45° bend was made 25-mm from the top of each electrode to allow a region of low field strength to allow droplets to form at the needle tip. A variable voltage–variable frequency power supply (California Instruments, 801-RP) was connected to these electrodes using high-voltage cable such that the two electrodes were of opposite electric potential.

### 3.2.5 Dispersion Test Procedures

The PLS and solvent phases prepared for each test were transferred to a separatory funnel and shaken for 2 minutes at room temperature. Unless stated otherwise the phases were allowed to disengage and then sit for a further 24 hours such that negligible mass transfer occurred during dispersion tests. Upon separating the phases, the feed reservoir was filled with PLS, the cell was filled with the solvent and the remainder of the PLS and solvent was set aside for testing to determine the physical properties. The feed needle was put in place 2 cm above the electrodes and the feed line flushed to remove any air bubbles. The electrodes were connected to the power supply and the desired voltage and frequency was selected. The camera was turned on, and the feed valve opened to allow an individual droplet to slowly form and detach from the needle tip. Once the droplet entered the region of high field strength, the droplets were allowed to fully disperse for 3 seconds, after which the applied field was quickly turned off to minimise droplet zigzagging and allow a clear picture of the dispersion to be taken. This process was repeated numerous times to ensure that a dispersion representative of the conditions being tested was recorded.

### 3.2.6 Measurement of Droplet Sizes

The sizes of the dispersed droplets were measured by analysing photographs taken with a 5.0 mega-pixel digital camera (Espio 5100, Pentax). A diagram of the experimental set-up is shown in Figure 3-2. The digital camera was mounted on an elevating stand, exactly 15 cm from the front of the test column and a size scale was mounted in front of the dispersion cell for droplet size measurement. Lights were located adjacent to and in front of the column, to illuminate the cell, droplets and the back screen. Numerous photographs of each experiment were taken, typically about 15 photographs, from which the clearest photograph with a representative of dispersion was selected for droplet size analysis.

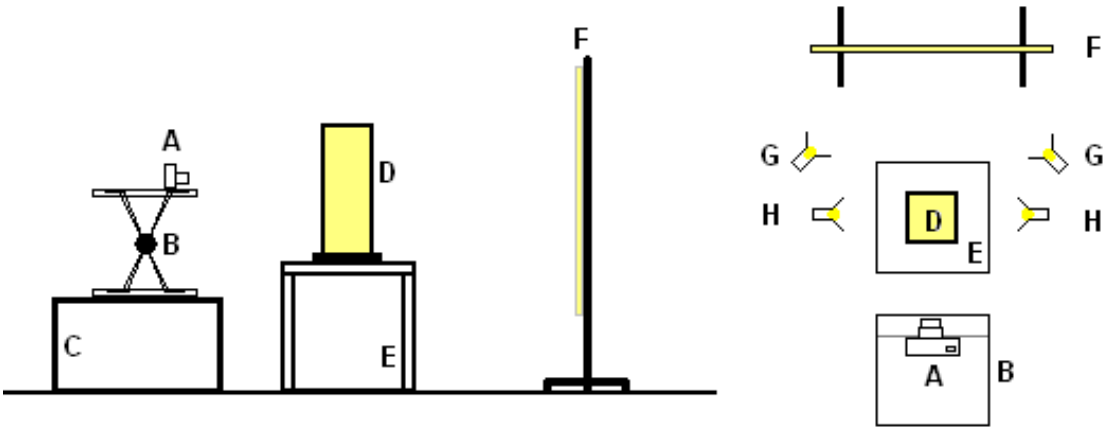


Figure 3-2. Diagram of droplet photography set-up. (A – digital camera, B – elevating stand, C – mounting block, D – test column, E – column stand, F – back screen, G – front directional lights, H – side directional lights)

Preliminary tests established that the camera settings which allowed clear and sharp pictures were a focal length of 0.15 m and a shutter speed on 1/250$^{th}$ of one second. Slight distortion of the droplets occurred as they zigzagged under the influence of the electrostatic field; momentarily switching off the electrostatic field during photographing eliminated this distortion.

After selection of the most suitable photograph for droplet size analysis, the raster image (i.e. jpeg) was converted to a vector image (i.e. .dxf or .cad) using a raster-vector image conversion program (VExtractor 2.95). This entailed manually circling the droplets and defining of the size scale. The vector image was then transferred to a CAD application (Surpac Vison V5.0) where the droplet sizes and droplet size distribution was calculated using a macro program. Typically, 600-800 droplets were sized in each photograph that was analysed. A detailed description of the droplet sizing procedure is in Appendix A1.

Some of the dispersed droplets were observed to be sticking to the walls of the column, which hindered acquiring representative droplet size data from the photographs. This was attributed to the slight surface charge on the cell wall attracting and retaining the droplets. To alleviate this problem, the glass column was thoroughly cleaned with methanol and bathed with a 2% solution of dichloromethane in 1,1,1-trichloroethane, as was described by Eow and Ghadiri (2002). This rendered the glass highly hydrophobic

and droplets that were attracted to the charged surface slid downward toward the settler; in some cases inducing turbulence within the solvent in the cell with a Pasteur pipette was required to prompt droplet movement.

The error in droplet size measurements was determined by measuring the aperture size of a range of sections of test sieve mesh. Sections of sieve mesh 2 x 4 cm in size were cut and suspended in the dispersion cell, and a photograph of the section was taken. Approximately 100 of the apertures in the photograph of the sieve mesh section were manually defined and the sizes calculated as described in Appendix A1. The measured errors for aperture sizes tested are shown Table 3-1. These error measurements were then applied to the droplets within a droplet size distribution and the overall error in average droplet size was calculated.

Table 3-1. Error in droplet size measurements.

| Aperture Size (um) | Maximum error in size measurement (%) | Droplet size range to which error is applied (µm) |
|---|---|---|
| 100 | 11.00 | 0 - 156 |
| 212 | 8.02 | 157 - 318 |
| 425 | 6.35 | 319 - 512 |
| 600 | 6.17 | 513 - 725 |
| 850 | 5.29 | 726 - 1025 |
| 1200 | 4.75 | 1026 - 1450 |
| 1700 | 4.12 | 1451 - 2050 |
| 2400 | 3.58 | 2051 - max |

## 3.3 Preliminary Experiments

### 3.3.1 Preliminary Investigation to Establish Test Conditions

The applied voltage of the electrostatic field used for all dispersion tests was 5.33 kV/cm (8 kV / 1.5 cm) as reported optimal previously (Steffens and Ibana 2005; Collard 2011). The applied frequencies of the electrostatic field investigated were 20, 35 and 50 Hz,

which covers the range of applied frequencies reported to be optimal previously (Scott 1987; Collard 2011). All procedures carried out in this work were at a temperature of 23 ± 1 °C.

Unless stated otherwise the PLS phase used in this section of the study was seawater with 5% blue colouring added to increase the visibility of dispersed droplets. Green colouring, as reported by Scott and Wham (1989), was not used because the yellow dye in the colouring was found to precipitate out in solutions of high ionic strength. The pH of all PLS phases was adjusted to pH 3 using sulphuric acid.

### 3.3.2 Modification of Ionic Strength

The ionic strength of the PLS was modified by addition of differing amounts of sodium chloride and sodium sulphate salts to distilled water containing 5% blue colouring and the solution pH was adjusted to pH 3. The sulphate to chloride ratio was maintained at 0.21 which was typical of the Bulong Nickel Operation PLS.

Solutions with ionic strengths of 0.00 M, 0.69 M, 2.06 M, 3.43 M and 4.80 M were prepared and 500 mL of each solution was individually equilibrated with 500 mL of solvent (15% Versatic 10 in ShellSol® 2046). Increases in the conductivity and viscosity of the PLS were measured with increases in the ionic strength.

### 3.3.3 Modification of PLS Viscosity

Carboxyl methyl cellulose (CMC) and sucrose have both previously been used to modify solution viscosity (Bircumshaw and Riddiford 1951; Hunt von Herbing and Keating 2003) and therefore their use in PLS as a viscosity modifier was assessed. Initial testing showed that CMC did not fully dissolve with globules remaining suspended in solution which, after equilibration with solvent, resulted in a droplet dispersion that was highly variable between tests using the same solution with respect to the dispersed droplet size. Such inconsistencies were not encountered when sucrose was used to modify the viscosity and therefore sucrose was used for PLS viscosity modification. An associated decrease in conductivity of the PLS was measured as the sucrose concentration was increased.

PLS solutions with viscosities ranging from 1.33 to 3.27 cP were prepared by weighing out appropriate amounts of sucrose and transferring to 500-mL volumetric flasks after which the flasks were filled partly with seawater that contained 5% colouring. The flasks were then placed on a hotplate at 40 °C overnight and agitated to allow the sugar to dissolve. The pH was adjusted to pH 3 and the flask was filled to the mark. Each solution prepared was then individually equilibrated with a 500 mL sample of solvent.

### 3.3.4 Modification of Solvent Viscosity

Solvent solutions ranging in viscosity from 2.45 cP to 8.01 cP were prepared by adding various amounts of a commercially used polyethylene-based viscosity index improver, Daelim 2400, to the 15% Versatic 10 in ShellSol® 2046 solvent phase. The required amount of Daelim 2400 was weighed out, transferred to a 1-L volumetric flask and the flask then partially filled with solvent and gently agitated overnight while on a hotplate at 40 °C. Upon cooling the flask was filled with solvent and the solvent then equilibrated with 500 mL of PLS.

### 3.3.5 Modification of Interfacial Tension

The following alcohols were investigated for modifying the interfacial tension (IFT): (1) pentanol, (2) octanol and (3) isotridecanol. These were selected over other reagents because their dielectric constant is low relative to other surface active reagents such as carboxylic acids and surfactants and also because they are not heavily surface active and therefore their loss from solution will be small in comparison to surfactants. After a detailed test work to assess these alcohols as IFT modifiers, octanol was selected as the most appropriate for this work as it provided adequate IFT modification with moderate alcohol dosages and negligible changes in dielectric constant.

PLS and solvent systems with varying interfacial tension were prepared by transferring 500 mL of solvent, 400 mL of seawater containing 5% colouring and the pre-determined amount of octanol to a 1-L volumetric flask, and then allowing the system to equilibrate. Associated changes in the conductivity, viscosity and dielectric constant of both solvent and PLS phases were measured and found to be negligible.

### 3.3.6 Modification of Solvent Conductivity

The solvent conductivity was modified by addition of a commercially-used solvent conductivity enhancer, Octastat® 3000. The addition of small amounts of Octastat® resulted in significant increases in the solvent conductivity; associated were significant decreases in interfacial tension which may be attributed to the high proportion sulphonic acid in the Octastat® reagent (Octel Company 2003). The solvent solutions were prepared by partially filling a 1-L volumetric flask with solvent, transferring the pre-calculated amount of Octastat® to the flask and gently mixing, after which the flask was filled to the mark with solvent.

It was found that pre-equilibrating the solvent bearing Octastat® with the PLS consisting of seawater with 5% colouring, resulted in the colouring extracting from the PLS to the solvent within 2 hours. The phases were therefore only gently agitated in a separatory funnel for 1 minute and then separated prior to the dispersion tests and testing of the solution properties.

## 3.4 Results and Discussion

### 3.4.1 Effect of Ionic Strength on Electrostatic Dispersion

The ionic strengths of common PLS feed solutions to hydrometallurgical solvent extraction circuits vary considerably and are largely dependent on the chemical systems used for leaching, the ore mineralogy and the quality of the process water. To determine the effects of the ionic strength of solutions on the droplet sizes and their distribution, dispersion tests were undertaken with synthetic PLS solutions of various ionic strengths. The results, summarised in Figure 3-3, show that a considerable change in the ionic strength had only a small effect on the average droplet size. Nonetheless, it is evident that there was an initial increase in average droplet size with an increase in ionic strength from 0, which was for deionised water, to 2 M, but further increases to 4.8 M resulted in a slight decrease in the average droplet size.

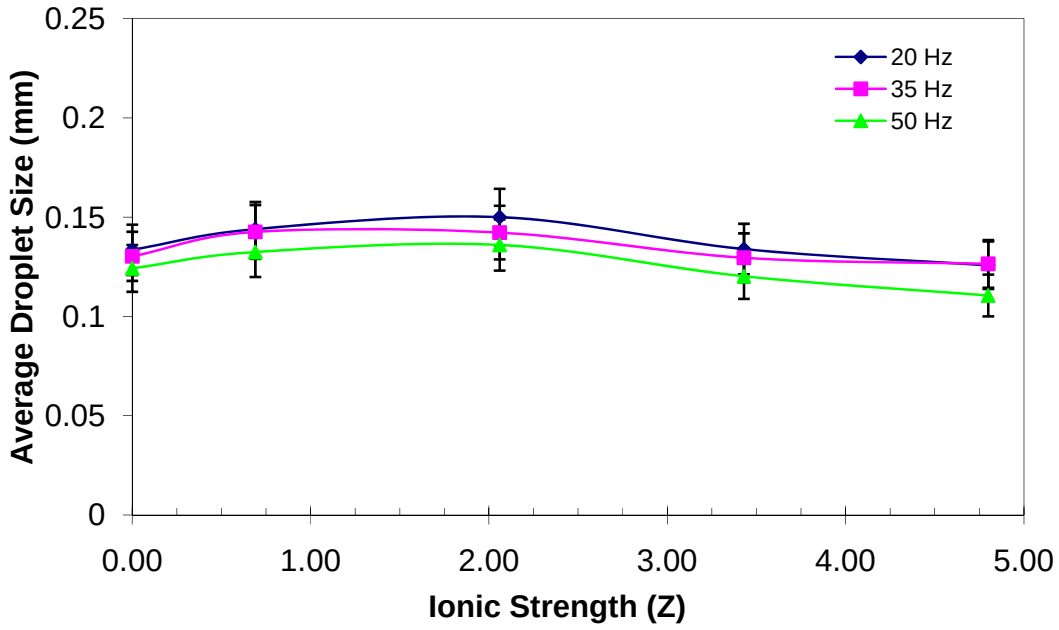


Figure 3-3. Effect of ionic strength on dispersed droplet size distribution for applied field frequencies of 20, 35 and 50 Hz and field strengths of 5.3 kV/cm.

The initial increase in average droplet size was owing to a slight increase in size of the larger droplets (>100 μm) and a decrease in the number of fine droplets being produced. On the other hand, the subsequent decrease in average droplet size is owing to an increase in the number of fine droplets formed with no appreciable change in the size of the larger droplets. It appeared that these differences were due to the particular dispersion mechanism that is predominantly operating under each of the conditions. That is, at high ionic strengths, the predominant dispersion mechanism appeared to be necking, which results in the formation of ultra-fine satellite droplets from the necking sites. This is illustrated in Figure 3-4.

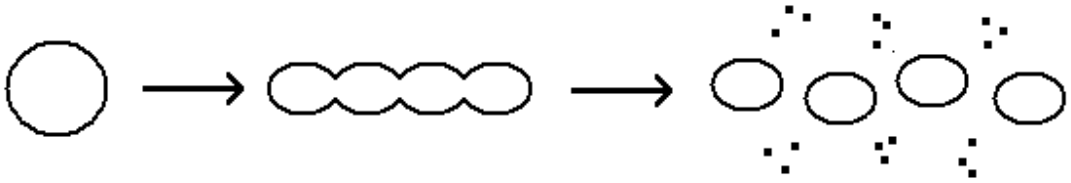

Figure 3-4. Formation of ultra-fine droplets during droplet breakage by the necking breakage mechanism.

In turn, this phenomenon appeared to be due to the increase in viscosity of the feed with substantial increases in the ionic strength. It makes sense that as the PLS becomes more viscous, it becomes more resistant to droplet deformation such that the regions of the droplet undergoing thinning have insufficient fluidity to report to one of the larger daughter droplets. To ascertain that it is in fact the increase in viscosity, not the increase in ionic strength of the PLS that is affecting the increase in the number of satellite droplets, the PLS viscosity will need to be increased independently of the ionic strength. This is discussed in Section 3.4.2.

There is a general trend that, under comparable conditions, increases in the frequency of the electrostatic field resulted in slight decreases in droplet sizes. The present investigator has no explanation for this.

### 3.4.2 Effect of PLS Viscosity on Electrostatic Dispersion

To explore the effect of the viscosity of PLS on droplet dispersion, dispersion tests were carried out under comparable conditions but different viscosities of the PLS, which were achieved by the addition of various amounts of sucrose. The results are summarised in Figure 3-5.

The trend is similar to that of the effect of the ionic strength but much more clearly evident. In particular, the size of the larger droplets (> 100 µm) slightly increased and the number of ultra-fine droplets formed was substantially higher at higher viscosities, indicating that it is indeed the increase in viscosity that favours necking as the dispersion mechanism to operate. It therefore seems appropriate to conclude that the increases in the size of larger droplets and increased formation of ultra-fine droplets is owing to increases in viscosity of the PLS rather than increases in ionic strength of the PLS.

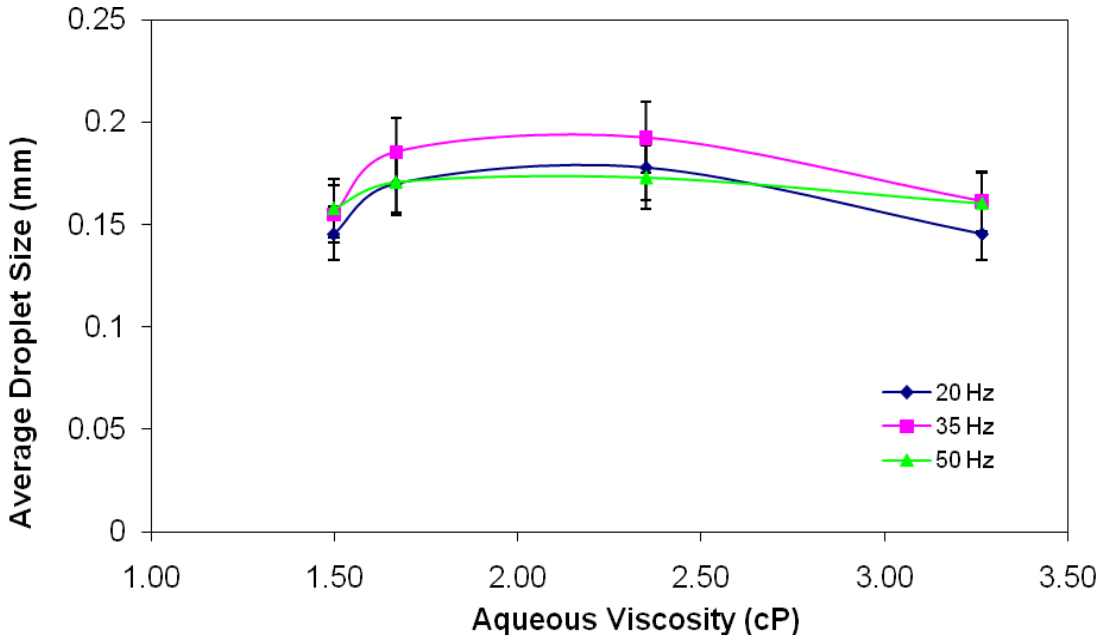


Figure 3-5. Effect of PLS viscosity on dispersed droplet size distribution for applied field frequencies of 20, 35 and 50 Hz and field strengths of 5.3 kV/cm.

These results may shed light on the observations in an earlier study by Collard et al. (2005). They reported a decrease in metal extraction as the ionic strength of solution increased but provided no explanation for it. They reported also a noticeable increase in the formation of much larger droplets. Possibly what they failed to realise is that increases in the ionic strength of the solutions resulted also in increases in the viscosity, resulting in the formation of much larger droplets as well as ultrafine droplets. It is logical that the formation of both much larger droplets and an array of ultrafine droplets leads to poor extraction efficiency. The difference in results achieved at the various electrostatic field frequencies tested is unclear to the present investigator.

These results have significant implications in the design of an ESX column. If a viscous PLS, such as for example a PLS of high ionic strength, is to be treated, then over time a myriad of ultra-fine satellite droplets will form. These can potentially be entrained in the solvent and consequently decrease process efficiency. Thus, an ESX column design

should provide a mechanism for minimising the formation of such ultra-fine satellite droplets or allow for their removal from the solvent in a timely manner.

### 3.4.3 Effect of Solvent Viscosity on Electrostatic Dispersion

The solvent viscosity within an SX circuit varies between plants but it is generally minimised by diluting the viscous extractant with a diluent to reduce phase entrainment. In this section, the effect of the solvent viscosity on dispersed droplet size was investigated by adding various amounts of Daelim 2400, a polyethylene-based viscosity index improver to the solvent consisting of 15% Versatic 10 in ShellSol® 2046. In addition, the effect of the frequency on the solvent viscocity was determined by carrying out the same experiments under comparable conditions but at different frequencies. The results are summarised in Figure 3-6.

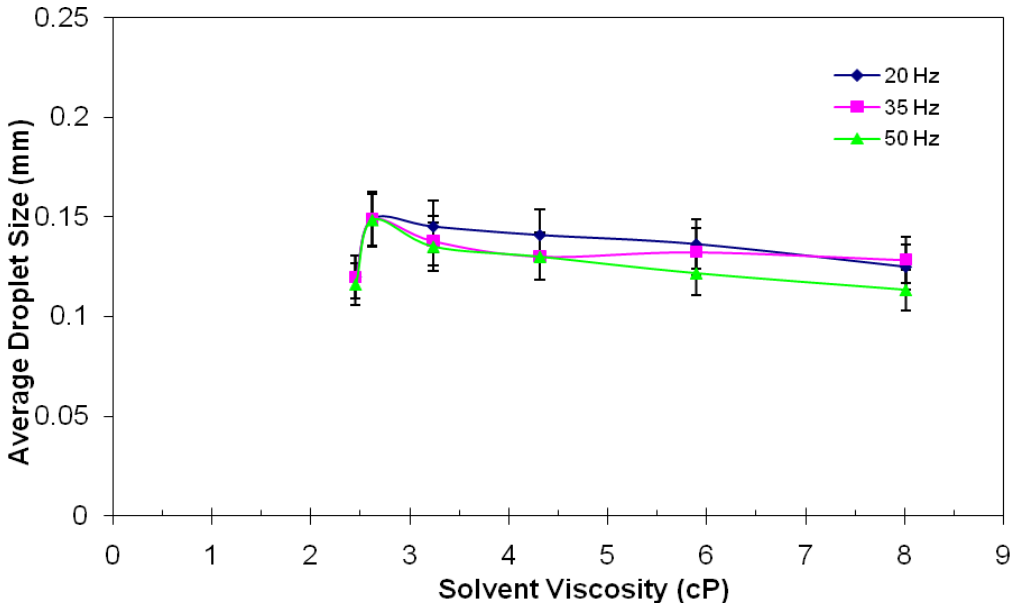


Figure 3-6. Effect of solvent viscosity on the droplet size distribution for applied field frequencies of 20, 35 and 50 Hz and field strengths of 5.3 kV/cm.

It is evident that for each of the frequencies investigated, an increase in the solvent viscosity from 2.42 to 2.62 cP led to an increase in the average droplet size from 0.12 to 0.16 mm, but further increases in the viscosity up to 8.02 cP resulted in decreases in the average droplet size except for the tests carried out at a frequency of 35 Hz, which had a rather unique pattern.

A closer look at the droplet size distribution revealed that the variation in the average droplet size was owing to increases in the number of ultra-fine droplets that were being formed accompanied by small increases in the sizes of the larger droplets that were being formed. This dispersion pattern appeared to be due to a shift in the predominant droplet dispersion mechanism from necking to jetting as the viscosity of the solvent was increased. It makes sense that increasing solvent viscosity leads to increasing hydrodynamic resistance to droplet deformation and thus, favouring the jetting mechanism of droplet dispersion. That is, the formation of conical tips at the ends of the droplet, from which ultra-fine droplets are ejected, is a droplet's pathway of lower hydrodynamic resistance to reduce its size and stabilise.

The formation of ultra-fine droplets over a large range of solvent viscosities highlights the need to incorporate in the design of an industrial ESX column a facility to minimise the formation of ultra-fine droplets or a facility to coalesce ultra-fine droplets. For example, using a lower electrostatic field strength could be one way of minimising the formation of ultrafine droplets when using a relatively viscous solvent.

### 3.4.4 Effect of Interfacial Tension on Electrostatic Dispersion

To determine the effect of interfacial tension (IFT) on droplet size distribution, various amounts of octanol were added to the solvent phase and then allowed to equilibrate with the PLS phase. The octanol concentration was increased from 0 to 9.1 vol.%, resulting in a decrease in IFT from 18.9 to 15.2 mN/m. The effect of IFT on the average droplet size of droplets larger than 100 µm is shown in Figure 3-7. It is evident that decreases in interfacial tension resulted in decreases in the average diameter of the droplets that were larger than 100 µm. This was true for all frequencies tested.

This is consistent with the results of a previous study (Heckley 2002) where the same trend was observed as the interfacial tension was decreased by the addition of salts of short-chain carboxylic acids. Further, this result may explain the reported difference in dispersion observed in the extraction and stripping compartments within an ESPLIM cell (Steffens and Ibana 2005).

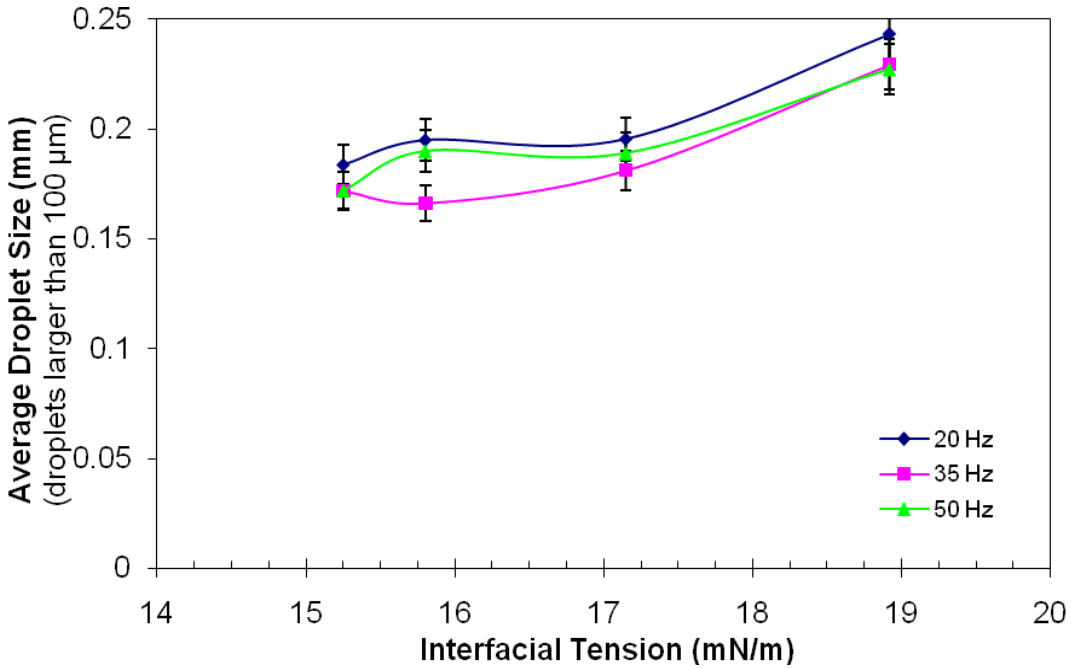


Figure 3-7. Effect of interfacial tension on dispersed droplet size distribution for droplets larger than 100 µm, applied field frequencies of 20, 35 and 50 Hz and field strengths of 5.3 kV/cm.

On closer examination, it was found that, as the interfacial tension decreased, and the average size of droplets larger than 100 µm also decreased, the overall average droplet size remained relatively constant, indicating that more ultra-fine droplets were formed when the interfacial tension was high. Attempts to take detailed photographs of the process of droplet dispersion, which could provide a good insight into how exactly and where the ultra-fine droplets were forming, were unsuccessful owing to a lack of affordable imaging technology at the time of this study. Nonetheless, this result reinforces the importance of a facility for coalescing ultra-fine droplets in an industrial ESX column.

### 3.4.5 Effect of Solvent Conductivity on Electrostatic Dispersion

To determine the effect of solvent conductivity on droplet dispersion, a commercially available conductivity enhancer, Octastat® 3000, was blended with the solvent phase. Increases in the Octastat® concentration from 0 mg/L to 4.6 mg/L resulted in increases in the conductivity of the solvent phase from 28 pS/m to 508 pS/m. The effect of this

additive on the viscosity of the solvent was negligible but associated decreases in the interfacial tension were significant. The effect of solvent conductivity on the droplet size, which is summarised in Figure 3-8, shows that when the solvent conductivity reaches 80 pS/m, droplet dispersion ceases completely despite the large decrease in interfacial tension. The same trend was observed for all frequencies tested.

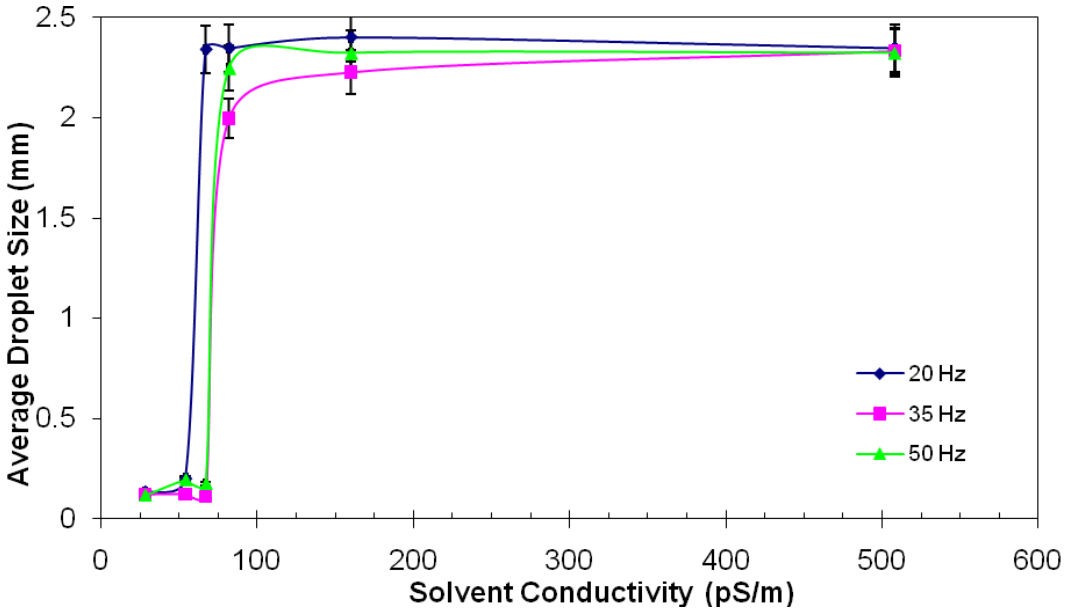


Figure 3-8. Effect of solvent conductivity on dispersed droplet size distribution for applied field frequencies of 20, 35 and 50 Hz and field strengths of 5.3 kV/cm.

Given that the applied voltage remained stable throughout all of the experiments, and that the dielectric constant of the PLS and solvent phases did not vary significantly between tests, these results show that the predominant mode of droplet polarisation in electrostatic dispersion, under conditions that are commonly encountered in ESX applications, is interfacial polarisation. This finding indicates a potential limitation of ESX in regard to pH control. That is, the use of solvent pre-neutralisation with reagents such as ammonium hydroxide that result in high solvent conductivities (Jaaskelainen and Paatero 1999) may inhibit droplet dispersion. Thus, it is desirable that other modes of pH control be explored.

## 3.5 Summary

This chapter investigated the effects of the physical properties of the solutions on electrostically generated droplet dispersions at conditions that are commonly encountered in solvent extraction. It includes the design and construction of a test cell that allowed detailed observation of droplet dispersion, the development of experimental procedures and methods for systematic variation of the desired physical properties of the solutions with as minimal effect on other variables as possible. It was found that:

- Increases in the viscosity of the PLS favours droplet breakage by the necking mechanism, but if the viscosity is sufficiently high, results in the formation of a myriad of ultra-fine droplets from necking sites on the droplet. Initial increases in the PLS viscosity from approximately 1.5 to 2.0 cP resulted in an increase in average dispersed droplet diameter from approximately 0.15 to 0.18 mm, with further increases in PLS viscosity from approximately 2.0 cP to 3.2 cP resulting in a decrease in average dispersed droplet diameter from 0.18 to 0.16 mm.
- The viscosity of the solvent affects the droplet size distribution largely by influencing the predominant mechanism of droplet dispersion. That is, initial increases in the viscosity of the solvent from 2.42 to 2.62 cP resulted in a marked increase in the average droplet size from 0.12 to 0.15 mm owing to the necking dispersion mechanism becoming more favourable, with further increases in solvent viscosity to 8.02 cP resulting in a continual and steady decrease in the average droplet size owing to the droplets breaking predominantly by the jetting dispersion mechanism.
- Increases in the interfacial tension from 15.2 to 18.9 mN/m resulted in increases in the average size of the larger (>100 μm) droplets from 0.17 to 0.23 mm accompanied by increases in the number of the ultra-fine droplets (<100 μm) and thus, a negligible effect on the overall average of the droplet size.
- The conductivity of the solvent has a significant effect on droplet dispersion. Increases in the conductivity of the solvent from 28 to 80 pS/m resulted in increases in the average droplet size and, eventually, cessation of droplet

dispersion, indicating that interfacial polarisation is the predominant mode of droplet polarisation.

Collectively, these results have significant implications on the design of an ESX column suitable for industrial application in process metallurgy. Firstly, an ESX column must either minimise the formation of ultra-fine droplets or have a facility for the coalescence of ultra-fine droplets. Secondly, the mode of pH control employed in an ESX column should minimise increases in the conductivity of the solvent.

Admittedly, the method of determining the sizes of the dispersed droplet used in the present study was tedious and not very precise. Further work using a high-speed camera would allow a more detailed and rigorous investigation into the modes of droplet dispersion under various conditions and a comprehensive droplet dispersion size analysis using a laser sizer would, by collecting significantly larger data sets, be particularly useful.

Chapter 4

# Development of an Electrostatically Assisted Solvent Extraction Column

## 4.1 Introduction

Several attempts to develop an electrostatically assisted solvent extraction (ESX) column have been reported but none has so far progressed to industrial application. This may be attributed to (1) the electrode designs being unsuitable for scale-up, (2) the inability to achieve sufficient aqueous fluxes, (3) the inability to coalesce ultra-fine droplets that inevitably form and (4) poor control of the operating variables allowed. This chapter describes the present investigator's efforts to develop an ESX column that is not limited by the aforementioned shortfalls and thereby suitable for industrial application.

As the first step of these efforts, the droplet dispersion, droplet agitation and droplet coalescence aspects of the design were established, and the findings from each aspect were then used to conceive the design of an ESX column that promises to be industrially applicable.

## 4.2 Materials and Methods

### 4.2.1 Reagents

The following reagents were used in this section of the work: blue colouring (commercial, Queen), dichloromethylsilane (99%) (LR, Sigma Aldrich), Loctite® 349 adhesive (Commercial, Henkel), magnesium chloride dihydrate (AR, UNIVAR), magnesium sulphate heptahydrate (Commercial, Faulding), nickel sulphate hexahydrate (AR, Ajax), ShellSol® 2046 (Commercial, Shell), sodium hydroxide (AR, Selby Biolab), sodium sulphate dihydrate (AR, BDH), sodium chloride (AR, BDH), sulphuric acid (98%, UNIVAR), 1,1,1-trichloroethane (TR, Ajax), Versatic 10 (Commercial, Resolution).

### 4.2.2 Preparation of Test Solutions

The synthetic pregnant liquor stream (PLS) was prepared by dissolving the required amounts of calcium, magnesium, nickel and sodium salts in a volumetric flask with distilled water to make a solution that simulated the Bulong Nickel Operation's (BNO) NiSX pregnant liquor stream (Table 4-1). Upon complete dissolution, blue colouring was added to make a 5% (v/v) colouring solution to increase the visibility of finely dispersed droplets, and the flask almost completely filled to the mark. The solution pH was then adjusted to pH 3, to prevent mass transfer during the experimental procedure, after which the flask filled to the mark. The resulting pH was between 2.95 and 3.05.

Table 4-1. Chemical composition of synthetic Bulong PLS prepared for this work.

| Species | $Ni^{2+}$ | $Mg^{2+}$ | $Na^{+}$ | $Cl^{-}$ | $SO_4^{2-}$ |
|---|---|---|---|---|---|
| Conc. (g/L) | 3 | 15 | 80 | 80 | 45 |

The solvent phase (15% (v/v) Versatic 10) was prepared by transferring the required amount of Versatic 10 into a volumetric flask, and filling to the mark with ShellSol® 2046 diluent. For all experiments, the PLS and the solvent were intimately contacted prior to experimental work to prevent any mass transfer effects.

A 2% (v/v) dichloromethylsilane solution was prepared by syringing 10 mL of dichloromethlysilane into a partially filled 500-mL volumetric flask, which was subsequently filled to the mark with 1,1,1-trichloroethane.

### 4.2.3 Power Supplies for Generation of Electrostatic Fields

To generate an AC-type high-voltage electrostatic field, a variable voltage – variable frequency power supply was used (801-RP, California Instruments). This power supply was capable of generating a 15 kV signal over a frequency range of 16 – 500 Hz. The instrument was connected to the electrodes with high voltage electrical leads.

To generate a DC-type high-voltage electrostatic field, a high voltage power supply similar to that used by Heckley (2002) was connected to a bridge rectifier to rectify the

AC signal to a DC signal, as described by Lee et al. (2001). The diodes used to construct the bridge rectifier were rated for high voltage and low current, with a maximum voltage of 8 kV (CS4308U050, High Voltage Power Systems Inc.). On each rectifier segment, three diodes were connected in series to allow a signal of up to 24 kV to be rectified.

To generate a pulsed-DC high-voltage electrostatic field, three high-voltage diodes were connected in series to the leads of the high voltage power supply.

### 4.2.4 Test Cells

Three test cells were used during the course of this work: (1) a small laboratory-scale dispersion cell, (2) a large laboratory-scale dispersion cell, and (3) a laboratory-scale counter-current column. Schematic diagrams of each are shown in Appendix B-1.

The small laboratory-scale dispersion cell was constructed of Perspex™ and had internal dimensions of 19 x 29 x 1500 mm (L x W x H). The left and right sides were 10-mm thick 29 x 150 mm sections and the front and back were made of 3-mm thick 38 x 150 mm sections. The base of the cell was made of 10-mm thick 50 x 50 mm section. An 8-mm diameter hole was drilled in the centre of the base, and a barbed Teflon® hose fitting was inserted. In the centre of each of the 10-mm thick side sheets, 7.5 x 23 x 100 mm cavities were milled to allow flat plate electrodes to be fitted outside the column. In addition, into the edges of these sheets, 13 mm from the top, 3-mm diameter holes were drilled to allow insertion of rod electrodes. All sections of this column were bonded using methylene chloride as the solvent to allow adhesion of sections.

The large laboratory-scale dispersion cell was constructed of glass and had internal dimensions of 50 x 50 x 200 mm. The cell sides were 10-mm thick 50 x 200 mm sections and the cell front and back were 3-mm thick 70 x 200 mm sections. The base was 10 x 150 x 150 mm in size and a 15-mm diameter hole was cut in the centre for a barbed Teflon® hose fitting to be inserted. The sections were assembled using Loctite® 349 adhesive.

The laboratory-scale counter-current column was constructed of glass and had internal dimensions 50 x 50 x 300 mm. The cell sides were 10-mm thick 50 x 300 mm sections and the cell front and back were 3-mm thick 70 x 300 mm sections. The base was 10 x

150 x 150 mm in size and a 15-mm diameter hole was cut in the centre for a barbed Teflon® hose fitting to be inserted. The organic outlet port was located on the side of the column, 30 mm from the top, and the organic inlet port was located on the opposite side of the column, 30 mm from the bottom. Both ports were made of 7.7-mm diameter glass tubing. The inlet port extended 45 mm into the column, and 3-mm diameter holes drilled along the sides of the port distributed solvent flow evenly about the column. All sections of this column were bonded using Loctite® 349 adhesive.

### 4.2.5 Electrode Configurations

Numerous electrode configurations were investigated in this work and a full description of each is provided in Appendices B2 – B4. The electrodes constructed and used in this work for dispersion with a DC-generated electrostatic fields were: (1) needle-point electrode, (2) Perspex™-coated rod electrode, (3) heat shrink Teflon® coated rod electrode, (4) copper ring electrode, (5) mesh electrode, (6) glass plate electrode and (7) glass cone electrode. The electrodes constructed and used in this work and used for dispersion with AC-generated electrostatic fields were: (1) glass plate dispersion (AC) electrode and (2) Teflon®-coated plate dispersion (AC) electrode. The electrodes constructed and used in this work for droplet agitation were (1) Teflon®-coated plate agitation electrode, (2) Teflon®-coated rod agitation electrode and (3) Tefzel®-coated rod agitation electrode.

### 4.2.6 Electrostatic Droplet Dispersion Test Procedure

The droplet dispersion test procedure followed for this work is similar to that described in Section 3.2.5. First, the PLS delivery needle (K3342-20, Becton Dickinson) was connected and the PLS flow rate adjusted to the required value by adjusting a pinch valve on the feed line. An on-off valve on the same feed line was then closed while the remainder of the apparatus was prepared. The PLS discharge line at the bottom of the dispersion cell was closed, the required electrode arrangement was inserted and connected to the power supply, and the cell was filled with solvent. The PLS was then allowed to flow into the cell for approximately 5 minutes, after which the volume of PLS entering the cell was recorded, and the an accurate PLS flow rate calculated; the

PLS delivery valve was then adjusted to provide the desired flow and the procedure repeated. Upon attaining the desired flow rate, droplet dispersion was observed and also photographed. The fluid level within the cell was controlled manually by periodically draining the PLS settler in the cell. Droplet size distributions of the dispersed droplets were generated following the procedure described in Appendix A1.

### 4.2.7 Electrostatic Droplet Agitation Test Procedure

First the PLS delivery flow rate was set to that required by adjusting a pinch valve in the PLS feed line. The cell was then filled with solvent, the agitation electrode inserted, and the needle-point dispersion electrode was inserted. The dispersion electrode was connected to a DC power supply with a potential of 1 kV and the agitation electrodes were connected to the variable voltage–variable frequency power supply and appropriate electrostatic field settings selected. The power supplies for the disperser and agitation electrodes were then turned on, after which the on-off valve in the PLS line was opened. Droplet agitation was measured by photographing agitating droplets with the camera shutter speed being 1/15 of one second, and then measuring the length of the droplet cycle path. This is illustrated in Figure 4-1.

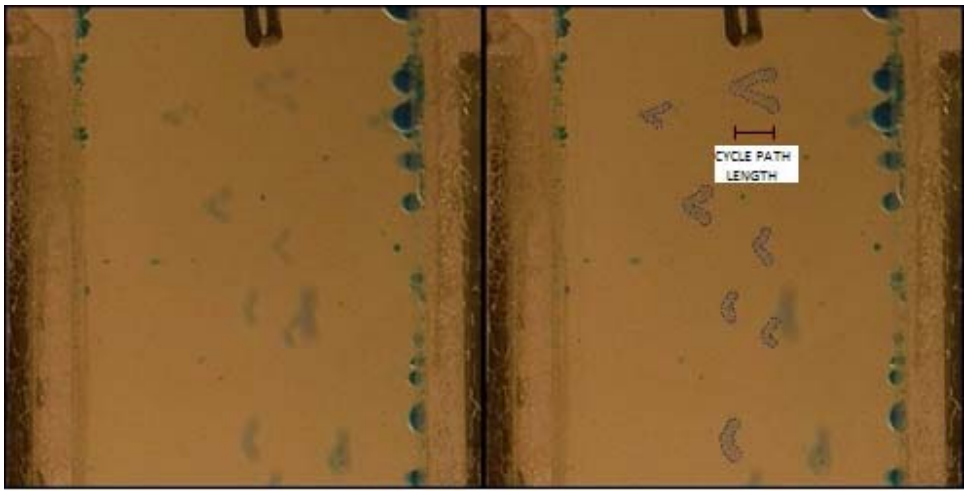


Figure 4-1. Photograph showing a single cycle of droplet zigzagging. (Zigzagging droplets are and cycle path length are outlined on the right hand side image)

### 4.2.8 Electrostatic Droplet Coalescence Test Procedure

The droplet coalescence was measured in the counter-current glass column by passing a 1% (v/v) PLS-in-solvent emulsion through the column and analysing the solvent overflow for PLS content over a range of electrostatic field conditions. The emulsion flow rate was calibrated to 1 L/hr, the electrode inserted into the column, after which the emulsion delivery pump and power supply for the electrostatic field were turned on. After 4 hours of operation, the PLS content of the solvent overflow was measured by collecting approximately a 100-mL solvent sample from the overflow port, weighing, and passing through phase-separation paper. The solvent collected was then weighed, and the fraction of PLS in the solvent overflow calculated. The procedure was performed in triplicate.

## 4.3 Exploratory Tests

Exploratory tests, aimed at alleviating unforseen problems, were undertaken prior to the planned experimental work. These tests found: (1) that the visibility of ultra-fine droplets needed to be enhanced, (2) the limitations of the electrostatic field conditions, (3) that electrostatic dispersers affected PLS flow into the cell, and (4) that droplets had a tendency to stick to the walls of the cell.

Tests showed that numerous ultra-fine droplets, which were difficult to see without magnification, were forming during dispersion. Blue food colouring was added to the PLS, as described in Section 3.3.1, which resulted in the ultra-fine droplets being readily visible and evident on photographs.

Testing of the electrostatic field strength showed that field strengths of up to 15 kV/cm, with a frequency of 50 Hz, could easily be achieved without damaging components of the test cell or the high-voltage power supplies. Testing of the electrostatic field frequency however, revealed that operating at high electrostatic field frequencies – that is above 250 Hz – resulted in arcing between the electrode connections. This was attributed to ionisation of the air at higher frequencies (Raju 2003, 133) and to prevent further arcing between the electrode connections the electrostatic field frequencies tested

were maintained below 100 Hz to allow a reasonable safety buffer. In addition, operating the power supply at high voltage-low frequency conditions (10 kV and 16 Hz), over an extended period (1.5 hours) resulted in the overheating of the power supply presumably owing to the increased strain on the transformer of the power supply (Heathcote 1998, 531). Subsequently, to reduce the risk of damaging the power supply, the use of high voltage-low frequency conditions was limited to short periods (~10-15 minutes).

These exploratory tests also indicated that at very low PLS flows, typically below 10 ml/hr, an electrostatic disperser influenced the flow of PLS into the cell; a similar observation was reported previously by Tsouris et al. (1998). To account for this additional suction, the exact PLS flow rate was calculated by running the dispersion test for a period of time – typically 5 minutes – and measuring the amount of PLS that had been allowed to flow from the feed reservoir.

Dispersed aqueous droplets were found to adhere to the sides of the cell, which hindered the taking of clear photographs of the dispersion within the cell. Washing the glass cells with a 2% solution of dichloromethylsilane, or inserting glass slides into the cells that had been washed with this solution, made the surface highly hydrophobic and reduced the number of droplets adhering to the sides. On some occasions, inducing turbulence to the solvent that was contained within the cell was required to dislodge droplets from the sides.

## 4.4 Electrostatic Dispersion

This study on electrostatic dispersion was split into three main categories: dispersion using a DC-generated field, a pulsed DC-generated field, and dispersion using an AC-generated field. The main aim of this part of the work was to identify the most appropriate type of applied field and disperser design.

### 4.4.1 Electrostatic Dispersion with DC Electrostatic Fields

To investigate electrostatic dispersion using a DC-generated electrostatic field, numerous electrode arrangements were constructed and tested, and their performance

considered on the basis of droplet uniformity and commercial applicability. Diagrams of the electrode arrangements investigated for dispersion with a DC-generated electrostatic field are shown in Figure 4-2.

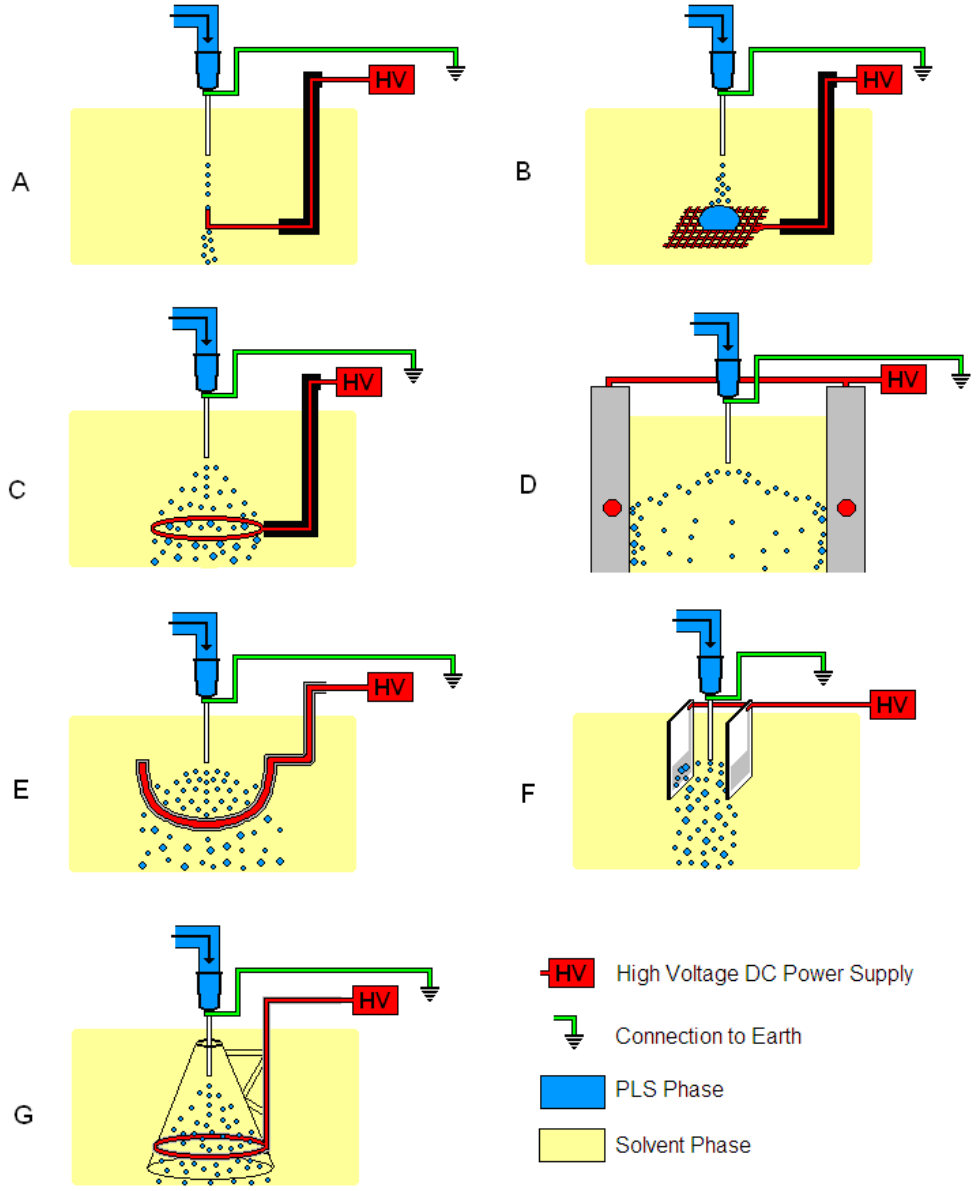


Figure 4-2. Diagrams of the various DC-field disperser arrangements. (A – needle-point electrode, B – mesh electrode, C – metal ring electrode, D – Perspex™ coated electrode, E – heat-shrink Teflon® coated electrode, F – glass plate electrodes, G – glass cone electrode).

The first arrangement to be tested was the needle-point electrode (Figure 4-2a). The set-up consisted of a stainless steel delivery needle, which was earthed, and 10 mm immediately below the needle was a stainless steel point that was connected to a high-voltage source. As the aqueous droplet was formed at the nib of the delivery needle, it was attracted toward the charged stainless steel point, causing it to detach from the delivery needle, and accelerate toward the charged point. The droplet then contacted the point, acquiring charge and then detaching to continue falling through the solvent phase.

It was found that this arrangement generated a dispersion in which the droplets were visibly uniformly sized but only when the PLS flow rate was below about 4 mL/hr. Higher PLS flow rates resulted in the droplets forming a bridge between the needle and the charged rod and consequently causing arcing. When the point electrode was moved further away from the needle, such that the needle and point were 30 mm apart, no significant increase in the maximum PLS flow rate was achieved. Given the low feed rate achievable, this disperser arrangement was deemed unsuitable for industrial application, where high feed rates are required.

In an attempt to alleviate the bridging of droplets, the point electrode was replaced with a mesh electrode (Figure 4-2b). The idea was that the mesh electrode provided a larger area than the point electrode for the PLS droplets to be attracted to, which may allow higher PLS flow rates without arcing. The results, however, revealed that small dispersed droplets would contact the mesh and, instead of falling through the mesh, would stick on it. Continual accumulation of droplets on the mesh resulted in one large droplet forming which would then bridge with the feed needle and consequently result in arcing.

The next electrode arrangement investigated was a metal ring electrode (Figure 4-2c). This disperser performed well at applied voltages between 1 and 12 kV/cm and flow rates between up to 34 mL/hr, with the resulting dispersion being uniformly sized. Exceeding these voltages and flow rates resulted in arcing between the needle and the ring. In addition, when higher flow rates were used, droplets were observed to attach to the ring and eventually coalesce to form larger droplets, which then detached and fell through the organic phase. Comparison of the maximum PLS flux achieved with the ring

electrode (0.15 $m^3/m^2/h$) to that used commercially in SX contactors (37 $m^3/h/m^2$) clearly show that the fluxes achievable with non-insulated electrodes are insufficient for a commercial application.

As the dispersion cell was made of Perspex™, which is a reasonably good insulator, parallel holes were drilled on either side of the cell and rod electrodes inserted; a diagram of this arrangement is shown in Figure 4-2d. When the voltage was first applied, the droplets forming at the tip of the needle were rapidly detaching and moving toward the electrodes, with the droplets being visibly uniformly sized. However, approximately 10 seconds after the electrostatic field was applied, the dispersion ceased completely. Subsequent increases in the voltage again affected dispersion, but again, after approximately 10 seconds the dispersion ceased. This was observed for all further increases in the applied voltage. Following this, a Teflon®-coated electrode was constructed and also tested; a diagram of this electrode arrangement is shown in Figure 4-2e. Similar to the performance of the Perspex™-coated electrodes, droplet dispersion again with the Teflon®-coated electrode occurred only momentarily for several seconds after which dispersion ceased.

Further investigation into this phenomenon indicated that the diminishment of the electrostatic field with Perspex™-and Teflon®-coated electrodes was owing to the insulation throttling off the electrostatic field, which is somewhat similar to that described previously by Jonassen (2002,132). That is, as the charge flowed from the DC power supply to the electrode, a potential difference developed across the thickness of the insulation. Subsequently, oppositely charged species within the dispersion cell were attracted to the electrode and then accumulated at the outside of the insulated electrode. This allowed for an electrostatic field between the metal electrode and the outer surface of the insulation but not between the two electrodes. Therefore, a non-conductor material cannot be used as electrode insulation when a DC field is used for dispersion.

Thus, the next step of this part of the work was to investigate the use of a semiconductor material (glass) as electrode insulation. This new arrangement is shown in Figure 4-2f. This electrode allowed continual droplet dispersion without any arcing occurring over a wide range of flow rates. The problem, however, was that a fraction of the droplets

adhered to the electrodes owing to electrostatic attraction. As more droplets adhered to the electrodes, they coalesced into larger droplets and then detached and fell through the solvent. In an attempt to alleviate this occurrence, the electrodes were coated with dichloromethylsilane to allow droplets to slide off the electrodes before coalescing but this made little difference.

In a further attempt to alleviate the adhesion of droplets on to the electrode, a glass cone electrode (Figure 4-2g) was investigated. The increased angle of the glass surface was to promote droplet detachment before the droplets became too large. Dispersion tests with this electrode arrangement revealed that PLS flow rates of up to 400 mL/hr were allowed and no significant accumulation of droplets on the electrode occurred. This electrode was thus found to be most promising among the DC dispersers and was further evaluated. The results are discussed in Section 4.4.4.

### 4.4.2 Electrostatic Dispersion with Pulsed DC Electrostatic Fields

Attempts to effect droplet dispersion using a pulsed DC-generated field were made under a variety of electrostatic field conditions and electrode arrangements. The voltage offset of the electrostatic field was varied between 1 and 8 kV, and the amplitude of oscillation was varied between 1 and 5 kV for all electrode arrangements evaluated. Using the ring disperser, droplet dispersion was achieved but arcing also occurred, which could not be circumvented. The use of both the Perspex™ coated and PTFE coated electrodes was found not suitable as continual dispersion could not be achieved. The glass cone disperser allowed droplet dispersion without any arcing but there was no observable benefit in using a pulsed DC-generated field over using a DC-generated field. The use of pulsed-DC fields was therefore not investigated further.

### 4.4.3 Electrostatic Dispersion with AC Electrostatic Fields

Given that electrode insulation is essential to achieve PLS fluxes required for commercial application, and also the success of the glass plate electrode for droplet dispersion with a DC field, the glass plate electrode seems an appropriate electrode with which to begin this section of the investigation. A larger version of the glass plate

electrode was constructed for these tests and a detailed description is provided in Appendix B3.

The glass plate electrode with an AC-generated electrostatic field applied allowed significantly higher fluxes and also continual dispersion. Droplets, however, were still observed to stick to sections of the glass owing to electrostatic attraction, and accumulation of the droplets resulted in their coalescence to form larger droplets before detaching from the electrode. To minimise such accumulation of droplets onto the electrode surfaces, the surfaces were silanated by washing the electrode with a solution of dichloromethlysilane to make the surface highly hydrophobic. This coating marginally reduced the retention of droplets on the electrode and thus, droplet coalescence, but not to an extent that was deemed sufficient to justify the use of glass insulation for an industrial application.

An electrode that was coated with hydrophobic Teflon® was subsequently constructed, a detailed description of which is provided in Appendix B3. Upon conducting dispersion tests, it was found that dispersion achieved with this Teflon®-coated electrode was comparable to that achieved with the glass plate electrodes and no arcing occurred at very high PLS fluxes. Also, coalescence of droplets on the electrodes was comparable to that observed with the previously tested glass-coated electrodes.

After longer testing times, however, i.e. after approximately 15 minutes of continual dispersion, a significant number of ultra-fine droplets were observed to be accumulating in the dispersion region. These ultra-fine droplets are deemed highly undesirable because they are likely to become entrained in the solvent stream that flows counter-currently to the PLS stream in an industrial column application.

Close observation of these ultra-fine droplets revealed that they did not oscillate or zigzag in the uniform field while other larger droplets rapidly oscillated and zigzagged. However, in the end regions of the electrodes, where the electrostatic field was non-uniform these small droplets were observed to migrate to an electrode and then coalesce with other droplets to form large droplets that subsequently fell. This observation suggests that a non-uniform field may be required, either in the dispersion region or in a solvent settler of a column design, to coalesce and remove such ultra-fine droplets.

### 4.4.4 Synopsis of Electrode Arrangements used for Electrostatic Dispersion

Of the dispersers tested, the most promising arrangements were the glass cone disperser which used a DC-generated electrostatic field for dispersion, and the Teflon®-coated plate electrode which used an AC field for dispersion. The glass cone disperser was tested over a range of PLS flow rates and electrostatic field strengths, and the Teflon® coated plate electrode was tested at a PLS flow rate of 400 L/hr and over a range of electrostatic field strengths at electrostatic field frequencies ranging from 20 to 80 Hz. The dispersion droplet size data for these configurations are shown in Figures 4-3 and 4-4 respectively.

From the dispersion data of the glass cone disperser shown in Figure 4-3, it appears that at higher PLS flow rates droplet dispersion is effected at lower applied voltages than when lower PLS flow rates are used. However, observation of drop breakage at these higher flow rates reveals that breakage at high PLS flow rates is owing to turbulence induced by injection of the PLS into the cell. Therefore, the electrostatic disperser itself was actually only capable of dispersing PLS at a flow rate of approximately 150 mL/hr, which equates to a flux of about 0.81 $m^3/hr/m^2$. In comparison, the Teflon®-coated AC plate disperser readily resulted in dispersion of the PLS at a flow rate of 400 mL/hr for all applied electrostatic field frequencies tested, which equates to around 1.8 $m^3/hr/m^2$; this disperser was capable of tolerating significantly higher flow rates.

In regard to droplet uniformity, the DC disperser allowed apparently more uniformly sized droplet dispersions to be generated than the AC disperser. The advantages of increased droplet uniformity however, are deemed to be outweighed by the large cross-sectional area of column required for a suitable flux. In addition, an independent coalescer can be placed above an AC disperser electrode to minimise PLS entrainment in the solid, or the dispersion electrode could be perforated to create a non-uniform electrostatic field and thereby promote, within the dispersion region, the coalescence of ultra-fine droplets. Therefore, using a Teflon®-coated electrode with an AC-generated electrostatic field is deemed most viable for an industrially applicable ESX column.

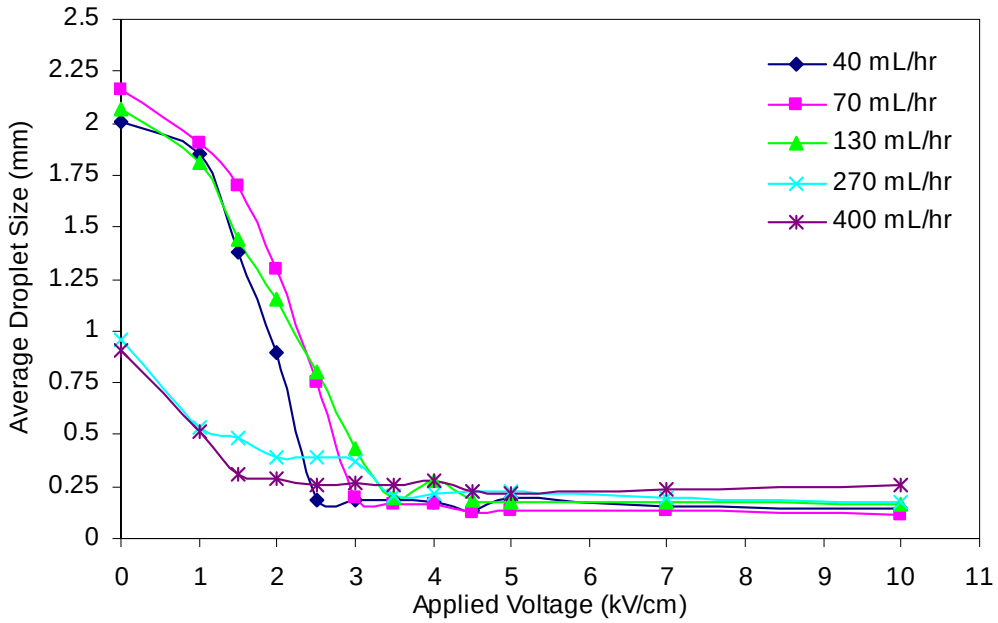


Figure 4-3. Dispersion data for the glass cone disperser with a DC-generated dispersion.

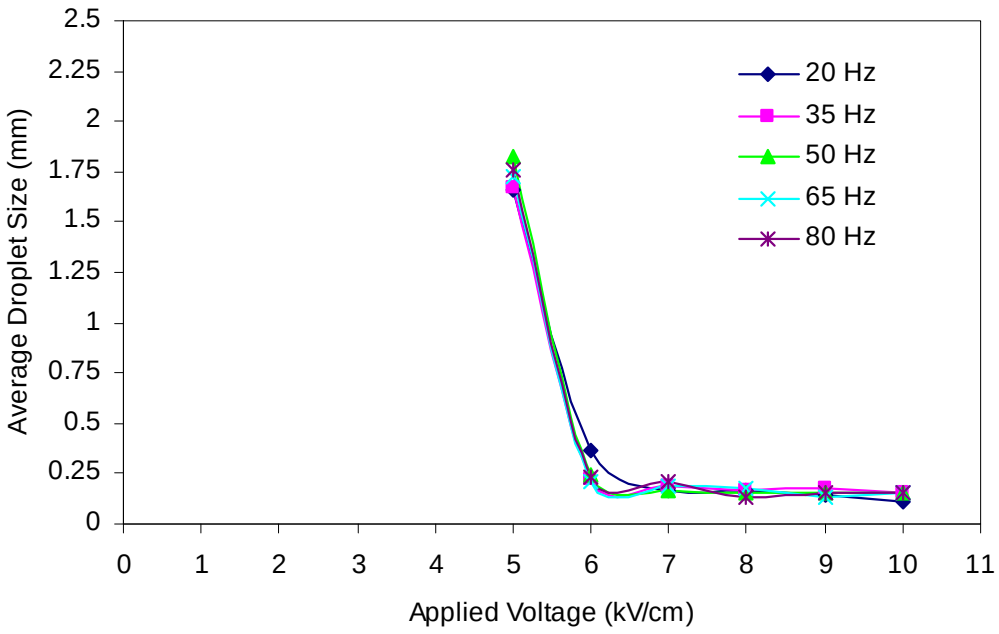


Figure 4-4. Dispersion data for Teflon® coated plate electrode with an AC-generated dispersion and PLS flow rate of 400 mL/hr.

## 4.5 Electrostatic Agitation

### 4.5.1 Nature of the Electrostatic Field

Only two ESX studies have used DC- or pulsed DC- generated electrostatic fields to effect droplet agitation (Thornton 1968; Scott 1994) and the agitation is deemed relatively mild in comparison to the agitation imparted by using an AC generated electrostatic field. That is, when a DC- or pulsed DC- generated electrostatic field is applied, agitation is due only to the turbulent wake resulting from the movement of a droplet through the continuous phase. Conversely, an AC generated electrostatic field provides intimate droplet mixing by oscillation of the droplets and zigzagging of the droplets through the organic medium (Yamaguchi et al. 1988; Yamaguchi 1995). Therefore, only the use of AC-generated electrostatic fields are investigated in this droplet agitation study.

### 4.5.2 Electrostatic Agitation with AC Generated Fields

Given the success of the Teflon®-coated plate electrodes for droplet dispersion with AC-generated fields, a larger version of this electrode was constructed and used for this section of the investigation. The dimensions and construction of this electrode is described in Appendix B4.

Observation of initial droplet agitation tests seemed to indicate that the amount of charge being carried by the droplet caused it to oscillate and zigzag when passing through the electrostatic field. When droplets fed into the cell contacted the top of an electrode before falling through the region of high field strength, they were more likely to oscillate and zigzag than when the droplet did not contact the top of an electrode. It was postulated that the droplets acquire a small amount of charge from the surface of the electrode, and the droplets that were then charged continually aligned themselves with the electrostatic field, causing oscillation and zigzagging. To ascertain this postulation, further experiments were conducted where the droplets were explicitly charged.

To explicitly charge droplets before they entered a region with an AC-generated electrostatic field, the needle-point disperser, as was used in Section 4.4.1, was located immediately above the agitation electrode and droplets fed through the delivery needle.

To the point electrode a DC voltage of 1 kV was applied to generate charged droplets and when uncharged droplets were required an earth lead was connected. To the agitation electrode a voltage of 4 kV/cm and frequency of 20 Hz was applied to agitate the droplets. The effect of droplet charge on droplet agitation is shown in Figure 4-5, where it is evident that charged droplets zigzag and agitate considerably more vigorously than uncharged droplets. This result highlights that droplet charging is crucial to the design of an efficient ESX contactor.

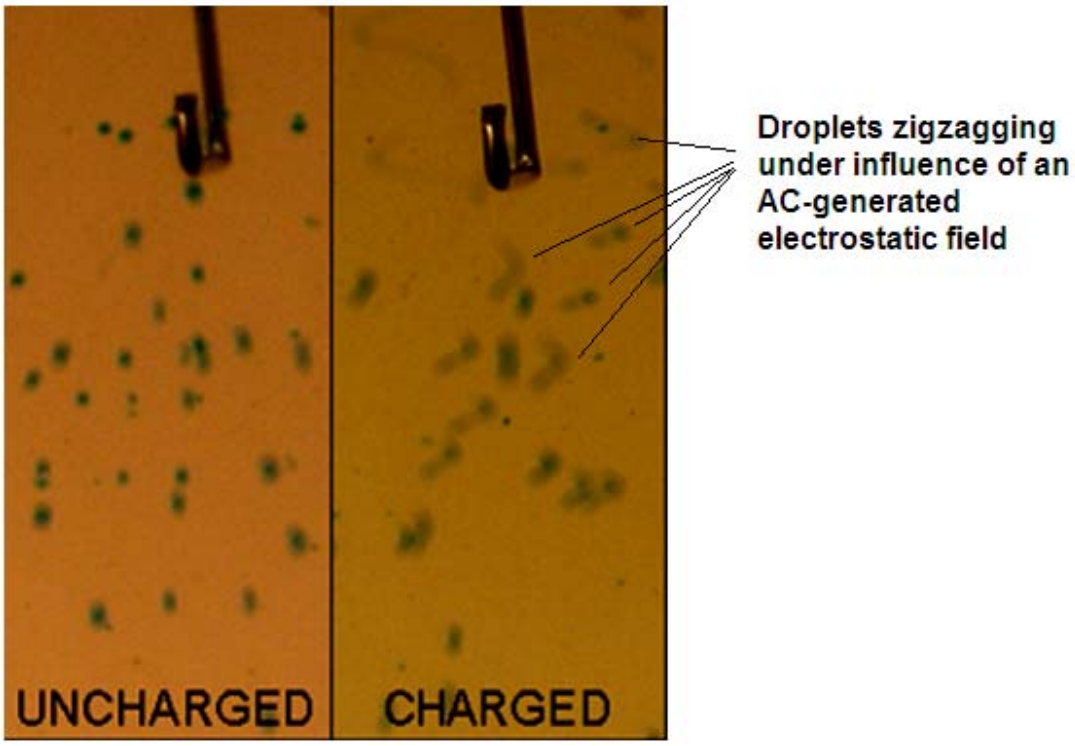


Figure 4-5. Effect of droplet charge on droplet agitation.

Note the droplet zigzagging in the photograph on the right hand side.

With droplet agitation is clearly evident in AC-generated electrostatic fields, the effect of the electrostatic field strength and the electrostatic field frequency on droplet agitation remains to be quantified. Such data are highly valuable for the design of an ESX column to allow appropriate electrostatic field conditions to be determined and column performance better understood.

To understand how the strength and frequency of the electrostatic field affect droplet agitation, droplet agitation was observed over a range of field strengths (2, 3.5 and 5 kV/cm) and field frequencies (20, 35 and 50 Hz). To eliminate variations in droplet size and droplet charge, the needle-point disperser was used to ensure that all droplets produced were between 1.10 and 1.20 mm in diameter. The effect of the electrostatic field frequency on lateral droplet motion is shown in Figure 4-6.

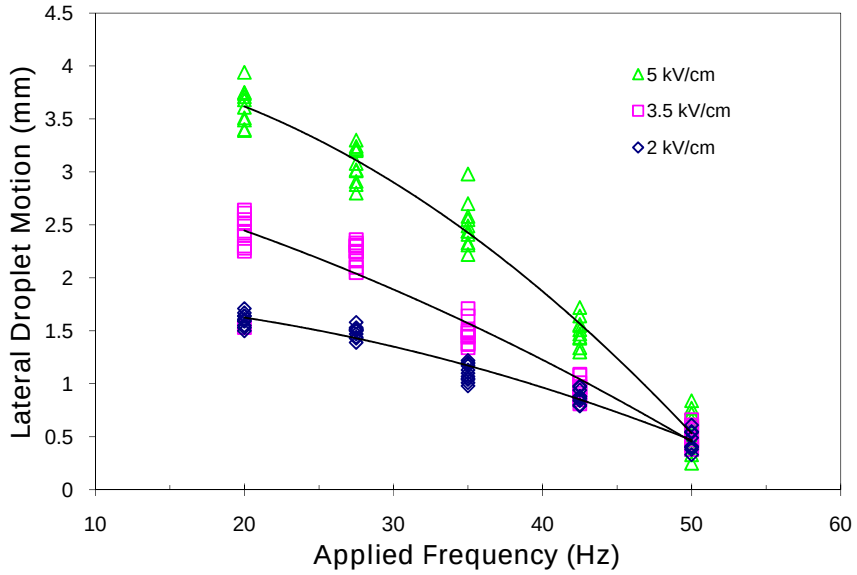


Figure 4-6. Lateral droplet motion within an AC-generated electrostatic field.

It is apparent that as the electrostatic field frequency was increased from 20 to 50 Hz for a constant electrostatic field strength, droplet zigzagging decreased and droplet oscillation seemed to increase. This was attributed to droplets having insufficient time to undergo large physical movement of zigzagging in the shorter cycles of the electrostatic field as the frequency was increased.

Also apparent is that as the applied voltage was increased from 2 to 5 kV/cm, with a constant electrostatic field frequency, the amount of droplet agitation (zigzagging and oscillation) increased. This is attributed to the greater force applied at the interface of the droplets causing greater zigzagging and oscillation. More detailed investigation using a high-speed camera would allow more accurate results to be attained.

While these data remain only indicative of the effect of electrostatic field conditions on droplet movement in commercial applications, a droplet agitation scheme for a commercial ESX column application may be postulated where different applied field frequencies are used in different sections of the column. In an extraction application, the concentrated aqueous feed solution contacts the highly loaded organic solution in the upper section of a column where it is likely that the replenishment of the droplet interface with “fresh” extractant molecules is the rate-determining step in extraction, and therefore using a low frequency applied field will promote droplet zigzagging and thereby interface replenishment with fresh extractant molecules. Conversely, in the lower sections of a column, after much of the metal has already been extracted into the organic phase, the aqueous droplets will be contacting a relatively unloaded organic phase. Here it is likely that the rate-determining step in extraction is the migration of the metal ions within the droplet to the interface, and using a higher frequency field to effect droplet oscillation will force convection within the droplet and replenish the interface with fresh metal ions.

To assess the viability of this postulated droplet agitation scheme, progressively less concentrated feed solutions can be fed into a small test column, and the optimum electrostatic field frequency for each solution concentration determined. If the optimum electrostatic field frequency for extraction increases as the feed concentration decreases, then droplet oscillation will be promoting mass transfer and independent agitation sections within a column are justified. Such an optimisation exercise however, would only be appropriate upon scaling-up to a commercial application as the results would be specific for the ESX contactor and the particular chemical system being evaluated.

### 4.5.3 Electrode Design

The main problem observed with using parallel-plate electrodes was the formation of a small number of ultra-fine droplets, which are too small to have sufficient mass to counteract drag forces that keep them from settling. With prolonged operation, these droplets collectively formed a swarm of ultra-fine droplets that subsequently formed an emulsion. Such small droplets will remain entrained in the solvent and thereby decrease

process efficiency and also, if the bulk conductivity of the continuous phase increases, they will hinder or completely prevent dispersion.

The other problem with parallel-plate electrodes is that some droplets fall through the region with electrostatic field without oscillating or zigzagging any great deal because of the little charge that they carry. This represents inefficiency in a contactor, as these droplets will require a longer residence time to allow complete extraction of the metal ions they contain, meaning that a larger column is required in comparison to where droplets are well agitated.

It appears that these problems may be overcome by incorporating a non-uniform electrostatic field and positioning charge-sources within the column. The non-uniform field would attract the ultra-fine droplets to central points and promote their coalescence, and positioning charge-sources in the path of falling droplets will effect droplet charging and thus droplet agitation. The most apparent way of achieving these conditions is to use rods as electrodes. Three configurations of this arrangement that were tested were (1) diagonally pitched electrode, (2) vertically pitched electrode and (3) horizontally pitched electrode. Cross-sectional diagrams of these configurations are shown in Figure 4-7.

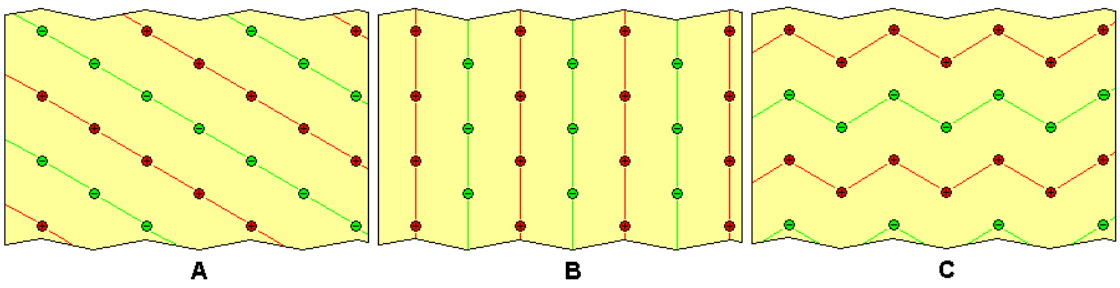


Figure 4-7. Diagram of rod electrode arrangements for droplet agitation. (a) diagonally pitched, (b) vertically pitched and (c) horizontally pitched electrodes. (The green and red points represent electrodes of opposite polarity, and the lines between represent the connections).

Initially a horizontal rod electrode with the electrodes pitched diagonally was constructed using 3-mm diameter stainless steel rods that were insulated with heat-shrink Teflon®. A picture of the electrode and the dispersion achieved is shown in Figure 4-8. It was observed that as the electrostatic field strength increased, droplet dispersion

increased although the dispersion was less uniformly sized in comparison to the dispersion when using parallel plate electrodes with the same field strength. In addition, nearly all of the droplets were observed to be agitating (oscillating and zigzagging) vigorously and free-falling droplets quickly contacted an electrode, became charged and subsequently agitated vigorously.

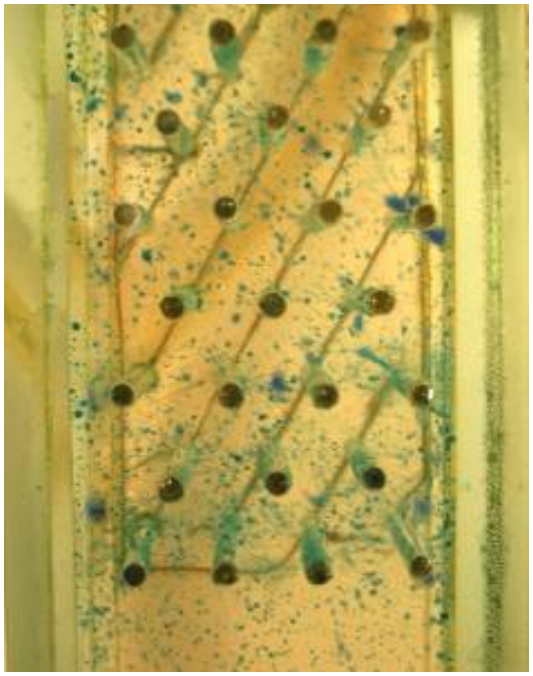

Figure 4-8. Photograph of the horizontal rod electrode with diagonal pitch.

To assess the viability of the vertically and horizontally pitched rod electrode arrangements, another electrode was constructed. Instead of again constructing a rod electrodes with heat-shrink Teflon® coating, which entailed lengthy and intricate construction, a Tefzel® coated wire electrode was constructed which consisted of a Perspex™ frame with holes drilled in a triangular pitch through which Tefzel® coated wire was woven with the appropriate electrode pitch. This allowed the performance of the diagonally, vertically and horizontally pitched rod electrode arrangements to be assessed comparatively. The droplet behaviour observed for these rod electrode arrangements is shown in Figure 4-9.

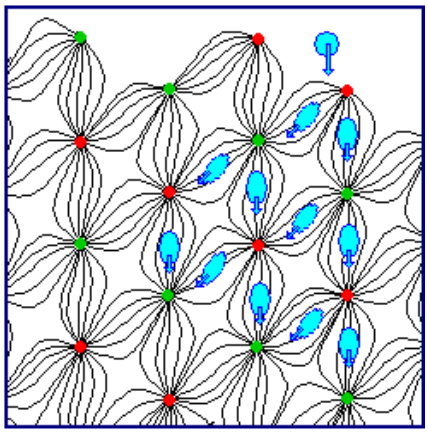

A

(1) Droplet contacts electrode, becomes charged and is attracted a lower electrode of opposite polarity.

(2) Upon touching lower electrode, droplet acquired opposite charge, and is attracted to neighbouring electrodes of opposite charge.

(3) Depending upon the frequency of the applied field and the droplet size, some droplets pass through large sections without electrode contact.

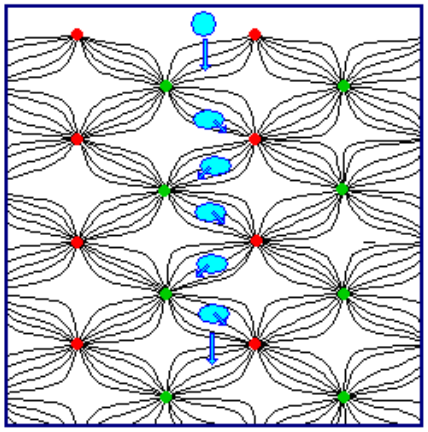

B

(1) Droplets fall down into the electrode region, and are channelled between electrodes of opposite polarity.

(2) Droplets oscillation was minimal, owing largely to the larger downward momentum of the larger droplets.

(3) Oscillation was largely dependent on the applied field frequency.

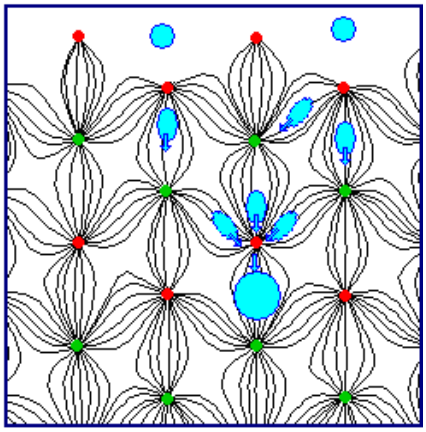

C

(1) Droplets disperse and behave in similar manner as to configuration (A).

(2) Owing to the horizontal zigzag configuration of the electrodes, droplets from three electrodes are attracted to one electrode of opposite charge below, causing a high localized aqueous phase hold-up, resulting in increased coalescence and increased non-uniformity in droplet size.

Figure 4-9. Droplet behaviour observed in rod-electrode arrangements with various pitches: (a) diagonal pitch, (b) vertical pitch and (c) horizontal pitch. Lines between point electrodes represent electrostatic field flux lines.

The diagonal pitched electrode, as shown in Figure 4-9a, allowed good dispersion, with a large majority of the droplets contacting an electrode falling downwards and towards one of two oppositely charged electrodes below; only a very small proportion of droplets went upwards again to contact an electrode above. Also, larger droplets (3-mm diameter) were found to zigzag freely without much physical interference from the rods.

The vertical pitched electrode, as shown in Figure 4-9b, produced poorer droplet dispersion and agitation than the diagonal pitched electrode for comparable electrostatic field strengths. When the aqueous droplets entered the electrode region, they already had considerable downward velocity. Regardless of whether the droplets contacted the uppermost rods, the droplets fell into the vertical channels between electrodes and were accelerated downward. The droplet oscillations prior to and whilst in the electrode region were comparable, and droplet zigzagging remained negligible. This was attributed to the large droplet having a higher downward momentum and velocity, and oscillating in its own wake. When higher electrostatic field strengths were applied increased droplet dispersion and also droplet agitation were observed.

The horizontal pitch electrode, as shown in Figure 4-9c, initially allowed quite good dispersion – in the upper 5 cm section of column – however droplet coalescence was much more predominant than for the diagonally pitched electrode in lower sections. Dispersed droplets that contacted a particular electrode became charged and attracted to the closest lower electrode of opposite polarity, usually resulting in droplets being channelled to a few electrodes where coalescence was quickly affected.

It is apparent that the diagonal pitch electrode is the most favourable for the nickel-Versatic 10 extraction system being investigated in this study; The other configurations however, may be favourable for other chemical systems, particularly for those with a tendency to emulsify.

## 4.6 Electrostatic Coalescence

Given the observation that rod electrodes also facilitated coalescence of ultra-fine droplets in addition to providing good dispersion (Section 4.5.3), the performance of this electrode configuration as a droplet coalescer was assessed. This was done by passing a 1% PLS-in-solvent emulsion through the laboratory-scale counter-current column with the Tefzel®-coated electrode at various strengths of applied voltage, and the amount of PLS that remained in the solvent discharge was measured.

The results, which are summarised in Figure 4-10, show that increases in applied voltage up to 3 kV/cm resulted in almost linear decreases in the PLS content of the solvent discharge but further increases in the applied voltage had no further effect.

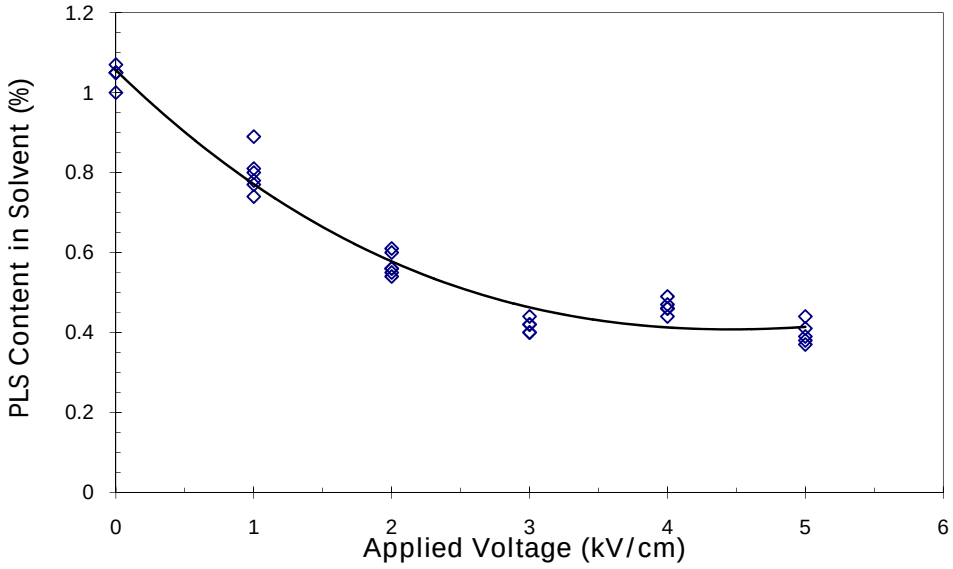


Figure 4-10. Effect of applied voltage on PLS remaining entrained in the solvent. (Constant 50 Hz applied frequency.)

In all experiments, it was observed that some coalesced droplets that formed on electrode surfaces, dispersed via the necking mechanism such that a part of each was ejected, a part remained on the electrode surface, and some ultra-fine daughter droplets were also formed. The ejected main daughter droplets were typically between 1 and 2 mm in diameter and fell down toward the settler, while ultra-fine daughter droplets moved upward with the solvent flow and some were again coalesced. It appears

therefore that for a given height of a coalescence column and a given flow rate, there is a limit as to the amount of the PLS that can be removed. It follows that adjusting the height and flow rate are keys to complete removal in this instance. Clearly, with some optimisation, this electrode arrangement can also be used as a coalescer that can be placed at the solvent settler of an ESX column allowing a more vigorous dispersion within the extraction stage.

The general trend of the coalescence observed here as a function of applied voltage is consistent with the observation of Galvin (1984) who investigated the use of electrostatic coalesce for dewatering crude oil.

## 4.7 Electrostatic Solvent Extraction Column Design

Based on the findings in the individual sections of this chapter, an electrostatic solvent extraction (ESX) column design was conceived. A diagram of this design is shown in Figure 4-11. Its key design features are as follows:

- The PLS feed is introduced into the column via a spray head to partially disperse the PLS. It was deemed that the benefit of a narrow droplet size distribution achievable by an individual electrostatic PLS feed disperser was not appropriate given the continual droplet dispersion-coalescence caused by a horizontal rod electrode arrangement would negate any benefit.
- A horizontal electrode arrangement is used to continually disperse, charge and coalesce PLS droplets as they fall downward within the column. The horizontal electrode arrangement allows for effective droplet dispersion and droplet charging which subsequently allows vigorous droplet agitation. In addition, a facility for the coalescence of any ultra-fine droplets is provided.
- Multiple sections of horizontal rod electrodes, to which individual AC power supplies are connected, are adopted to allow for the electrostatic field to be optimised for the varying conditions along the column.
- A horizontal rod electrode droplet coalescer is included in the solvent settler to remove entrained PLS droplets in the solvent, if any.

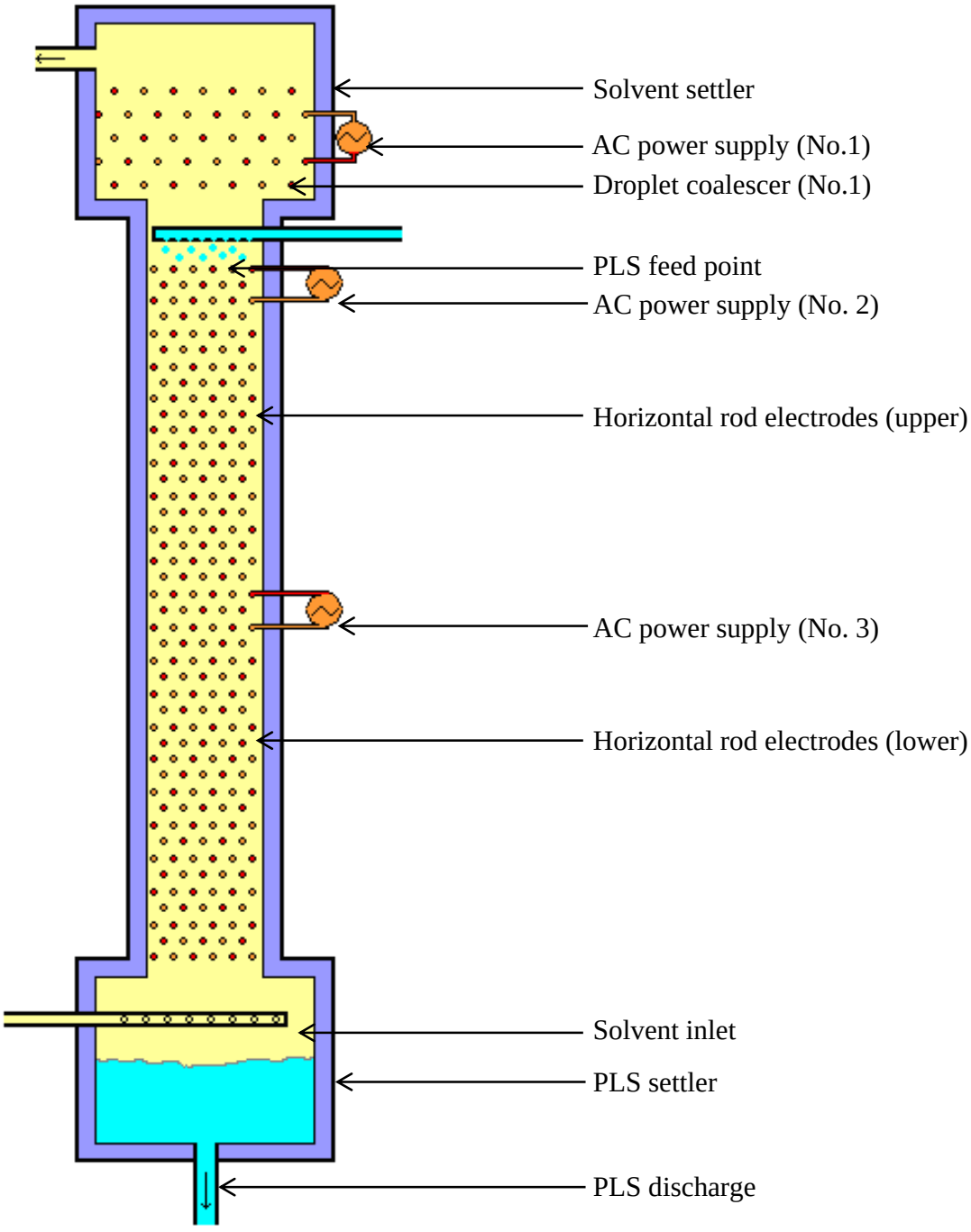


Figure 4-11. Design of the electrostatic solvent extraction (ESX) column.

## 4.8 Summary

In this chapter it was found that:

- An individual electrostatically assisted PLS disperser is not appropriate for a commercial ESX column. Dispersers utilizing a DC-generated electrostatic field allowed apparently more uniform droplet sizes but did not allow fluxes suitable for commercial application. Dispersers utilizing AC-generated electrostatic fields did not provide any benefit in regard to droplet uniformity.
- The electric charge carried by a droplet has a significant effect on droplet agitation. Droplets that carried an electric charge were observed to zigzag and oscillate markedly more than droplets that did not carry any electric charge.
- Vertical plate electrodes are unsuitable for droplet agitation. Droplet dispersion using vertical plate electrodes invariably results in the formation of ultra-fine droplets that become entrained in the solvent, and this electrode arrangement does not allow a facility for the effective removal of these ultra-fine droplets.
- The horizontal rod electrode arrangement seems the most suitable arrangement for droplet agitation within a commercially applicable ESX column. The horizontal rod electrode arrangement allowed continual droplet dispersion, droplet charging and droplet agitation, and also coalescence of ultra-fine droplets that formed during droplet dispersion.
- Coalescence of ultra-fine droplets is effectively achieved using a horizontal rod electrode arrangement. The horizontal rod electrode was found to markedly reduce the amount of PLS entrained within a solvent phase.
- An ESX column with horizontal rod electrodes throughout the body of the column seems the most promising design for commercial application.

Chapter 5

# Design, Construction and Commissioning of the Pilot-Scale ESX Column and Associated Equipment for the Pilot-Scale Study

## 5.1 Introduction

This chapter describes the effort to design, construct and commission a pilot-scale ESX column, the refurbishment of a sieve-plate pulsed column and the assembly of a pilot plant suitable for exploring the potential industrial application of an ESX column. Several modifications to the design of the ESX column presented in Chapter 4 were incorporated into the pilot-scale ESX column to simplify construction, namely: (1) the coalescence electrode in the solvent settler was omitted but facility for later installation if required was allowed, (2) all sections of electrode were connected to the same power supply and thus the voltage and frequency of the electrostatic field applied were the same along the entire length of the column and (3) the electrode spacing was decreased from 11 mm to 8 mm to lower the voltage required to maintain a sufficient electrostatic field strength, and thus preventing potential damage to the power supply and electrode insulation when operating at high voltages and low frequencies over prolonged periods.

This work is part of the effort to assess the potential industrial application of the ESX column that was developed in the previous chapter. To achieve this, its performance needed to be compared directly with another contactor that has already received industrial application. Considering the structural similarities that the ESX column and pulsed column share, the pulsed column seemed the most appropriate contactor for this comparison.

## 5.2 Construction of the Pilot-Scale ESX Column

### 5.2.1 Design Philosophy

To make a direct comparison of the ESX column and the sieve-plate pulsed column, the active cross-sectional area of the ESX column was made to match that of the pulsed column, i.e., 20 $cm^2$. Given that the minimum diameter of pulsed column from which scale-up data can be obtained is 5-cm (Ritcey 2006c, 313), the diameter of the pulsed column used for this comparison should be no smaller than 5 cm. To accommodate this active cross-sectional area, the true ESX column cross-sectional area needed to be larger to allow space for the electrode frame. In addition, the height of the active contacting area of each column should be the same, i.e. 3.60 m, to simplify comparison and discern any variations in dispersion and mixing along the column.

Owing to limitations with respect to available materials and fabrication equipment, a column of this size must be constructed in sections that are connected together using flange joints. These joints must allow application of sufficient joining pressure to prevent leakage, while allowing relatively simple assembly and disassembly for any repair and modifications. Also, the materials of construction must provide sufficient structural strength to hold the column together and maintain stable operation.

The upper and lower settlers need to be large enough to allow sufficient phase disengagement to occur but not be too large to minimise the residence time of fluid within them and thereby allow reasonable run-times for experiments. Given that the expected maximum PLS and solvent throughputs are each 80 L/hr, a upper settler with capacity of 7 L will provide a solvent residence time of 5.25 min and a lower settler with a capacity of 10 L will provide a PLS residence time of 10.5 min. Phase disengagement tests indicated this time is comfortably sufficient for complete phase disengagement. Also, a large dump valve fitted in the lower settler will allow quick and simple drainage of the column if required.

The PLS injection port should allow droplets to be formed evenly about the cross-section of the column. In addition, the injection port should not hinder counter-current solvent flow and also be easily removable to allow the removal of the electrodes if

required. The organic inlet port should be located in the upper half of the lower settler to prevent obstructing downward flow of aqueous droplets, and also distribute the organic phase evenly about the column cross-section.

### 5.2.2 Materials

The following commercial materials were used for the construction of the pilot-scale ESX column: Perspex™ (5-mm and 10-mm thick, Dotmar Industries), stainless steel bolts, nuts and washers (Grade 316, 14 mm-diameter x 30 mm), stainless steel rod (Grade 316, 4.76-mm diameter), cork sheeting (3-mm thick, Beldam Burgmann), PVC conduit glue (Industrial grade, Clipsal), stainless steel screws (Grade 304; 6 g x 12 mm pan-head, 6 g x 18 mm countersunk, 8 g x 25 mm countersunk), O-rings (Viton®, 12-mm and 25-mm diameter), various polyethylene hose fittings (12-mm diameter, Nylex Australia), PVC hosing (12-mm diameter, Nylex Australia), heat-shrink Teflon®, (1.76-mm diameter, Zeus Industries) and Tefzel®-coated stainless steel wire (M22759/16 AWG22, Avial Australia).

### 5.2.3 Column Supports

To provide structural support to the column and allow seamless operation, a suitable column stand was made by refurbishing and modifying an existing leach column stand. Rusted sections were replaced and the stand was painted to prevent corrosion after which the stand was affixed to the concrete floor. A photograph of the column stand is shown in Figure 5-1a. The upper part of the column, which was not supported by the stand, was supported by a custom-made cradle that was attached to the hand-rail of the first floor of the laboratory. This cradle directly supported the flange connecting the upper settler and the first column section. A photograph of the cradle is shown in Figure 5-1b.

Figure 5-1. Photographs of column supports: (a) column stand and (b) column cradle.

### 5.2.4 Column Body

To make the cross-sectional area of the ESX column match that of the pulsed column, the internal dimensions were made 45 x 58 mm: this allowed 6.5 mm on either side of the column for the electrode frame, yielding an active cross-sectional area same as the pulsed column (20.25 $cm^2$). The body sides were made of 10-mm thick Perspex™ and the front and rear were made of 5-mm thick Perspex™. The column body was made in 1.2-m sections that were connected with flanges. Schematic diagrams of the column body sections and flanges are shown in Appendix C-1.

Sections of body side were cut to 60 mm wide 1.25 m lengths. The width was then reduced to 58 mm by passing over a bench planer, which ensured a perfectly straight edge. Holes (3-mm diameter) were then drilled centrally along the edges of the column side sections (50 mm apart) to allow for the front and rear sections to be affixed. The body front and rear were cut 65 mm wide 1.25 m lengths and holes (3.5-mm diameter)

were drilled along the lengths (5 mm from the edge and 50 mm apart) to fit the screws (6 g x 12 mm pan head) for fastening the sections together.

The side, front and rear sections were then thoroughly cleaned with methylated spirits, conduit glue was applied to the ends of the side sections, and the body assembled. Screws were then placed into the pre-drilled holes and fastened to secure the column and provide pressure to the glued joints. Two days were allowed for the glue to cure after which the column sections were cut to lengths of 1.18 m.

The flanges were cut from 10-mm thick Perspex™ to 150 x 150 mm sections. Equidistantly around the side of the flange, 30 mm from the edge, twelve holes (15-mm diameter) were drilled. At the centre of each flange a 45 x 58 mm section was cut using a machining mill; outward 5 mm from each 58-mm long side, three 4.5-mm diameter holes were drilled equidistantly apart to allow the flanges to be screwed to the column sections. These holes in the flanges were countersunk so that the heads of the screws were below the flange surface. The flanges and column ends were cleaned with methylated spirits, jointing cement applied to the column ends, and the flanges affixed to the column ends by fastening the screws (8 g x 25 mm countersunk) through the flange and into the column wall.

### 5.2.5 Upper and Lower Settlers

The two settlers, the upper settler and lower settler, were constructed of 10-mm thick Perspex™, with sections being affixed together with screws (6 g x 18 mm countersunk) and the joints sealed with jointing cement. Each settler had a flange to allow connection to the column body. These flanges are described in Section 5.2.4 and their fitting to the settlers was same as the fitting of flanges to column body sections. Schematic diagrams and photographs of the settlers are shown in Appendix C-2.

The upper settler was rectangular (100 x 100 x 7500 mm) and had a flange attached to one side. It was constructed as follows: The front and rear sections of the compartment (120 x 750 mm) had 4.5-mm diameter holes pre-drilled 5 mm from the edge of the 750-mm lengths, with each hole being 50 mm apart. The two side sections of the compartment (100 x 750 mm) had 4-mm holes pre-drilled on the sides of the 750-mm lengths, with each hole also being 50 mm apart. All sections were then cleaned with

methylated spirits, the two side sheets held upright 100 mm apart, and conduit glue applied to the edges. The front and rear sections were then clamped to the side sections, and affixed by inserting and fastening screws in the pre-drilled holes. Upon curing of the cement, the ends were planed level and a flange attached to the bottom.

On one of the side sections, 100 mm from the top, a 26-mm diameter hole was made for an organic overflow port to be fitted. The port was a standard polyethylene threaded pipe fitting, with a 10-mm internal diameter, which had a barbed outer connection for a hose to be fitted.

The lower settler was made of two compartments: a lower compartment and an upper compartment. The lower compartment had internal dimensions of 200 x 200 x 350 mm, above of which an upper compartment with internal dimensions of 45 x 60 x 150 mm was connected. A flange was fitted to the top of the upper compartment.

The lower compartment was constructed as follows: The front and rear sections of the compartment (220 x 350 mm) had 4.5-mm diameter holes drilled 5 mm from the edge of the 350 mm length, with each hole being 50 mm apart. The two side sections of the compartment (200 x 350 mm) had 3-mm holes pre-drilled on the side of the 350 mm lengths, with each hole also being 50-mm apart: The holes drilled in each of the sections aligned when placed together. The sections were cleaned with methylated spirits, the two side sheets held upright 200 mm apart and jointing cement applied to the edges. The front and rear sheets were then clamped onto the side sheets, and affixed by inserting and fastening screws in the pre-drilled holes. Two days were allowed for the glue to cure, after which the ends were planed flat. A base section (220 x 220 mm) was made and sixteen 3.5-mm diameter holes were pre-drilled equidistantly around the base, 5 mm inside from each edge. The edges were cleaned with methylated spirits, glued and then fastened to the end of the compartment by fastening screws in the pre-drilled holes.

The 150-mm long body of the upper compartment was cut from a test section of the column body, which was constructed following the procedure described in Section 5.2.4. To the top of the upper compartment body, a flange for connection to the column body was fitted, and to the bottom of the body a larger flange (220 x 220 mm), which also was the lid to the lower compartment, was fitted. In the centre of this larger flange, a 45 x 58

mm section was milled out, around which the upper compartment was fastened. Both of the flanges were connected in the same manner as flanges were connected to column body sections. Sixteen 4.5-mm holes were pre-drilled equidistantly around the large flange base, 5-mm inside from each edge.

The connection points of the upper and lower compartments were then cleaned with methylated spirits, conduit glue applied and the upper compartment placed on top. Screws were placed into the pre-drilled holes in the large flange and fastened to the walls of the lower compartment.

On the side of the lower compartment, 250 mm from the base, a 26-mm hole was drilled to allow an organic injection port to be inserted. Also, at the centre of the base of the lower compartment, another 26-mm diameter hole was made to allow the fitting of a standard polyethylene discharge port with an outer barbed connection to allow drainage of raffinate.

### 5.2.6 Electrodes

The rod electrode design, as proposed and investigated in Section 4.11, with a diagonal rod arrangement was used in this pilot-scale column. To circumvent the prohibitive construction time that would be required for a 3.6 m Teflon®–coated rod electrode, a Perspex™ frame was constructed in which numerous holes were drilled, and Tefzel™-coated stainless steel wire weaved through. To lower the voltage required to maintain sufficient electrostatic field strength, and thus preventing potential damage to the power supply and electrode insulation, the electrode spacing was shortened to 8 mm from the 12 mm gap used in the bench-scale work. A photo of a section of an electrode length is shown in Figure 5-2 and schematic diagrams provided in Appendix C-3. To construct each of the three electrode frames required for the column, i.e., one frame in each body section, two sections of 5-mm thick Perspex™ were cut to size (40 x 1200 mm). Along both lengths of both sections, 5 mm inward from the edge, holes (4.5-mm diameter) were drilled 3-mm deep and 15 cm apart. Stainless steel rods (4.76-mm diameter) were cut to 51-mm lengths and firmly inserted into the holes along the edge of both Perspex™ sections to make a rigid frame with a 45-mm space between sections. On each of the

frames, 1.18-mm diameter holes were drilled 9 mm apart on a triangular pitch, through which the Tefzel® coated wire was weaved.

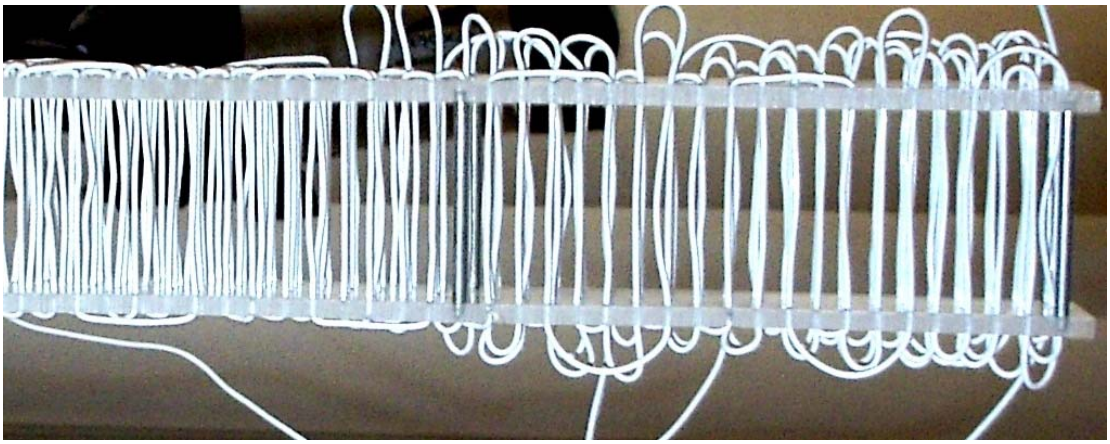

Figure 5-2. Photograph of Tefzel® coated wire electrodes during tightening of the electrode wires.

Each of the electrode frames were inserted into their respective section of the column body. To make one continuous electrode, the wire ends were passed through the flanges, soldered to the corresponding electrode wire in the adjacent section and covered with heat-shrink Teflon®. The wires exiting the first section of the column were passed upward through the upper settler and connected to the power supply, and the wire exiting from the third column section were cut and sealed with heat shrink Teflon®.

### 5.2.7 Injection Ports

Injection ports for the PLS and solvent were installed on the side of the column body 10 cm below the flange connection to the upper settler and on the side of the lower settler 250 mm from the base, respectively.

The PLS injection port was designed to be easily removable to allow the removal of electrodes from the column for repair. It was fabricated from a 20-mm diameter stainless steel bolt and two fitting nuts. A diagram of the injection port is shown in Figure 5-3 and photograph shown in Appendix C-4. The shaft of the bolt was machined to 15-mm diameter and the bolt length was cut to 75 mm such that a 30 mm length was threaded. A 70 mm long, 10-mm diameter tunnel was machined from the threaded side of the bolt.

Along the shaft of the bolt, three rows of seven 1-mm diameter holes were made on one side of the port to allow the flow of fluid evenly about the cross-section of the column. Along the first 15 mm of tunnel, a thread was cut to allow the fitting of a barbed connector for tubing.

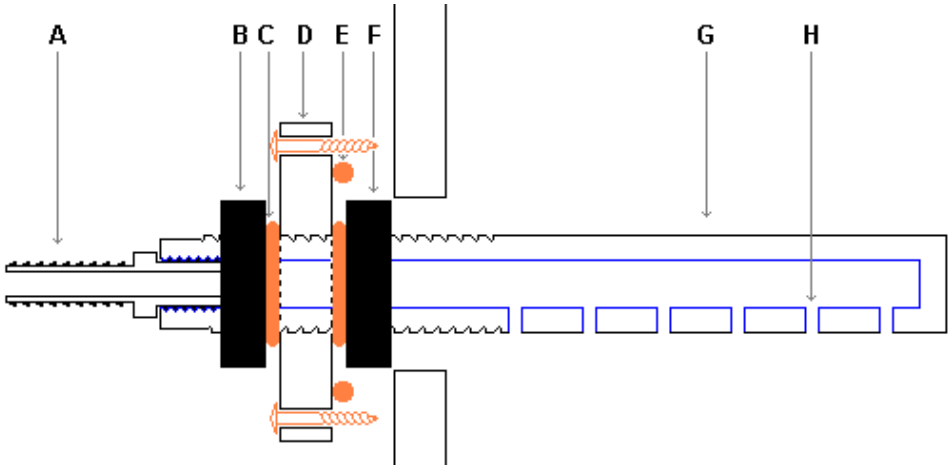


Figure 5-3. Diagram of PLS injection port. (A – barbed fitting, B – outer tightening nut, C – o-ring, D – Perspex™ fitting section, E – o-ring, F – inner tightening nut, G – main shaft, H – discharge holes)

The injection port was fitted into a hole in the centre of a 45 x 45 x 5 mm section of Perspex™, and two nuts were tightened on either side of the section. Between the nuts and Perspex™ section, Viton® o-rings were located to provide a leak-proof seal upon tightening of the nuts. On the edge of the Perspex™ section, screws (12-mm pan-head) were inserted into 3.5 mm diameter pre-drilled holes, and upon inserting the injection port into the column, these screws were fastened into the body of the column. Another Viton® o-ring was placed in between the Perspex™ section and the body of the column to provide a leak-proof seal.

The organic injection port was modified from a fabricated polyethylene fitting. A diagram of the port is shown in Figure 5-4 and a photograph shown in Appendix C-4. The fitting consisted of a 170-mm long, 25-mm diameter threaded pipe moulded to a large flanged nut. Along the sides of the threaded pipe, eight 10-mm diameter holes were drilled to allow solvent flow evenly across the settler. This fitting was inserted into

the 26-mm diameter hole in the side of the lower settler, a Viton® washer was placed over the threaded pipe and a second flanged nut was screwed onto the pipe. An end cap was screwed onto the pipe to seal the end. The second flanged nut was tightened, thereby providing a leak-proof seal. A barbed fitting was then attached to the outside nut to allow connection of a solvent feed hose.

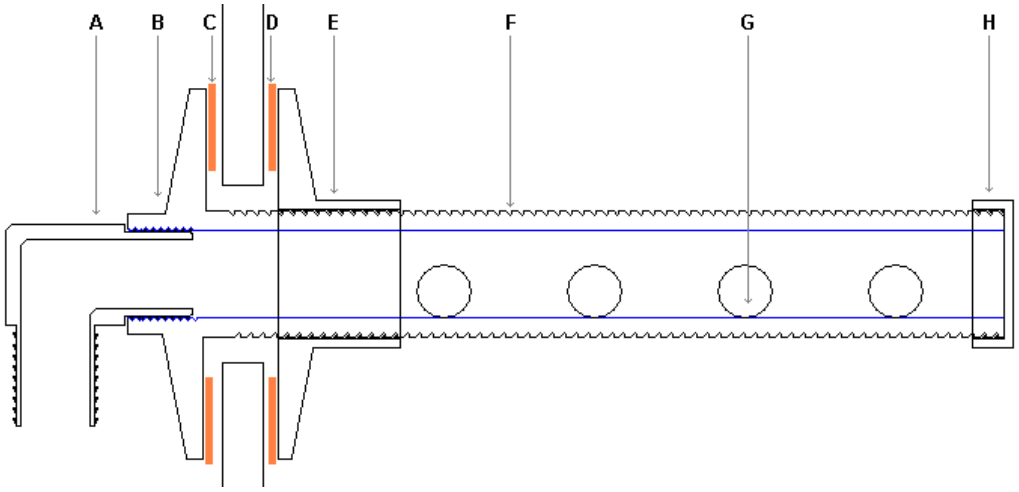


Figure 5-4. Diagram of the solvent injection port. (A – barbed fitting, B – flanged nut moulded to main shaft, C – gasket, D – gasket, E – outer fitting nut, F – main shaft, G – discharge holes, H – end cap)

### 5.2.8 Column Assembly

The electrode frames were inserted into their column sections, and the three column sections aligned. A custom-cut cork gasket was placed in between the flanges and the corresponding electrode wires of adjacent sections of the column were connected. The wire connections were soldered and covered with heat-shrink Teflon®. The sections were connected and sealed by tightening the bolts through the flanges. The upper settler was then connected to the top column section in a similar manner to how the column sections were connected, with the electrode wire passing through to exit at the top of the settler. The short wire sections remaining from the lower body section were sealed with heat-shrink Teflon® tube.

The lower settler was placed on the column cradle, and the platform adjusted such that the flange of the settler was exactly horizontal. The connected column body with the upper settler was then carefully lifted upright, placed onto the lower settler and the sections joined and sealed by fastening the flange bolts. The cradle supporting the upper section of the column was fitted around the upper settler flange, ensuring that the column was sitting vertically and that lateral stresses on the column were minimised.

The injection ports were then inserted into their appropriate holes which were cut and fastened. The wires exiting from the upper settler were further shielded with PVC tubing and prepared for connection to the power supply. Finally, hosing was connected to the injection and discharge ports.

## 5.3 Refurbishment of the Sieve-Plate Pulsed Column

The sieve-plate pulsed column that was constructed previously by Donegan (2001) was used in this study. The column is 6.7 m tall, has an active zone of 3.6 m and active cross-sectional area of 20 $cm^2$. Preliminary attempts to operate the column revealed that it was unsuitable for piloting because the pulsing mechanism, the sieve-plate spine and the solvent discharge fitting required refurbishment.

### 5.3.1 Pulsing Mechanism

The existing pulsing mechanism was a simple piston pump that was powered by a small variable speed motor. Initial testing showed that the pulsing pump was struggling with pulsing against the static head of the column fill, which was causing excessive vibration of the column thereby increasing the risk of damage, and also the piston was leaking a considerable amount of liquid. The existing motor was replaced with a larger one to provide more fluent pulsing, and two grooves were machined into the Teflon® pulsing piston and Viton™ o-rings placed inside to allow a better seal and prevent leakage. Subsequent operation was deemed acceptable, however its performance deteriorated after several hours. Thus, to allow consistent performance without any leakage, an air pulsing mechanism was installed.

The design of the air pulsing mechanism presented by Brunet et al. (2005) and shown in Figure 5-4 was adopted. It consists of two solenoid valves on either side of a T-piece that is connected to an air-leg line on the column. The valve between the high-pressure air and the T-piece controls the flow of air into the air-leg, and the valve on the other side of the T-piece controls the flow of air from the air leg. The valves are operated out of phase so that when one valve is open the other valve is closed and thereby controlling the airflow into and out of the air leg and effecting a pulsing motion within the column. Changing the supplied air pressure and the frequency of valve opening/closing cycle allows control of the pulsation amplitude and frequency, and therefore pulsation intensity.

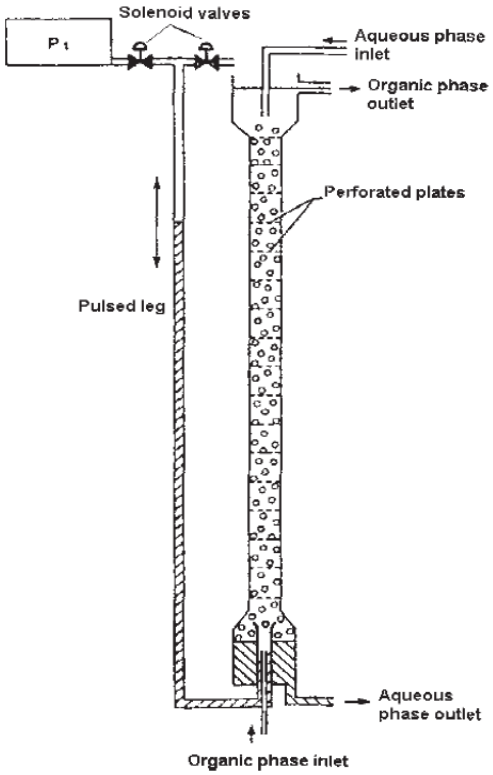


Figure 5-5. Air pulsing mechanism for a pulsed column. (Brunet et al. 2005)

The air leg was constructed as follows: The existing 50-mm diameter stainless steel piston shaft that was attached to the lower settler had a thread cut onto its outer side, and a standard 50-mm polypropylene elbow fitting attached. To the other side of the elbow, a 25-mm barbed fitting was fitted, to which a length of 25-mm diameter Nylon hose was

attached. This hose ran alongside the pulsed column and was connected to the pulsing mechanism located adjacent to the organic settler.

A diagram of the complete pulsing mechanism is shown in Figure 5-6. It consists of a compressed air source, a 1-250 kPa pressure regulator, two 25-mm diameter solenoid-actuated diaphragm valves (B55-6-25-5V, Process Systems Aust.), and a custom made relay box that boosted the signal generator (TG 215, Thurlby Thandar Instruments) output sufficiently to power the solenoids. The relay box was configured such that the two valves were open at alternate times. Photographs of the set-up are shown in Appendix D.

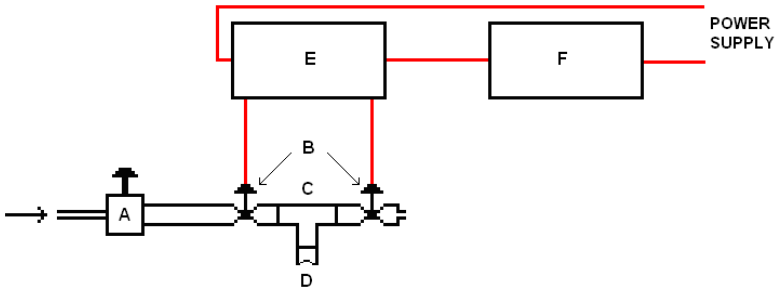


Figure 5-6. Air pulsing mechanism constructed for the sieve-plate pulsed column. (A – air pressure regulator, B – solenoid valves, C – T-piece, D – barbed fitting, E – relay box and F – signal generator)

Diaphragm valves with 25-mm ports were selected to ensure that the high pressure air within the air leg could flow out before the next pulsing cycle begins. Within the relay box, solid-state switches were used instead of conventional relays as they are more robust and therefore appropriate for the continual on-off valve timing required.

### 5.3.2 Column Spine

Preliminary testing of the pulsed column also showed that the sieve plates moved significantly when the column contents were being pulsed. This was attributed to the flexing of the Teflon® shaft between the uppermost sieve-plate and the supporting frame at the top of the upper settler from which the plate assembly was suspended. A 20-mm stainless steel tube was placed over this section of Teflon® shaft, and the resulting plate motion was significantly decreased, however was still sufficient to impede dispersion. The entire Teflon® shaft was therefore completely replaced with a stainless steel shaft.

The shaft was made of stainless steel tube with internal and external diameters of 10-mm and 4-mm, respectively. Three sections of tube, 1.2-m long, were cut and inside each end a thread was cut. Threaded rod was then used to connect these individual sections to make a 3.6 m long shaft. The Teflon® sieve-plates were fitted on the rod alternately with 50 mm long sections of 10-mm diameter PVC tubing to allow a 50 mm space between plates. Subsequent testing of the pulsed column revealed that there was negligible plate movement over a range of pulsation intensities.

### 5.3.3 Discharge Outlets

The solvent discharge outlet on the column was 8 mm in diameter and initial testing showed that solvent flow from this outlet was intermittent because the outlet was too small. Owing to long procurement time for column parts, a larger diameter discharge outlet was made in-house. A Perspex™ sheet was cut to size to cover the flange, and holes drilled so that it could be attached to the existing holding frame. In the centre of the sheet, a 16-mm hole was drilled and a thread cut into the sheet. A barbed polypropylene fitting was then fitted into the sheet and a Nylon hose was attached and secured. This arrangement allowed fluent and steady solvent flow.

## 5.4 Design and Assembly of the Pilot Plant for Concurrent Testing of the ESX Column and Sieve-Plate Pulsed Column

To operate the pilot-scale ESX and sieve-plate columns, miscellaneous pilot-plant equipment were procured and prepared including:

- feed and solvent storage capacity for adequate testing times,
- pumping capacity to deliver reagents at the required flow rates,
- a suitably sized mixer-settler contactor for solvent stripping,
- a solvent pre-neutralisation vessel for continuous operation, and
- hosing to transfer reagents about the pilot plant.

Four 1-$m^3$ Bulki containers were sourced for the (1) PLS make-up tank, (2) PLS feed tank, (3) solvent feed tank and (4) raffinate storage tank. Also, one 200-L fibreglass tank was prepared for solvent pre-neutralisation. The containers were thoroughly cleaned using a high-pressure cleaner and copiously flushed with water. The solvent feed and pre-neutralisation tank were also thoroughly washed with diluent. An overhead motor (0.4 hp, C&H Australia) with a stainless steel marine type turbine (200-mm diameter) agitated the contents of the PLS make-up tank.

The PLS and solvent were transferred from the storage tanks to their respective column inlets with peristaltic pumps (7554-20, Masterflex®), the speed of which were controlled using the corresponding solid-state speed controllers. The pump tubing was made of Viton™ (64112-18, Masterflex®), and was connected to the PVC tubing used throughout the plant with barbed Teflon® connectors. The loaded solvent and raffinate exiting the columns were transferred through the PVC tubing to the stripping mixer-settler and raffinate storage tank respectively. The flow rates of the raffinates exiting the columns were controlled using pinch-valves.

A Perspex™ mixer-settler, with a 200 x 200 x 250 mm mixing compartment and 200 x 350 x 250 mm settling compartment, was used to strip the solvent. The mixer used was a Rushton turbine with an 85-mm disc and six 25 x 25 mm blades, and was driven with a variable speed overhead drive (0.25 hp, C&H Australia). A Perspex™ picket-fence with 5 x 5 mm pickets and 5-mm gaps was located in the settler, 50-mm from the mixer overflow, and extended to 100-mm from the bottom of the settler.

The stripping solution was pumped from a 25-L container into the mixer using a peristaltic pump (7554-20, Masterflex®) with Viton™ (64112-18, Masterflex®) tubing. The stripping acid that exited the settler flowed back to the stripping solution storage container and was recycled. Periodically the stripping solution in the storage tank was drained and replaced with fresh stripping solution. The stripped solvent exiting the settler flowed into the solvent pre-neutralisation tank where it was contacted with ammonia gas before being transferred to the solvent feed tank.

The complete pilot-plant set-up is illustrated in Figure 5-7 and the refined pilot-plant start-up procedures are as follows: (1) The PLS is prepared in the PLS feed tank. (2) The

valves on the raffinate discharge lines of the columns are closed and the columns filled with solvent. (3) The agitators for the stripping mixer-settler and the stripping solution pump are turned on. (4) The solvent feed pumps are turned on and calibrated to the desired flow rate. (5) The agitation mechanism (pulsing or electrostatic field) is turned on. (6) The PLS feed pump is turned on and adjusted to the desired flow rate. (7) After the PLS/solvent interface within the solvent settler reached the desired position, the raffinate discharge valves are opened and adjusted to maintain the position of the interface. (8) The strip solution tank is periodically drained and refilled with fresh strip solution. (9) The stripped solvent flowing into the pre-neutralisation tank is sparged with ammonia gas and periodically released to the solvent feed tank.

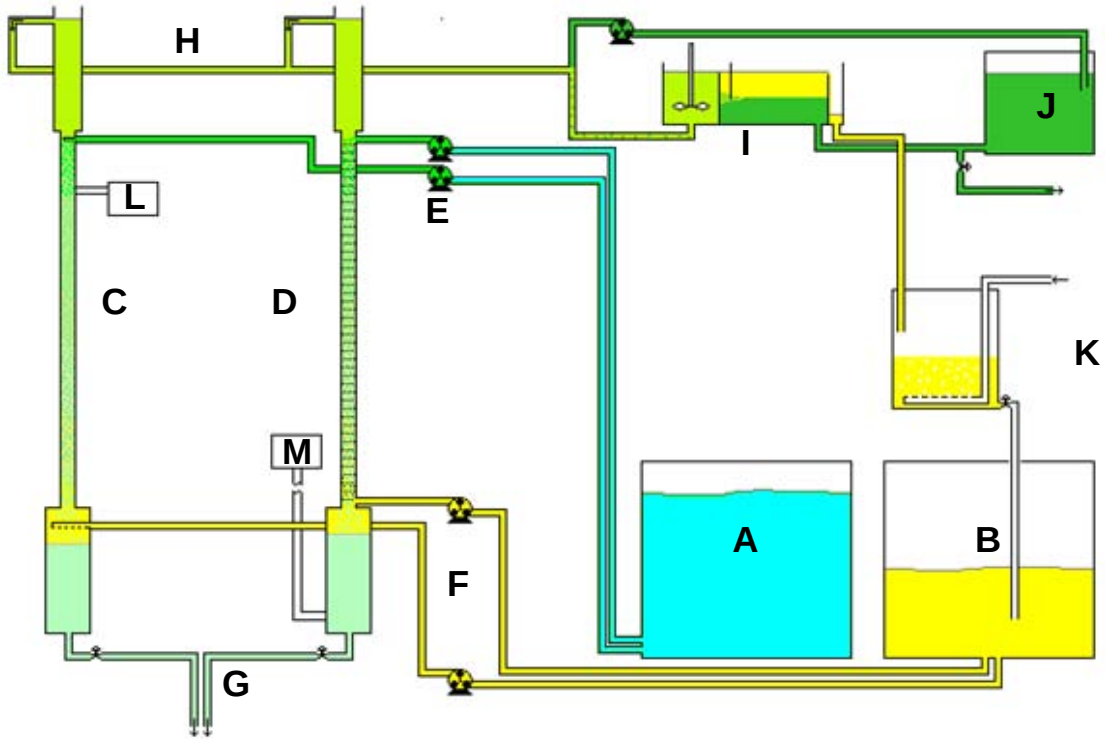


Figure 5-7. Schematic diagram of the pilot plant. (A – PLS feed tank, B – solvent feed tank, C – ESX column, D – sieve-plate pulsed column, E – aqueous feed delivery pumps, F – organic delivery pumps, G – aqueous raffinate discharge, H – loaded organic overflow, I – stripping mixer-settler, J – stripping acid reservoir tank, K – ammonia gas sparging tank, L – high-voltage power supply, M – pulsing mechanism).

## 5.5 Commissioning of the ESX Column

The ESX column and the associated pilot-plant equipment were all checked and tested, after which the plant was commissioned to ensure the plant operated as intended.

Initially all pumps were tested to ensure solution would flow through pipes at the required flow rates, after which calibration curves of pump speed against flow rate were prepared for each pump. Both the ESX and pulsed column were then filled with solvent for the first time to identify any leaks; several leaks were found which were subsequently repaired. Once the leaks were repaired, the columns were again filled with solvent to ensure all leaks had been sealed. Subsequently, the discharge valves on the PLS settler of the ESX and pulsed columns were tested to ensure stable flow at the desired flow rate could be achieved. It was found that the discharge valve on the bottom of the pulsed column was too large, which resulted in difficulty in accurately maintaining the desired flow rate. This valve was instead used as an on-off valve and flow was controlled with a more sensitive pinch valve. Also, the flow of solvent from the solvent settler of each column to the stripping mixer-settler was tested and found that the PVC tubing was too small to allow steady and continual flow. This tubing was replaced with larger diameter tubing, after which flow through this pipe was steady and continual.

The mixer-settler was tested with stripping acid recirculating from the mixer-settler into a holding tank and then pumped into the mixer. Solvent was allowed to flow into the mixer at a flow rate which was approximately what was expected during operation, and the acid was recirculated at a similar flow rate, which allowed the aqueous phase to be the continuous phase. The mixer speed was then adjusted to allow adequate dispersion in the mixing cell without encountering phase disengagement issues in the settler.

The ammonia gas sparge in the solvent pre-neutralisation tank was tested and it was found that the ammonia was passing through the solvent as large bubbles. A new sparge was constructed which had smaller holes and the resulting ammonia bubbles in the solvent were significantly smaller, allowing more efficient ammonia usage and significantly quicker neutralisation of the solvent.

When the columns were full of solvent and the PLS pumps were operational, the dispersion occurring within each column was assessed. The air-pulsing mechanism installed into the pulsed column allowed excellent dispersion, and varying the air pressure and timing of the solenoid valves within the pulsing mechanism allowed good control of the pulsed amplitude and frequency. When the variable voltage – variable frequency power supply was connected to the electrodes within the ESX column, no dispersion was evident, which was determined to be owing to arcing between wires in the electrode. Examination of the electrodes revealed some fine cracks in its insulation. The electrodes were removed from the column and the damaged sections of wire were replaced with new wire. A further dispersion test was then carried out and it was found that the repair was successful as good dispersion resulted. The dispersed droplets were observed to be somewhat rapidly slinking between the electrodes as they travelled down the length of the column, indicating good droplet agitation.

### 5.5.1 Repairs to the ESX Column

As discussed earlier in this section, the two main problems encountered during commissioning of the ESX column were (1) solvent leaks from column flanges and small cracks in column sections and (2) arcing between electrodes.

Upon detecting leaks when the column was filled with solvent, the column was drained, dismantled and thoroughly cleaned. The leaks that occurred between the jointing flanges were fixed by replacing the cork gasket that was free from any kinks or imperfections. The leaks through small cracks in the column sections were fixed by milling out the cracks using a hand-held grinder to roughen the surface and then filled with conduit glue. Both techniques proved successful as no leaks were detected upon reassembling and refilling the column with solvent.

Upon application of a voltage to the electrodes while a small volume of PLS was fed into the column, no droplet dispersion or agitation were apparent. Inspection of the column at night time when the pilot plant was completely dark revealed that there were several points of electrode within the column where arcing were occurring between the electrodes. This created a short circuit and thus prevented the generation of an electrostatic field. The column was then dismantled again; the sections of wire where

arcing was occurring replaced and the column was again reassembled. Subsequent operation of the column allowed droplet dispersion and agitation. It was apparent that the sections of wire where arcing was occurring were damaged during the construction of the electrodes.

## 5.6 Conclusions

To assess the commercial viability of the ESX column developed in the previous chapter, a pilot plant that allowed co-current operation of an ESX column and a sieve-plate pulsed column was constructed and assembled. This involved constructing a pilot-scale ESX column, refurbishing an existing sieve-plate pulsed column, assembling associated pilot plant equipment and commissioning the ESX column.

# Chapter 6

# Comparative Pilot-Scale Studies of an ESX Column and Sieve-Plate Pulsed Column

## 6.1 Introduction

This chapter describes the present investigator's attempt to assess the industrial feasibility of the pilot-scale ESX column developed, constructed and commissioned as described in Chapters 5 and 6 of this work. The aims of this chapter were to (1) gain an understanding of the performance of the ESX column while operating under industrially applicable conditions, particularly the flux of the PLS, (2) compare the performance of the ESX column with a sieve-plate column and (3) determine aspects of the column design that need improvement.

As the first step of this task, a method of controlling the pH was established. This was followed with the generation of data to construct extraction isotherms and McCabe-Thiele diagrams to determine the required equilibrium pH and the column height equivalent to a theoretical stage (HETS). The performance of the sieve-plate pulsed column was then optimised followed by the optimisation of the performance of the ESX column. Finally, the ESX column and sieve-plate pulsed columns were operated concurrently under comparable conditions to allow a direct comparison of the two contactors.

## 6.2 Materials and Methods

### 6.2.1 Reagents

The following reagents were used in this experimental work: ShellSol® 2046 (Industrial, Shell), Versatic 10 (Industrial, Resolution), nickel hydrogen reduction (Ni-HR) feed solution (~ 95 g/L Ni, Murrin-Murrin Nickel Operations), sodium chloride (Industrial, Pool Supply), sodium sulfate (Industrial, Sigma), sulfuric acid (AR, Sigma), sodium hydroxide (LR, Sigma), and ammonia gas (99.4%, BOC Gasses Australia). All reagents were used as supplied.

The nickel feed solution was prepared by diluting the Ni-HR solution with tap water and adding salts ($MgCl_2.2H_2O$, NaCl, $Na_2SO_4.2H_2O$) as necessary. This was to simulate the nickel feed solution typical in the direct solvent extraction of nickel such as that at the former Bulong Nickel Operations which had the following composition: 3 g/L $Ni^{2+}$, 15 g/L $Mg^{2+}$, 80 g/L $Cl^-$ and 45 g/L $SO_4^{2-}$; The solution did contain residual ammonium. The pH of the PLS was adjusted to 5.5 for mass transfer experiments and to 3.0 for maximum flux tests using either sodium hydroxide or sulfuric acid.

The solvent was prepared by mixing the appropriate amount of Versatic 10 with ShellSol® 2046 to make a 10 % (v/v) solution. The concentration was verified titrimetrically using the procedures used by Jääskelainen and Paatero (2000). For mass transfer tests the solvent was sparged with ammonia gas to pre-neutralise the extractant.

### 6.2.2 Set-up of Pilot-Scale Columns and Pilot-Plant

The ESX column and sieve-plate pulsed column, as well as the associated pilot plant used for this work are described in Chapter 5 and therefore are here only briefly summarised.

The ESX column had an active column length of 3.6 m and cross-sectional area of 20 $cm^2$. The internal dimensions of the upper and lower settlers were 10 × 10 × 75 cm (7.5-L) and 20 × 20 × 35 cm (14.5-L), respectively. The electrodes were Tefzel™-coated stainless steel, with electrodes spaced 8-mm apart. The electrostatic field was generated using a variable voltage – variable frequency power supply (California Instruments, 801RP).

The sieve-plate pulsed column used was that constructed by Donegan (2001), but major refurbishments were made by the present investigator. It is constructed of double-toughened glass and has active column and cross-sectional areas of 3.6 m and 20 $cm^2$, respectively. The sieve plates were made of Teflon® and spaced 50 mm apart. The sieves had 3-mm diameter holes and a 22% open area.

The pilot-plant was set-up as follows: The PLS and the solvent feed were each stored in individual 1000-L storage tanks. From these containers, the PLS and solvent feeds were pumped to their respective column injection ports. The raffinate from the column

discharged to a raffinate storage tank and the loaded solvent flowed to a stripping mixer-settler, which had an 8-L mixer and 16-L settler, where the solvent was stripped with a 1 mol/L sulphuric acid stripping solution. The stripping acid was continually recycled, with pregnant strip solution being drained and replenished with fresh stripping solution periodically. The stripped solvent exiting from the settler flowed into a pre-neutralisation container where it was intimately contacted with ammonia gas and subsequently released to the solvent feed tank.

### 6.2.3 Pilot-Scale Test Procedures

The maximum flux tests were carried out as follows: The column was first filled with the solvent, and the agitation mechanism (pulsing or electrostatic field) was applied. For the given phase ratio being tested, specific solvent and PLS flow rates were selected after which the solvent and then the PLS pumps were turned on. The column was allowed to reach steady state for 20 minutes and, if flooding had not occurred, the flow rates were increased step-wise. These steps were repeated until the maximum flux was achieved.

The mass transfer tests were carried out as follows: First the column was completely filled with the solvent and the solvent and PLS delivery pumps calibrated to the desired flow rate. The agitation mechanism was turned on (pulsing or electrostatic field) with the appropriate settings selected, and the stripping mixer and acid pump turned on, after which the solvent and the PLS feed pumps were turned on. The column operation was allowed to stabilise for approximately 1.5 h after which the feed, raffinate and loaded organic samples were collected at 15 minute intervals for nickel analysis by inductively coupled plasma – optical emission spectrophotometer (ICP-OES) (Varian, Liberty 200).

## 6.3 Exploratory Extraction Tests

### 6.3.1 Mode of pH Control within the ESX Column

The mode of pH control within an ESX contactor is significant to its success and commercial feasibility, as was discussed in Section 2.8. Previous studies that used salts of weak acids to buffer the pH of the feed stream to maintain a favourable extraction pH were successful but, industrially, ammonium hydroxide or ammonia are more

appropriate. Therefore bench-scale tests were undertaken to establish which is most suitable.

Neutralising the solvent with ammonium hydroxide caused the solvent to become highly conductive (>2000 pS/m), which was attributed to the micro-emulsions that formed. Given that electrostatic dispersion is hindered by high solvent conductivity, as reported in Section 4.6, the use ammonium hydroxide for pH control in ESX was not explored further.

Neutralising the solvent with ammonia gas resulted in minimal increases in the solvent conductivity; the highest solvent conductivity measured was 42 pS/m, which was found to be suitable for ESX in Section 3.4.5. This conductivity value is consistent with that reported by Jääskelainen and Paatero (1999). The ammonia gas was used to pre-neutralise the solvent prior to it being fed into the ESX and pulsed columns instead of the ammonia gas being injected directly into the columns, as this eliminated differences in solvent pre-neutralisation between columns and thereby allowed direct comparison. At the same time, it allowed pre-neutralisation of the solvent away from the central area of the pilot plant.

### 6.3.2 Development of Extraction Isotherm

An isotherm for the extraction of nickel from the synthetic PLS with 10% (v/v) Versatic 10 solvent was developed to: (1) establish the extraction behaviour of the particular nickel test solution used in this study, (2) determine the required raffinate pH and (3) determine the effect, if any, of the residual ammonium ions contained within the PLS.

The extraction isotherm was developed by contacting 500 mL of synthetic PLS with 500 mL of the solvent in a 2-L beaker, with incremental pH changes being made by means of drop-wise addition of 0.5 M or 1.0 M sodium hydroxide solution. At selected pH values, 10 mL of the aqueous phase was collected and passed through phase separation paper to remove any entrained solvent. From the filtrate a 1-mL sample was collected, diluted and the nickel concentration determined by means of ICP-OES. The remaining filtrate was returned to the 2-L beaker, and further pH changes made. The resulting nickel-Versatic 10 extraction isotherm, together with the nickel-Versatic 10 isotherms reported by Donegan (2006) and Cheng (2006) are shown in Figure 6-1.

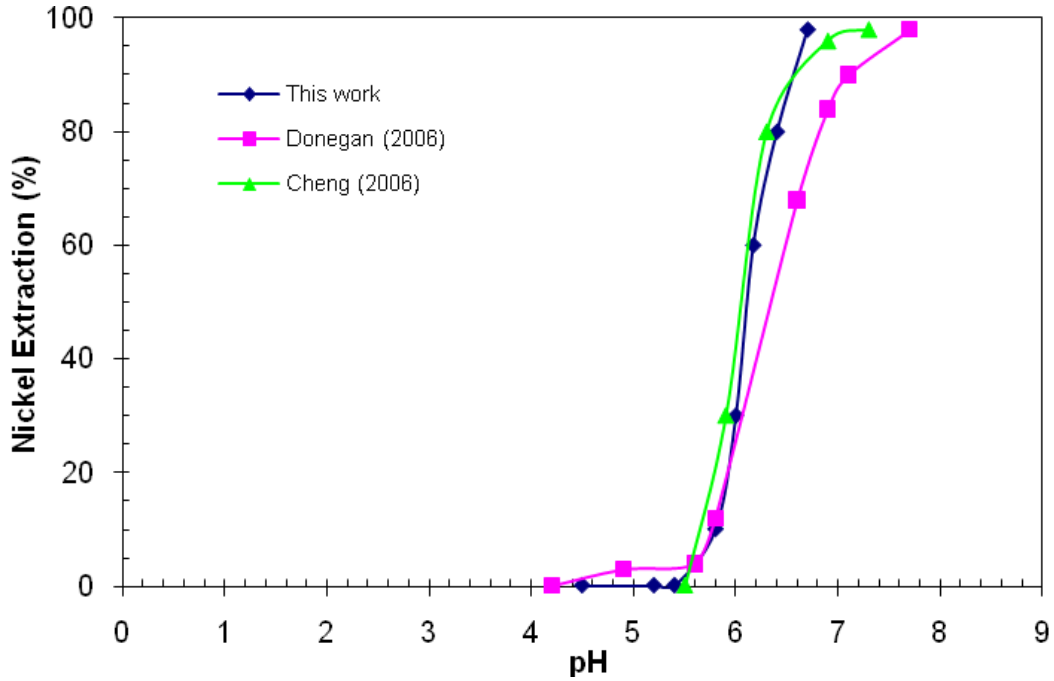


Figure 6-1. Nickel extraction isotherms for Versatic 10.

From these isotherms it is evident that: (1) the isotherm constructed in this work is comparable to those reported by Cheng (2006) and Donegan (2006), (2) an equilibrium pH of 6.5 should be targeted for complete nickel extraction, and (3) that the residual ammonia/ammonium in the PLS had no significant effect on nickel extraction, which is consistent with the results of Jaaskelainen and Paatero (1999). The slight difference in nickel extraction at higher pH values reported by Donegan (2006) may have been owing to co-extraction of calcium given the high concentration of calcium in his test solutions, and the achievement of maximum nickel extraction at a pH lower than that reported by Cheng (2006) could possibly be owing to the presence of an impurity in the solvent.

### 6.3.3 McCabe-Thiele Diagram Analysis

A McCabe-Thiele diagram analysis was carried out to determine the number of theoretical stages achieved within the ESX and sieve-plate columns. The equilibrium line data was generated by equilibrating PLS and solvent samples with phase ratios of A:O = 1:4, 1:2, 1:1, 2:1, 8:1 and 16:1 to pH 6.5 using ammonia gas. Analyses for the nickel content of the PLS and back calculation of the nickel concentration of the solvent

phase allowed the points on the equilibrium curve to be determined. The operating line, with a slope of O/A = 1/2, represents a flow ratio (A:O) of 2:1. Starting on the operating line at a nickel concentration of 3000 mg/L Ni, stages were drawn between the operating and equilibrium lines. The McCabe-Thiele diagram is shown in Figure 6-2.

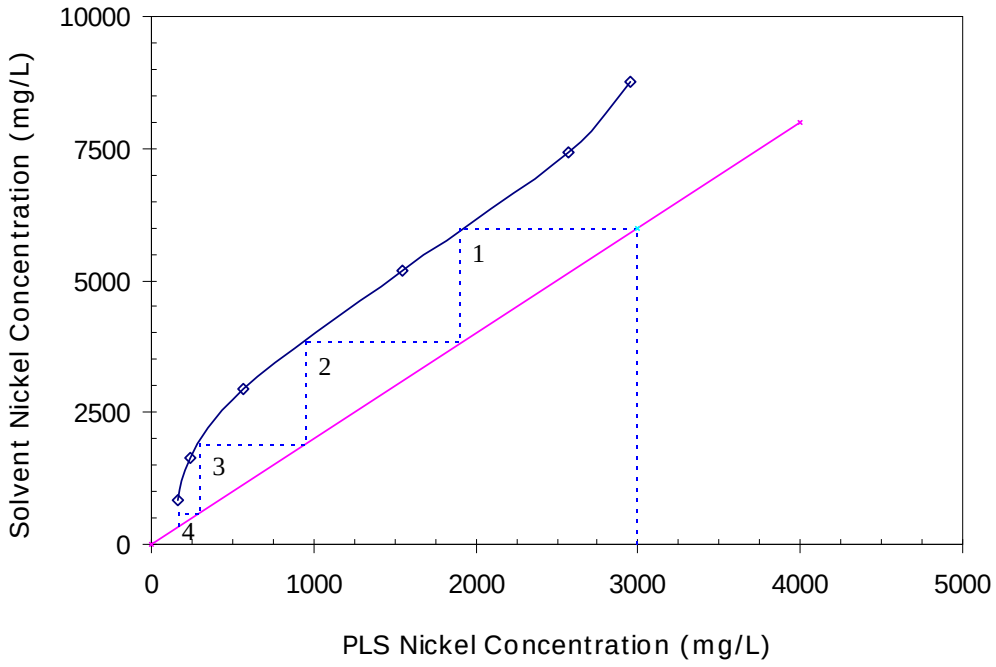


Figure 6-2. McCabe-Thiele diagram analysis for phase ratio of A:O = 2:1.

Analysis of the McCabe-Thiele diagram revealed that four theoretical stages are required to reduce the nickel concentration in the PLS from 3000 mg/L to about 150 mg/L. This is comparable to the values found previously under comparable conditions by Soldenhoff et al. (1998).

### 6.3.4 Optimisation of the Sieve-Plate Pulsed Column

The sieve-plate pulsed column was optimised by first generating flooding curves to establish approximate throughputs achievable over a range of phase ratios and pulsation intensities, and then undertaking mass transfer tests to verify optimum flux and also attain the optimum pulsation intensity – combination of pulsed frequency and pulsed amplitude – to minimise axial and back-mixing. Flooding occurs when insufficient

pulsation intensity is applied to the contents of the column, and is identified by the intended dispersed phase pooling and accumulating near the dispersed phase inlet.

The flooding curves were constructed as follows: For a given phase ratio, a pulsation intensity was selected and the combined flux incrementally increased until flooding occurred. This was repeated over a range of pulsation intensities, and the flooding points constituted the flooding curve. The procedure was then repeated for other phase ratios. The flooding curves for phase ratios of A:O = 2:1, 1:1 and 1:2 are shown in Figure 6-3.

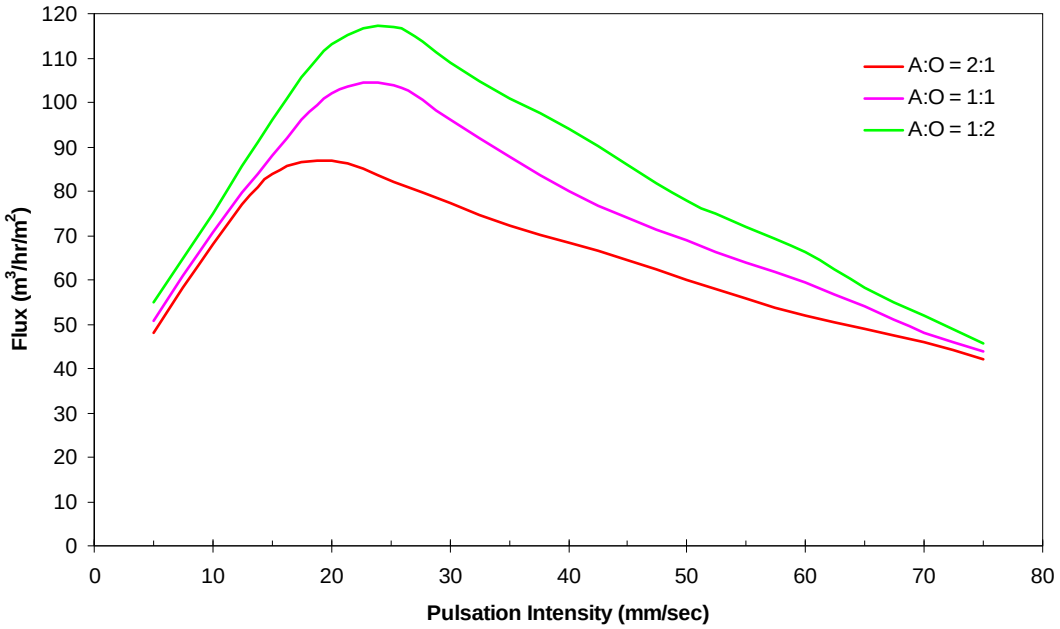


Figure 6-3. Pulsed column flooding curves for phase ratios of A:O = 2:1, 1:1 and 1:2. (Waters 2007)

The flooding curves collectively show that the column is more difficult to flood at moderate pulsation intensities; at low pulsation intensities the pulsation energy is insufficient to effect intimate dispersion and thus the system is more prone to flooding, and at high pulsation intensities the dispersed droplet size is smaller thus the system is more prone to emulsification.

For the phase ratio A:O = 2:1, which is a typical ratio for an extraction circuit, the highest combined (A + O) flux attained was 85 $m^3/hr/m^2$ with a pulsation intensity of 20 mm/s. This combined flux of 85 $m^3/h/m^2$ equates to an aqueous flux of 56 $m^3/h/m^2$.

Typically columns are operated at about 80% of the flooding capacity to allow for variation within column operation, giving a flux rate of 45 $m^3/h/m^2$. Further, considering that these flooding curves were produced under conditions with no mass transfer, the tendency for emulsification was decreased and therefore a lower flux between about 35 – 40 $m^3/h/m^2$ seemed appropriate. This is consistent with a flux of 37 $m^3/h/m^2$ reported to be appropriate for nickel SX systems (Ritcey 2006c).

Mass transfer tests, in which the solvent was pre-neutralised and thus the interfacial tension between the solvent and PLS was lower, were undertaken to validate the achievable flux and also optimise the pulsation intensity. This was done by first varying the pulsation intensity to determine the true achievable flux and then varying the pulsed frequency and amplitude to minimise axial and back mixing. This confirmed that a flux of 37 $m^3/h/m^2$ was appropriate. Fiigure 6-4 depicts the resulting dispersion.

Figure 6-4. Droplet dispersion achieved within the pulsed column after optimisation.

### 6.3.5 Preliminary Investigation into ESX Column Operation

Preliminary tests were undertaken to compare operation of the bench-scale and pilot-scale ESX columns and to establish baseline conditions for: (1) the electrostatic field strength, (2) the frequency of the electrostatic field, (3) the flow rates of the aqueous and organic phases and (4) the phase ratio for this piloting work.

The results of Chapter 4 as well as the results of previous studies (Heckley 2002; Steffens and Ibana 2005), indicated that an applied voltage of 5 kV/cm was approximately optimal for operation; lower applied voltages did not allow sufficient

dispersion and higher voltages reduced the size of the droplets such that their settling velocity was significantly lower than that required to prevent flooding. It was found that the dispersion observed in the pilot-scale column was markedly different from that observed in the bench-scale column, photographs of which are shown in Figure 6-5. Primarily, the droplets that were forming in the pilot-scale ESX column, as shown in Figures 6-5A and 6-5B, were significantly larger than those which had formed in the bench-scale column, as shown in Figure 6-5C. This may be attributed to a larger initial droplet size in the pilot-scale column owing to the larger PLS flow-rate into the column.

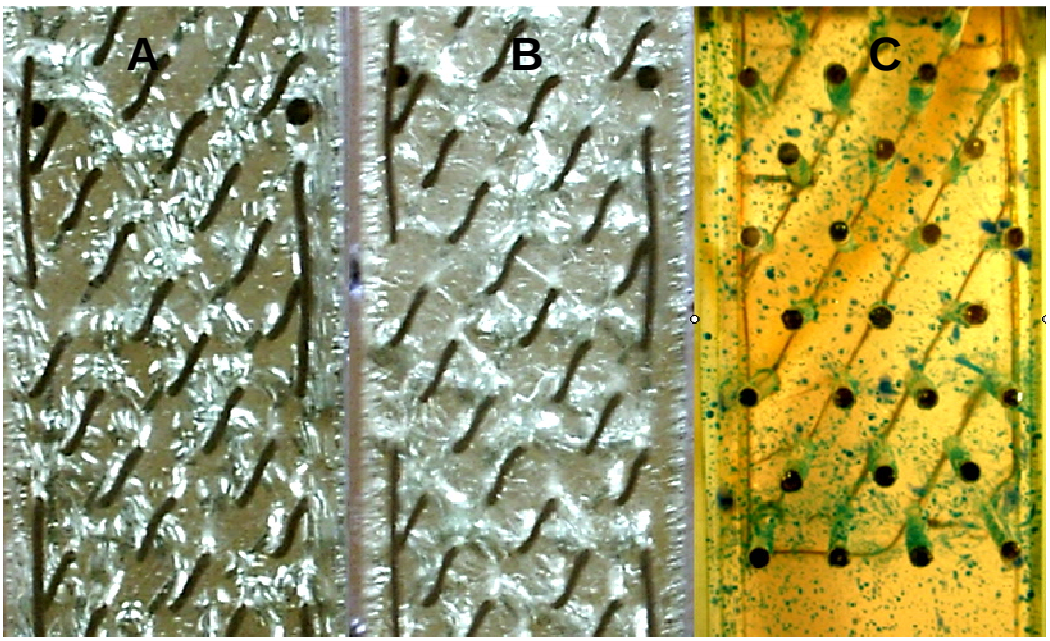


Figure 6-5. Droplet dispersion observed with horizontal rod electrodes. (A – Pilot-scale column with 0 kV/cm applied electrostatic field, B – Pilot-scale column with 5 kV/cm applied electrostatic field, C – Bench-scale column with 5 kV/cm applied electrostatic field).

The agitation observed in the pilot-scale column was also apparently different to that in the bench-scale column. In the bench-scale column, the droplets were clearly zigzagging; in the pilot-scale column the droplets were moving vigorously and moving between the rods in a manner that is analogous to a slinky travelling down a flight of stairs (Figure 6.5b). Varying the electrostatic field frequency was found to affect droplet motion and agitation, with the greatest droplet movement being estimated at a frequency

of 20 Hz; this frequency was used for early parts of this study prior to the frequency being optimised.

A phase ratio A:O = 2:1 is common for extraction circuits and therefore was used throughout this investigation. Also, with a feed nickel concentration of 3000 mg/L and a Versatic 10 concentration of 10% (v/v), the molar ratio nickel to Versatic 10 entering the column is approximately 1:5, meaning that the extractant (Versatic 10) is in excess and its availability in the system should not limit mass transfer.

The flow rate of PLS and solvent were each maintained at 20 L/h throughout the initial parts of this study. This was deemed an appropriate compromise between maintaining hydrodynamic conditions within the column comparable to the column operating at full capacity and minimising the risk of damaging the electrodes as well as minimising the amount of PLS that was required to be prepared.

## 6.4 Results and Discussions

### 6.4.1 The Effect of Electrostatic Field Strength on Nickel Extraction

The effect of the electrostatic field strength on column performance was determined by measuring the nickel extraction achieved over a range of electrostatic field strengths. The flow-rates of both the PLS and solvent phase were maintained at 20 L/h, and the electrostatic field frequency was maintained at 20 Hz. The results are summarised in Figure 6-6.

The overall trend in nickel extraction obtained was comparable to those obtained in bench-scale studies (Gu 1992; Steffens and Ibana 2005; Collard et al. 2005). The initial decreases in nickel extraction with increases in electrostatic field strength (0 - 2.5 kV/cm) indicated that the column was operating at droplet coalescence regime. The small increases in nickel extraction with further increases in electrostatic field strength signified the start of the dispersion regime although the field strengths were clearly insufficient to effect significant dispersion. Only when the electrostatic field strength reached 5.7 kV/cm did the nickel extraction exceed that obtained when no field was

applied, signifying the start of a significant dispersion regime. Electrostatic field strengths above 6.5 kV/cm were not explored to avoid damaging the electrode insulation by arcing.

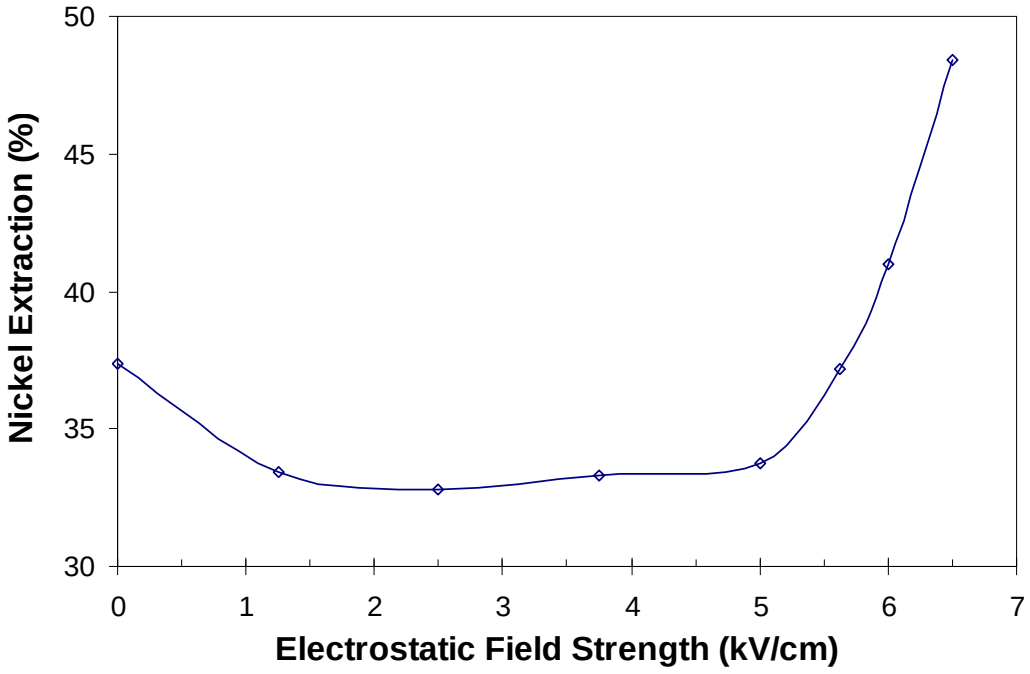


Figure 6-6. Effect of electrostatic field strength on nickel extraction.

The main difference between these results and those obtained in previous bench-scale studies (Steffens and Ibana 2005) was the significantly higher electrostatic field strength required to achieve optimal nickel extraction, which is a direct result of the electrode spacing and design. That is, the larger than expected PLS droplets together with the shortened electrode spacing did not allow for a good dispersion of droplets because droplets were sufficiently large to bridge oppositely charged electrodes. Although it was apparent that droplets were moving rather vigorously and thus, mixing well, it was clear, based on the extents of extraction, that droplet dispersion is critical to producing high metal extraction.

To increase the amount of dispersion either the initial droplet size needs to be decreased or the electrode spacing increased. An alternative spray head with smaller PLS discharge holes was tested but the droplet size was apparently similar to that achieved with the

original spray head; the high amount of PLS being delivered resulted in the individual PLS streams exiting the spray head to merge. A new electrode with larger electrode spacing was not constructed because of the extensive time required for its fabrication and fitting into the column. In addition, the higher voltages that would be required by an electrode arrangement with larger electrode spacing to allow a comparable electrostatic field strength to be maintained would place a higher load on the electrode insulation making it more prone to break down owing to arcing. Undertaking further investigations with an electrode arrangement with a larger electrode spacing and more robust electrode insulation is highly desirable but given the time required for this additional work being beyond that allowed for this research work, it was decided that they be included in the recommendation for further work.

### 6.4.2 The Effect of the Frequency of the Electrostatic Field on Nickel Extraction

The frequency of the electrostatic field influences droplet oscillation and lateral motion and thus mass transfer, as was shown in Section 4.5.2 of this work. As this electrode configuration differs from all those previously presented and the droplet dispersion-agitation regime within this contactor is unique, the effect of the applied frequency of the electrostatic field on nickel extraction had to be optimised.

To establish the optimum electrostatic field frequency, it was systematically varied from 20 to 50 Hz, while the electrostatic field strength was maintained at 6 kV/cm. The flow-rates of both the PLS and solvent phase were again maintained at 20 L/h. The results are summarised in Figure 6-7. This indicates that the optimal frequency of 40 Hz provided optimal oscillation and lateral motion of the droplets at the electrostatic field used in this particular column.

These results are consistent with those obtained in previous bench-scale studies (Collard 2011) except that in this present study low frequencies did not result in such large increases in extraction and also the maximum nickel extraction was achieved at a higher frequency; both of these differences may be attributed to the larger droplet sizes observed in this work. This is consistent with the proposal of Scott (1987) with regard to

the relationship of droplet size and droplet motion. The differences in physical properties of the PLS and solvent phases may have also contributed to differences in results.

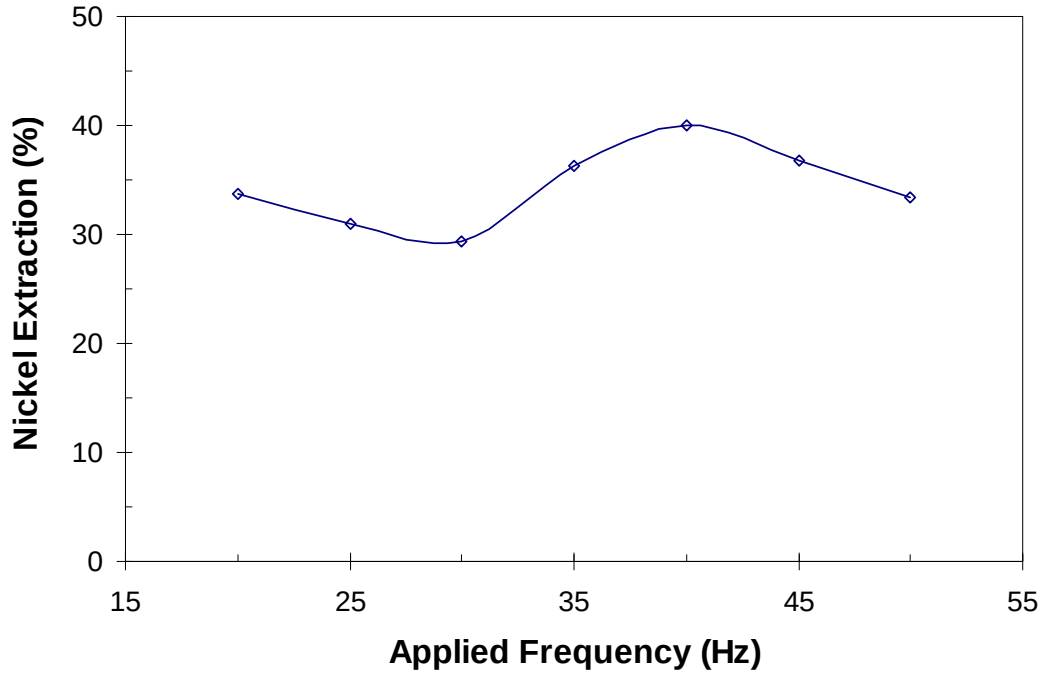


Figure 6-7. Effect of electrostatic field frequency on nickel extraction.

### 6.4.3 Determination of Maximum Flux

The maximum flux achievable within the ESX column used in this study was determined at various phase ratios by increasing the PLS and solvent flow rates stepwise until flooding occurred. All tests were carried out at an electrostatic field strength and frequency of 6 kV/cm and 40 Hz, respectively. The flooding curve obtained is shown in Figure 6-8.

The increases in the flux required to effect flooding with decreases in the phase ratio from 4:1 to 2:1 and thus, the proportion of A:O, may be attributed to the lessening tendency for phase inversion. The substantial decreases in the maximum aqueous flux achievable with further decreases in the phase ratio appeared to be due to greater upward flow of organic within the column hindering the downward flow of the dispersed aqueous droplets leading to flooding. Nonetheless, the maximum fluxes achievable within this column (35-55 $m^3/h/m^2$) were much higher than those achieved by previous

investigators on ESX columns ($9.15\times10^{-4}$ to 3.77 $m^3/h/m^2$) and comparable to that typically used in conventional sieve-plate pulsed columns treating a comparable chemical system, as detailed previously in Table 2-2. This result is particularly significant as it demonstrates that ESX columns are physically capable of tolerating the fluxes required for commercial application addressing what was perceived by many as the main limitation of the use of electrostatic agitation in solvent extraction.

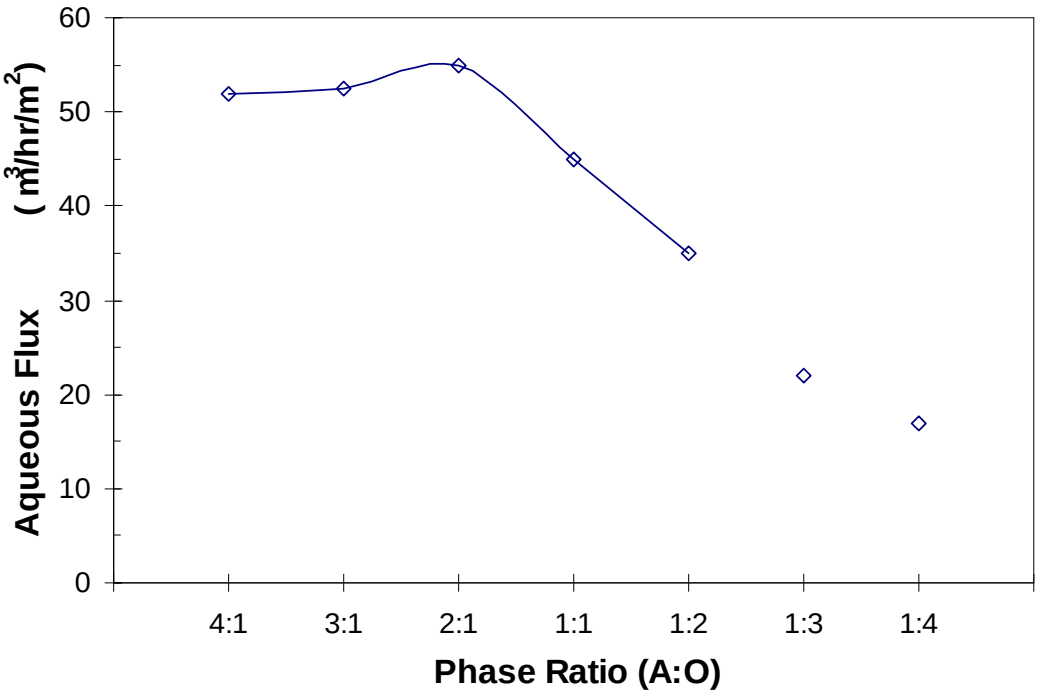


Figure 6-8. Effect of phase ratio on maximum aqueous flux. (Free points indicate flooding was not reached owing to pump capacity)

### 6.4.4 The Effect of Flux on Nickel Extraction

A good flux without adequate mass transfer would provide no advantage over conventional contactors. Thus, the effect of the flux on the nickel extraction at a 2:1 phase ratio, which provided maximum throughput in the column used in this study, was investigated. The results, summarised in Figure 6-9, showed increases in nickel extraction with increases in flux from 15-25 $m^3/h/m^2$, after which further increases in the flux to 40 $m^3/h/m^2$ yielded slight decreases in nickel extraction.

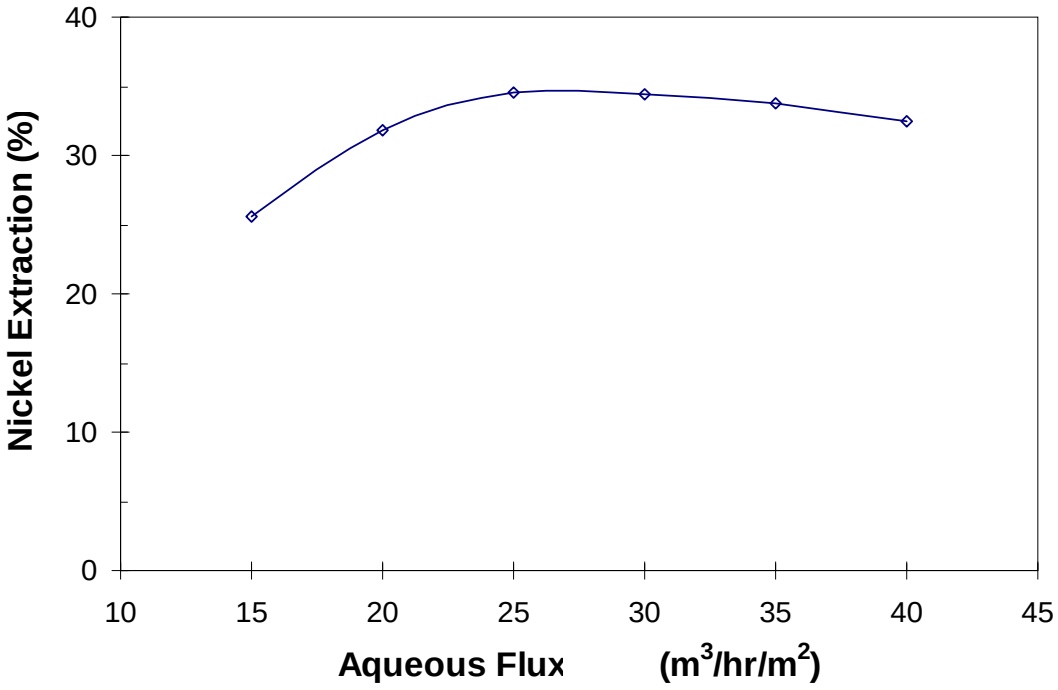


Figure 6-9. Effect of PLS flux on nickel extraction (A:O = 2:1).

This trend is comparable to that observed in conventional pulsed columns (Sege and Woodfield 1954), where the initial increases in extraction have been attributed to corresponding increases in dispersed phase hold-up and thus, contact time, and the ensuing slight decreases have been attributed to increases in droplet coalescence. Again, this is a major finding as it demonstrates that an ESX column can tolerate commercially applicable PLS fluxes while maintaining high mass transfer.

An attempt, however, to run the sieve-plate pulsed column at the same flux as the ESX column at 40 $m^3/hr/m^2$ failed due to flooding, which was attributed to the sieve-plates being a larger physical barrier to the downward PLS flow than the horizontal electrodes in the ESX column. This higher tolerance of ESX columns to flooding is a significant advantage that they have over conventional sieve-plate pulsed columns.

### 6.4.5 Comparison of Performance of the ESX Column and Sieve-Plate Pulsed Column

The ESX column and sieve-plate pulsed column were operated concurrently for 2.5 hours under conditions where the agitation provided was that found optimal for each but

the phase ratio and flux were the same for both. That is, both columns had a PLS flow rate of 70 L/hr and solvent flow rate of 35 L/hr, and thus a phase ratio of (A:O) = 2:1. The field conditions for the ESX column were an electrostatic field strength of 6.5kV/cm and frequency of 40 Hz, and the pulsing conditions for the pulsed column was a pulsation intensity of 20 mm/s. The pH of the feed solution was adjusted to 5.70 and the solvent was pre-neutralised with ammonia gas. The results of co-current operation are shown in Figure 6-10.

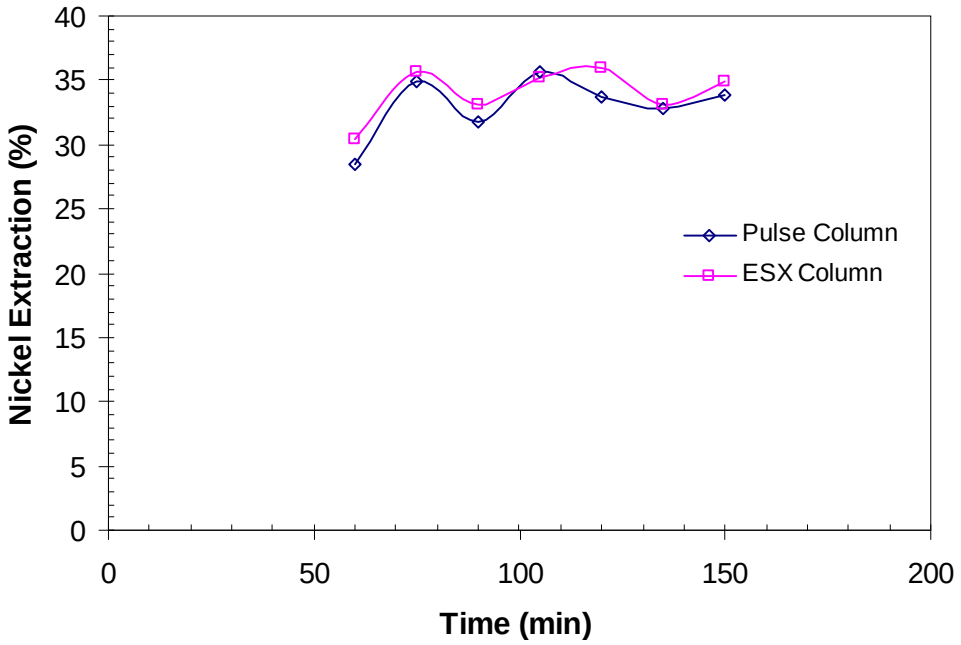


Figure 6-10. Nickel extraction achieved within the ESX column and sieve-plate pulsed columns during concurrent testing.

The extractions achieved by the use of the ESX column and the pulsed column are comparable at about 33% each. Whilst a nickel extraction of 33% is low compared to commercial operations, this result is good for two reasons. Firstly, it has demonstrated the agitation intensity that is achievable in an ESX column is comparable to that of commercially established columns. This is the first time that this has been achieved circumventing what the previous investigators thought was the major weakness of ESX columns. Secondly, this result indicates that similar to commercially established columns, adequate nickel extraction in ESX column can be achieved simply by increasing the height of the column.

The minor fluctuations in nickel extraction evident in Figure 6-10 are attributed to the manual operation of the columns, difficulty in maintaining steady interface levels within the lower settler and also temporary stalling of pumps. Also observed during the start-up of the columns was that the pulsed column required the PLS feed to be temporarily stopped to prevent the column from flooding.

To determine whether the extraction achieved in this testing was owing to limited agitation provided by the columns and not by other factors, such as the degree of solvent pre-neutralisation, samples of the loaded solvent and raffinate were collected and further contacted in a mixer. The result showed that further nickel extraction occurred, confirming that the extraction reaction was only limited by agitation and suggesting that a taller column would allow more than the 33% nickel extraction observed in the current column.

With both columns achieving about 33% nickel extraction, the raffinate nickel concentration was approximately 1750 mg/L. From the McCabe-Thiele diagram analysis undertaken, as was shown in Figure 6-2, a raffinate concentration of 1750 mg/L nickel is achieved in approximately 1.15 theoretical stages. Given that the active length of both columns is 3.60 metres, the height equivalent to a theoretical stage (HETS) is approximately 3.20 metres. Therefore, to reduce the raffinate nickel concentration to approximately 150 mg/L, an ESX or pulsed column with a 12.80 m active height is required. The differences in HETS achieved by the pulsed column in this study and that reported by Golding and Lee (1981), who also investigated the extraction of nickel using a sieve-plate pulsed column, may be attributed to differences in the applied flux and or temperature, both of which have been identified by Grinbaum (2006) and Ritcey (2006) as possible causes.

## 6.5 Conclusions

A comparative pilot-scale study on the performance of an ESX column and a sieve-plate pulsed column was undertaken and it was found that:

- The optimal electrostatic field conditions for the ESX column developed in this investigation were an electrostatic field strength of 6.5 kV/cm and an electrostatic field frequency of 40 Hz. These conditions allowed the highest amount of metal extraction. Significant improvement in extraction appeared readily achievable by increasing the electrode spacing to allow for greater droplet dispersion.
- The flux achievable within an ESX column is comparable to that achievable within a sieve-plate pulsed column, which is particularly significant as it disproves what was perceived by many as the main limitation of the use of electrostatic agitation in solvent extraction. The maximum PLS fluxes achieved at various phase ratios were in the range of 35-55 $m^3/h/m^2$, which are much higher than those achieved by previous investigators of ESX columns. At a phase ratio of A:O = 2:1 and PLS fluxes ranging from 20 to 40 $m^3/h/m^2$, metal extraction between 30 and 35% was maintained.
- The nickel extractions achieved with the sieve-plate pulsed column and the ESX column were comparable. From a McCabe-Thiele diagram analysis, the height equivalent to a theoretical stage for both was approximately 3.20 m.
- Under commercially applicable conditions, the performance of the ESX column is comparable to that of a sieve-plate pulsed column. Concurrent operation of the ESX column and sieve-plate pulsed column, with the performance of each optimised and both operating under comparable conditions, showed that the metal extraction achieved in both was comparable. A McCabe-Thiele diagram analysis showed a theoretical stage height of 3.20 m, requiring a 13 m column for complete extraction of nickel at 25 °C.

Chapter 7

# Conclusions and Recommendations

## 7.1 Conclusions

The commercial application of solvent extraction (SX) in hydrometallurgy has steadily increased over the past 50 years as the technique has been increasingly used for traditional and also for novel applications. With this extensive industrial application, limitations that are inherent to the design of contactors used have become apparent. That is, the high-shear mechanical agitation used in conventional SX contactors favours the formation of crud, non-uniform droplet size distributions and numerous ultra-fine droplets. Electrostatically assisted solvent extraction (ESX) contactors appear to eliminate these limitations and are therefore a promising alternative to mechanically agitated contactors.

In bench-scale studies ESX contactors have been found to provide high rates of mass transfer by simultaneously combining high interfacial area with high interfacial renewal, good control of contactor performance through precise control of droplet size, a substantial reduction of the energy requirement and also, literature suggests that problems inherent to mechanically agitated contactors such as high shear mixing can be eliminated. However, no commercial application has been realised, which may be attributed to a poor understanding of electrostatically assisted droplet dispersion over a range of commercially applicable solution properties, the designs of ESX contactors already proposed in literature being unsuitable for scale-up and the performance of an ESX contactor never having been evaluated on a pilot scale.

The main objectives of this study were, firstly, to further the understanding of electrostatic dispersion over a range of commercially used solution properties, secondly, to develop an ESX column suitable for commercial application and, thirdly, to construct and investigate the performance of a pilot-scale ESX column.

In pursuing the first objective it was found that:

- The viscosity of the PLS influences the number of ultra-fine droplets that are formed by electrostatic droplet dispersion. Initial increases in the PLS viscosity resulted in a slight decrease in the number of ultra-fine droplets forming and thus, an increase in the average dispersed droplet size. Further increases in the PLS viscosity resulted in an increase in the number of ultra-fine droplets and thus, a slight decrease in the average size of the dispersed droplets. This trend may be attributed to changes in hydrodynamic resistance of the droplet to deformation.
- The viscosity of the solvent influences whether a PLS droplet will break by the necking or jetting droplet dispersion mechanism. At low solvent viscosities, droplets were found to break predominantly by the necking mechanism, which resulted in a larger average droplet size owing to fewer ultra-fine droplets forming. At higher solvent viscosities, droplets were found to break predominantly by the jetting mechanism, which resulted in a smaller average droplet size owing to more ultra-fine droplets forming.
- The interfacial tension has a significant effect on droplet dispersion. Increases in the interfacial tension result in increases in the average dispersed droplet size of droplets larger than 100 μm but have only a negligible effect on the overall dispersed droplet size distribution. This is owing to increases in the interfacial tension resulting in increases in the number of ultra-fine droplets forming.
- The dispersion of a droplet of conducting liquid under the influence of an electrostatic field occurs largely by interfacial droplet polarisation and thus, the conductivity of the solvent is critical in allowing dispersion. Under the conditions used in the present study, droplet dispersion ceased completely when the conductivity of the solvent reached 80 pS/m.

In pursuing the second objective it was found that:

- An individual electrostatically assisted PLS disperser is not appropriate for a commercial ESX column. Although dispersers utilising DC- and AC-generated electrostatic fields allow more uniformly sized droplets and higher PLS fluxes,

respectively, they provide no substantial benefit to the performance of a commercially applicable ESX column.

- Droplet zigzagging is favoured at low applied field frequencies and droplet oscillation is favoured at high applied field frequencies. Within an ESX column, enhanced metal extraction seems achievable by operating sections of the column at different applied field frequencies to favour either zigzagging or oscillation.
- Flat-plate electrodes are unsuitable for application in a commercially used ESX column. These electrodes result in the formation of an excessive number of ultra-fine droplets, and this electrode arrangement does not provide sufficient facility to coalesce such droplets.
- The horizontal rod electrode promotes droplet charging owing to the rods being in the path of falling droplets. Charged droplets zigzag vigorously when located within a transient electrostatic field.
- The horizontal rod electrode arrangement seems the most suitable arrangement for droplet agitation within a commercially applicable ESX column. The horizontal rod electrode arrangement allowed continual droplet dispersion, droplet charging and droplet agitation, and also coalescence of ultra-fine droplets that formed during droplet dispersion.
- The horizontal rod electrode is also effective when used exclusively for coalescing ultra-fine aqueous droplets that are entrained within a solvent, and thus can be placed in a solvent settler to remove any entrained aqueous droplets.

In pursuing the third objective, a 5.5 m tall pilot-scale ESX column with an active length of 3.6 m and cross-sectional area of 20 $cm^2$ was constructed, an existing pilot-scale sieve-plate pulsed column was refurbished, and associated pilot plant equipment to allow concurrent testing of the columns was assembled. From these tests, it was found that:

- An electrostatic field strength of 6.5 kV and an applied electrostatic field frequency of 40 Hz yielded the highest metal extraction.

- The fluxes achieved with the pilot-scale ESX column were directly comparable to those commercially used in sieve-plate pulsed columns. Over the range of fluxes tested, both above and below that commercially used in sieve-plate pulsed columns, a metal extraction in excess of 30% was maintained.
- Operation of the ESX and sieve-plate pulsed columns concurrently, under comparable conditions and with each column individually optimised, showed that nickel extraction achieved by both columns was comparable. A McCabe-Thiele diagram analysis showed a theoretical stage height of 3.20 m, requiring a 13 m column for complete extraction of nickel at 25 °C. Further improvements to the design of the electrode spacing of the ESX column promise enhanced results.

## 7.2 Recommendations

While this study has contributed significantly to the understanding of electrostatic dispersion and agitation under industrially applicable conditions, as well as significantly advancing the technique towards commercialisation, further improvements and understanding of the technique may be achieved by:

- **A fundamental study into electrostatic droplet dispersion and agitation.** With a high-speed camera and laser particle sizer, data can be collected to verify droplet dispersion mechanisms and provide droplet size data with greater statistical confidence. Unfortunately the required instrumentation remains expensive at this time.
- **A fundamental study into mass transfer in electrostatic solvent extraction**. While droplet zigzagging, droplet oscillation as well as electromigration of metal and extractant species to the droplet interface influence the mass transfer rate, how much each of these factors quantitatively contribute remains unknown. Such data would assist in optimising an ESX column.
- **Improvement in the design of the pilot-scale ESX column**. The droplet dispersion observed in the pilot-scale ESX column was significantly different from that observed in the bench-scale ESX column, which was attributed to the

electrode spacing being too small. Manufacturing an electrode with a greater spacing and testing it on a pilot-scale promises to produce a more desirable dispersion and thus allow higher mass transfer rates.

- **Investigate alternative ESX contactor designs**. With the high mass transfer rates shown to be achievable in ESX contactors, a tall column arrangement may not necessarily be required. Instead simpler and shorter fibreglass tanks could be modified, with appropriate fittings and electrode frames inserted, which would allow a greatly reduced construction cost.
- **Investigations using other extraction systems**. Most of the ESX studies undertaken to date have used acidic extraction systems; few studies have used chelating and solvating systems. Additional work investigating the performance of ESX contactors with other extraction systems would significantly assist in further developing this technique.

# References


Allan, R. and Mason, S. 1962. Particle Behaviour in Shear and Electric Fields I – Deformation and Burst of Fluid Drops. *Proceedings of the Royal Society A* 267**:** 45-61.

Austin, L., Banczyk, L. and Sawistowski, H. 1971. Effect of Electric Field on Mass Transfer across a Plane Interface [Short Communication]. *Chemical Engineering Science* 26: 2120-2121.

Bailes, P. 1981. Solvent Extraction in an Electrostatic Field. *Ind. Eng. Chem. Process Des. Dev.* 20:564-570.

Bailes, P. and Wade, I. 1980. *International Solvent Extraction Conference*, 1980: *Electric Solvent Extraction*, Leige, Belguim: ISEC.

Basaran, O. and Scriven, L. 1982. *The Second International Colloquium on Drops and Bubbles*, November 19-21, 1981: *Profiles of electrified drops and bubbles*. California, United States.

Bircumshaw, L. and Riddiford, A. 1951. The Kinetics of the Dissolution of Zinc in Aqueous Iodine Solutions – Part II. *Journal of the Chemical Society*: 1490-1493.

Brazier-Smith, P. 1971. Stability and Shape of Isolated and Pairs of Water Drops in an Electric Field. *Physics of Fluids* 14(1): 1-6.

Briggs, M., Cheng, C. and Ibana, D. 2000. An Electrostatic Solvent Extraction Contactor for Nickel-Cobalt Recovery. *Minerals Engineering* 13:1281-1288.

Brunet, L., Prat, L., Wongkittipong, R., Gourdon, C., Casamatta, G. and Damronglerd, S. 2005. A New Pulsation Policy in a Disk and Doughnut Pulsed Column Applied to Solid-Liquid Extraction of Andrographolide from Plants. *Chemical Engineering Technology* 28(1): 110-118.

Cheng, C. 2006. Solvent Extraction of Nickel and Cobalt with Synergistic Systems Consisting of Carboxylic Acid and Aliphatic Hydroxime. *Hydrometallurgy* 84: 109-117.

Collard, J. 2011.Extraction of Cobalt from Pregnant Liquor Steams using Electrostatic Pseudo-Liquid Membrane. PhD diss. [Under Examination], Curtin University of Technology.

Collard, J., Ibana, D. and Browner, R. 2005. *Nickel and Cobalt 2005: Challenges in Extraction and Production*, August 21-24, 2005: *Extraction of cobalt from acidic leach solutions using Electrostatic Pseudo Liquid Membrane*. Calgary, Canada: MetSoc of CIM.

Donegan, S. 2006. Direct solvent extraction of nickel at Bulong operations. *Minerals Engineering* 19: 1234-1245.

Donegan, S. 2001. Development of a Sieve-Plate Pulsed Column for Hydrometallurgical Solvent Extraction. Honours diss., Curtin University of Technology.

Eow, J. and Ghadiri, M. 2002. Electrostatic enhancement of coalescence of water droplets in oil: a review of the technology [Short communication]. *Chemical Engineering Journal*, 85: 357–368.

Galvin, C. 1984. Design Principles for Electrical Coalescers. *IChemE Symposium Series* 88: 101-113.

Garton, C. and Krasucki, Z. 1964. Bubbles in insulating Liquids: Stability in an Electric Field. *Proceedings of the Royal Society A* 280: 211-226.

Goldburg, A. and Florsheim, B. 1966. Transition and Strouhal Number for the Incompressible Wake in Various Bodies. *Physics of Fluids* 9: 45-50.

Golding, J. and Lee, J. 1981. Recovery and Separation of Cobalt and Nickel in a Pulsed Sieve-Plate Extraction Column. *Ind. Eng. Chem. Process Des. Dev.* 20(2): 256-261.

Godfrey. J. 1994. Mixers. In *Liquid-Liquid Extraction Equipment*, eds J.C. Godfrey and M.J. Slater, 399. Chichester: John Wiley & Sons Ltd.

Grinbaum, B. 2006. The Existing Models for Simulation of Pulsed and Reciprocating Columns – How Well do they Work in the Real World?. *Solvent Extraction and Ion Exchange* 24(1): 795-822.

Gu, Z. 1990. A New Liquid Membrane Technology – Electrostatic Pseudo Liquid Membrane. *Journal of Membrane Science*, 52: 77-88.

Gu, Z., Zhou, Q. and Jin, L. 1990. Recovery of Nickel (II) from Rinse Water from Nickel Plating with Liquid Membranes. *Water Treatment*, 5: 170-178.

Gu, Z., Wu, Q., Zheng, Z., Li, X., Jiang, Y., Tang, C. and Lin, P. 1994. Laboratory and Pilot Plant Test of Yttrium Recovery from Wastewater by Electrostatic Pseudo Liquid Membrane. *Journal of Membrane Science*, 93: 137-147.

Hanson, C. 1982. *Proceedings of a NATO Advanced Research Institute on Hydrometallurgical Process Fundamentals*, July 25-31, 1982: *Equipment Selection and Design for Metals Solvent Extraction*. Cambridge, UK: Plenum Press, New York.

Heatchcote, M.J., 1998, *J and P Transformer Handbook*, Biddles Ltd.

He, W., Chang, J. and Baird, M. 1997. Enhancement of Interphase Mass Transfer by a Pulsed Electric Field. *Journal of Electrostatics* 40 & 41: 259-264.

Heckley, P. 2002. Extraction and Separation of Cobalt from Acidic Nickel Laterite Leach Solutions using Electrostatic Pseudo Liquid Membrane (ESPLIM). PhD diss., Curtin University of Technology.

Heckley, P., Ibana, D. and McRae, C. 2002. *International Solvent Extraction Conference*, March 17-21, 2002: *Extraction and Separation of Nickel and Cobalt by Electrostatic Pseudo Liquid Membrane (ESPLIM)*. Cape Town, South Africa: Chris van Rensburg Publications Pty. Ltd.

Huh, C. and Mason, S. 1975. A Rigorous Theory of Ring Tensiometry, *Colloid and Polymer Science*, 253: 566-580.

Hund, M. and Lancelot, F. 1986. *International Solvent Extraction Conference*, September 11-16 1986: *Interfacial Transfer under Electrostatic Field in Solvent Extraction.* Munich, Germany: DECHEMA.

Hunt von Herbing, I. and Keating, K. 2003. Proceedings of the 26th Annual Larval Fish Conference, August 20-23, 2003. Temperature-induced changes in viscosity and its effects on swimming speed in larval haddock. Santa Cruz, CA: Institute of Marine Research.

Iyer, P. and Sawistowski, H. 1974. *International Solvent Extraction Conference*, September 8-14, 1974: *Effect of Electric Field on Mass Transfer across a Plane Interface*. Lyon, France.

Jääskeläinen, E. and Paatero, E. 2000. Characterisation of Organic Phase Species in the Extraction of Nickel by Pre-neutralised Versatic 10. *Hydrometallurgy* 55:181-200.

Jääskeläinen, E. and Paatero, E. 1999. Properties of the Ammonium Form of Versatic 10 in a Liquid-Liquid Extraction System. *Hydrometallurgy* 51: 47-71.

Jeffreys, G. 1987. Review of the Design of Liquid Extraction Equipment. *Chemistry and Industry* 6: 181-185.

Jonassen, N. 2002. *Electrostatics*. Kluwer Academic Publishers.

Kowalski, W. and Ziolkowski, Z. 1981. Increase in Rate of Mass Transfer in Extraction Columns by Means of an Electric Field. *International Chemical Engineering*. 21(2): 323-327.

Lerner, O. 2006. Bateman Pulsed Columns. In *Solvent Extraction: Principles and Practice*, ed. G. Ritcey. 334-349. Canada: G.M. Ritcey and Associates.

Martin, L., Vignet, P., Fombarlet, C. & Lancelot, F. 1983. Electrical Field Contactor for Solvent Extraction, *Separation Science and Technology*, 18, (14&15): 1455-1471.

McEwan, A. D., de Jong, L. N. J., (1966). Addendum, *Proceedings of the Royal Society A* 291, 166.

Melcher, J. 1976. Electric Fields and Forces in Semi Insulating Liquids. *Journal of Electrostatics*. 2: 121-132.

Melcher, J. and Taylor, G. 1969. Electrohydrodynamics: A Review of the Role of Interfacial Shear Stresses. *Annual Review of Fluid Mechanics.* 1: 111-146.

Octel Company. 2003. *Safety Data Sheet – Octastat® 3000* [Brochure]. Cheshire UK: The Associated Octel Company Ltd.

Pohl, H. 1973. Nonuniform Field Effects: Dielectrophoresis. In *Electrostatics and its Applications*, ed. A. Moore, 336-361. Canada: Wiley Interscience.

Proceedings of the 3rd International SX Workshop. 2003. *State of the Art and Future Directions in Solvent Extraction*. [Workshop Proceedings]. Digby: ICST.

Raju, G. 2003. *Dielectrics in Electric Fields*. Marcel Dekker Inc.

Ritcey, G. 1980. Crud in Solvent Extraction Processing – A Review of Causes and Treatment. *Hydrometallurgy* 5: 97-107.

Ritcey, G. 2004. Industrial Solvent Extraction Processes. In *Solvent Extraction Principles and Practice*, eds. J. Rydberg, M. Cox, C. Musikas and G. Choppin, 293. New York: Marcel Dekker.

Ritcey, G. 2006a. Solvent Extraction in Hydrometallurgy: Present and Future. *Tsinghua Science and Technology* 11 (2): 137-152.

Ritcey, G. 2006b. *Solvent Extraction: Principles and Applications to Process Metallurgy – Vol. 2*. Ottawa: G.M. Ritcey and Associates Inc.

Ritcey, G. 2006c. *Solvent Extraction: Principles and Applications to Process Metallurgy – Vol. 1*. Ottawa: G.M. Ritcey and Associates Inc.

Rosenkilde, C. 1969. A Dielectric Fluid Drop in an Electric Field. *Proceedings of the Royal Society A* 312: 473-494.

Sato, M. 1990. *International Solvent Extraction Conference*, July 18-21, 1990: *Formation of Uniformly-Sized Emulsions by Means of Applied Electrostatic Field*. Kyoto, Japan: Elsevier Science Publishers B.V.

Scott, T. 1987. Surface Area Generation and Droplet Size Control Using Pulsed Electrostatic Fields [R&D Notes]. *J. AIChE* 33(9): 1557-1559.

Scott, T. 1989. Use of Electric Fields in Solvent Extraction: A Review and Prospectus. *Separation and Purification Methods*. 18(1): 65-109.

Scott, T. and Sisson, W. 1988. Droplet Size Characteristics and Energy Input Requirements of Emulsions formed using High-Intensity Electric Fields, *Separation Science and Technology*. 23(12+13):1541-1550.

Scott, T. and Wham, R. 1987. Surface Area Generation and Droplet Size Control in Solvent Extraction Systems Utilising High Intensity Electric Fields. United States Patent 4,767,515, filed July 30, 1987 and issued Aug. 30, 1988.

Scott, T. and Wham, R. 1989. An Electrically Driven Multistage Counter-current SX Device: The Emulsion Phase Contactor. *Ind. Eng. Chem. Res.*, 28, 94-97.

Scott, T., Basaran, O. and Byers, C. 1990, Characteristics of Electric-Field-Induced Oscillations of Translating Liquid Droplets, *Ind. Eng. Chem. Res.* 29: 901-909.

Scott, T., DePaoli, D. and Sisson, W. 1994. Further Development of the Electrically Driven Emulsion-Phase Contactor. *Ind. Eng. Chem. Res.* 33: 1237-1244.

Sege, G. and Woodfield, F.W. 1954. Pulsed Column Variables. *Chemical Engineering Progress* 50 (8): 396-402.

Sherwood, J. 1991. The Deformation of a Fluid Drop in an Electric Field: A Slender Body Analysis. *J. Physics A* 24: 4047-4053.

Slater, M. 1978. *Solvent Extraction Technology: Course Notes for AMF Workshop*, November 20-24, 1978*: Fundamental Aspects of Column Design*. Adelaide, SA: Australian Mineral Foundation.

Smoot, L., Mar, B. and Babb, A. 1959. Flooding Characteristics and Separation Efficiencies of Pulsed Sieve-Plate Extraction Columns. *Industrial and Engineering Chemistry* 51 (9): 1005-1010.

Soldenhoff, K., Hayward, N. and Wilkins, D. 1998. *TMS Extraction and Processing Division Congress*, February 15-19, 1998: *Direct Solvent Extraction of Cobalt and Nickel from Laterite-Acid Pressure Leach Liquors*. San Antonio, TX: The Minerals, Metals and Materials Society.

Steffens, M. and Ibana, D. 2005. *Nickel and Cobalt 2005: Challenges in Extraction and Production*, August 21-24, 2005. *Extraction of nickel from acidic leach solutions using Electrostatic Pseudo Liquid Membrane*. Calgary, Canada: MetSoc of CIM.

Stewart, G. and Thornton, J. 1967. Charge and Velocity Characteristics of Electrically Charged Droplets, Part II: Preliminary Measurements of Droplet Charge and Velocity. *IChemE Symposium Series* 26: 37-42.

Suyama, T. Awakura, Y., Hirato, T., Konto, M. and Majima, H. 1993. Extraction and Stripping Characteristics of Ni(II) with D2EHPA under High Electrostatic Field. *Materials Transactions JIM* 34(1): 37-42.

Taylor, G. 1964. Disintegration of Water Droplets in an Electric Field. *Proceedings of the Royal Society A* 280: 383-397.

Taylor, G. 1966. Studies in Electrohydrodynamics I: The Circulation Produced in a Drop by an Electric Field. *Proceedings of the Royal Society A* 291: 159-166.

Thornton, J. 1968. The Applications of Electrical Energy to Chemical and Physical Rate Processes. *Reviews of Pure and Applied Chemistry* 18: 197-218.

Thornton, J. 1989. A method of enhanced solvent extraction and apparatus therefore. European Patent 356,030-B1, filed July 31, 1989 and issued Oct. 13, 1993.

Thornton, J. and Brown, B. 1966. Liquid/Fluid Extraction Process. UK Patent 1,205,562, filed June 29, 1966 and issued Sept. 16, 1970.

Thunaes, A. and Colborne, G. 1969. *Proceedings of the Ninth Commonwealth Mining and Metallurgical Congress*, 1969: *Pulsed columns for solvent extraction from aqueous solutions and slurries*. London, UK: The Institution of Mining and Metallurgy.

Torza, S., Cox, R. and Mason, S. 1971. Electrohydrodynamic Deformation and Burst of Liquid Drops. *Proceedings of the Royal Society A* 269: 295-319.

Tsouris, C., Shin, W. and Yiacoumi, S. 1998. Pumping, Spraying and Mixing of Fluids by Electric Fields. *The Canadian Journal of Chemical Engineering* 76: 589-599.

Usami, T., Enokida, Y. and Suzuki, A. 1993. Application of Electrically Driven Liquid-Liquid Dispersion to Solvent Extraction Using Tri-n-Buthyl Phosphate. *Journal of Nuclear Science and Technology* 30(10): 1017-1023.

Vancas, M. 2003. Pulsed Column and Mixer-Settler Applications in Solvent Extraction. *JOM* 55 (7): 43-45.

Warren, K. and Prestridge, F. 1979. Apparatus for Application of Electrostatic Fields to Mixing and Separating Fluids, United States Patent 4,161,439 filed on Apr. 3, 1978 and issued Jul. 17, 1979.

Waters, T. 2007. Direct Extraction of Nickel from Pressure Acid Leach Solutions by Sieve-Plate Pulsed Column using Versatic 10. Honours diss., Curtin University of Technology.

Weatherley, L., Campbell, I., Slaughter, J. and Kirton, D., 1990. Electrically enhanced extraction of penicillin G into dichloromethane. *Journal of Chemical Technology and Biotechnology*: 48, 427–438.

Wildberger, A. and Bart, H. 2002. *International Solvent Extraction Conference*, March 17-21, 2002: *Influencing the Rate of Mass Transfer in Reactive Extraction using High Voltage*. Cape Town, South Africa: Chris van Rensburg Publications Pty. Ltd.

Williams, T. , Bailey, A. and Broan, C., 1997, Ion Extraction Using the Electrostatic Pseudo Liquid Membrane Technique, *Journal of Electrostatics*, 40&41, 729-734.

Yamaguchi, M. Sugaya, H. and Katayama, T. 1988. Hydrodynamic Behaviour of Dispersed Phase in a Spray Column with an Electric Field for Liquid-Liquid Extraction. *Journal of Chemical Engineering of Japan* 21: 179-183.

Yamaguchi, M., Sugaya, H. and Katayama, T. 1989. Liquid-Liquid Extraction Characteristics of a Spray Column with a DC Electric Field. *Journal of Chemical Engineering of Japan* 22: 25-29.

Yamaguchi, M. 1995. Application of Electric Fields to Solvent Extraction. In *Electrical Field Applications in Chromatography and Chemical Processes*, ed. T. Tsuda, 185-203. Weinheim: VCH Publishers.

Yamaguchi, M. and Kanno, M. 1996. International Solvent Extraction Conference, 19-23 March 1996: Hydrodynamics in an Electrostatic Liquid-liquid Contactor – Hold-up, Drop Size and Drop Velocity. Melbourne, Australia: University of Melbourne Press.

Yamaguchi, M. 1997. Extractive Separation of Pr and Nd by D2EHPA in the Presence of Water Soluble Complexing Agents using and Electrostatic Liquid-Liquid Contactor. *Trans. IChemE* 75: 447-452.

Yang, X., Gu, Z. and Wang, D. 1995. Extraction and Separation of Scandium from Rare Earths by Electrostatic Pseudo Liquid Membrane, *Journal of Membrane Science*, 106(1-2), 131-145.

Yang, X. Gu, Z. & Fane, A. 1998. Multicomponent separations by a combined extraction/electrostatic pseudo-liquid membrane: (I): Separation of Al, La, Sm, and Y. *Hydrometallurgy* 49(3): 275-288.

Yang, X. Gu, Z. & Fane, A. 1999. Multicomponent separation by a combined extraction/electrostatic pseudo-liquid membrane (II): extraction and group separation of rare earths from simulated rare earth ore leach solutions. *Hydrometallurgy* 53(1): 19-29.

Yoshida, F., Yamaguchi, M. and Katayama, T. 1986. An Experimental Study of Electrohydrodynamic Dispersion from a Liquid Film Flowing Down an Inclined Plate into a Continuous Phase. *Journal of Chemical Engineering of Japan* 19: 1-7.

Yoshida, F., Yamaguchi, M. and Katayama, T. 1988a. An Experimental Study of Electrohydrodynamic Dispersion from a Liquid Film Flowing Down an Inclined Plate into a Continuous Liquid Phase. *Journal of Chemical Engineering of Japan* 19 (1): 1-7.

Yoshida, F., Yamaguchi, M. and Katayama, T. 1988b. Characteristics of Electrical Dispersion from Water Film Flowing Down an Inclined Plate into a Dielectric Liquid Phase – Drop diameter, Drop Velocity and Dispersed-phase Hold-Up. *Journal of Chemical Engineering of Japan* 21(2): 123-128.

Zeleny, J. 1916. Instability of Electrified Liquid Surfaces. *Physical Review* 10:1-6.

Zhou, Q. and Gu, Z. 1988. Studies on the Extraction of $Eu^{3+}$ by Means of Electrostatic Pseudo Liquid Membrane. *Water Treatment* 3: 127-135.

# APPENDICIES

# APPENDIX A - DROPLET SIZING

## Appendix A1: Droplet Sizing Procedure

(1) Photograph selection

Digital photographs taken under the required experimental condition were compared, and the most representative and clear photograph(s) selected for droplet size analysis.

(2) Conversion of raster image to vector image (i.e. .jpg to .vff)

Using raster-to-vector image conversion software, VExtractor 2.95, the droplets and size scale in the raster photograph were manually defined; the defined droplets and scale were then saved as a vector image. Figure 1 shows a screen image of dispersed droplets in a raster photograph were being manually defined by circling each individual droplet. Manual definition was required because the software could not adequately define droplet boundaries.

Figure 1. Conversion of raster image to vector image using VExtractor 2.95.

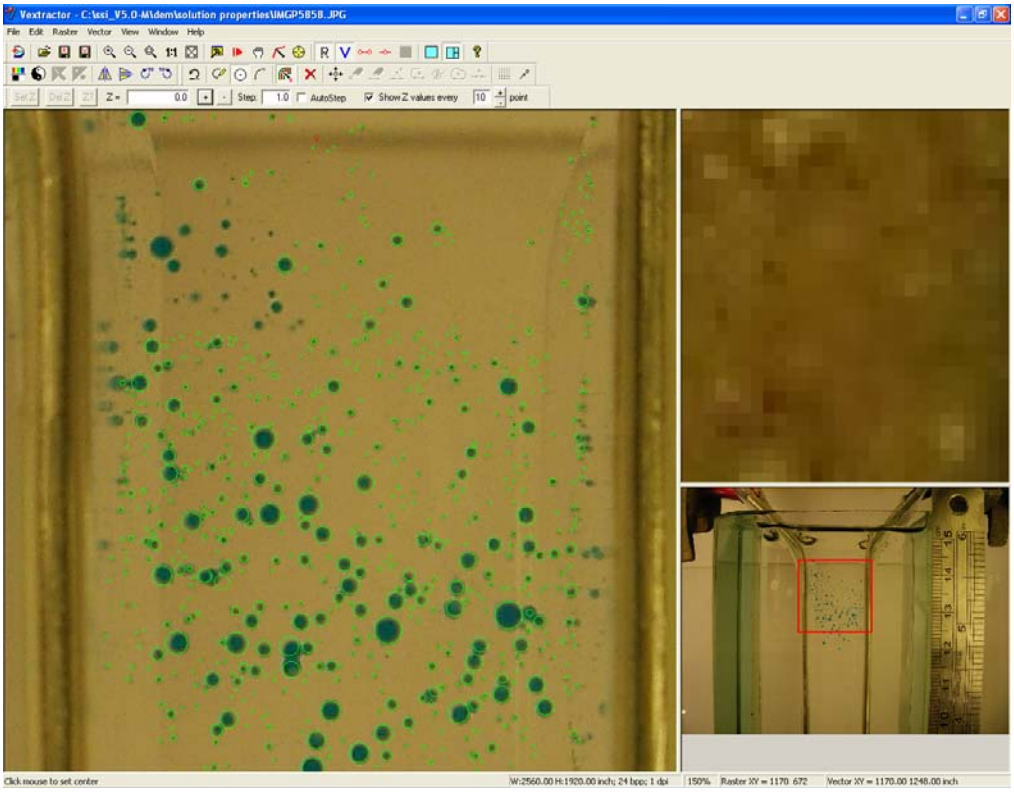


(3) Conversion between vector image formats and image scaling

The vector image file was analysed using a CAD application, Surpac Vision 5.0 (Surpac). Firstly, the vector image file was converted from '.vff' to '.dxf' format for compatibility with required Surpac functions.

The resulting '.dxf' file was then opened in Surpac, which allowed viewing of the droplet dispersion and sizing scale, as shown in Figure 2. The dispersion is the cluster of circles on the left side of the viewing pane and the sizing scale is the 5 circles, which together represent a distance of 5-mm, on the right side of the viewing pane.

Figure 2. The vector image of droplet dispersion in the Surpac software.

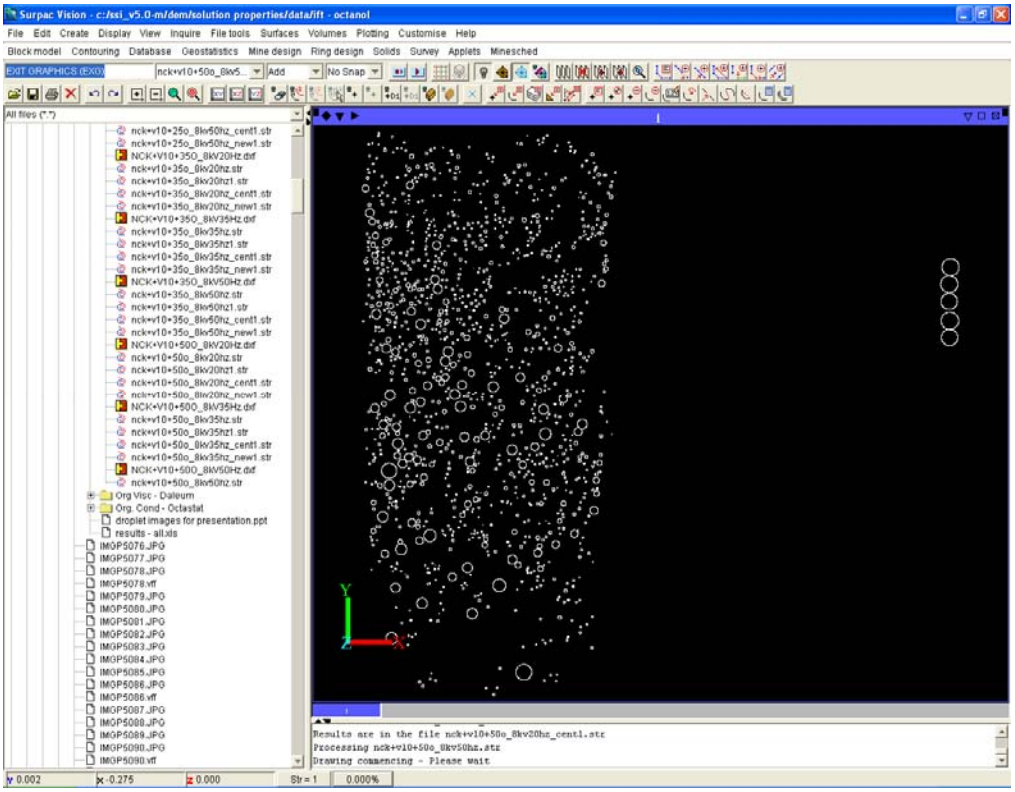


The "virtual" distance between the ends of the 5-mm scale was measured, the scale deleted and the vector file saved. The virtual distance measured was divided by 5 to provide the virtual distance of 1-mm, which was then inversed to provide the scale factor. This was used for rescaling the image so that the droplet data was accurate.

(4) Rescaling and calculation of cross-sectional areas of droplets

The image was rescaled and the area of each of the droplets calculated with the aid of a macro. The macro was opened, the input file and scale factor were specified, as shown in Figure 3, and after calculating the cross-sectional area of each droplet, a string (.str) file was created with all droplet area data.

This string file was opened with Microsoft Excel, and the droplet area data copied into a pre-formatted template, as shown in Figure 4. Here the diameter of each droplet was calculated using the relationship $A = \pi(d/2)^2$.

Figure 3. Macro view of entering in data for droplet area analysis.

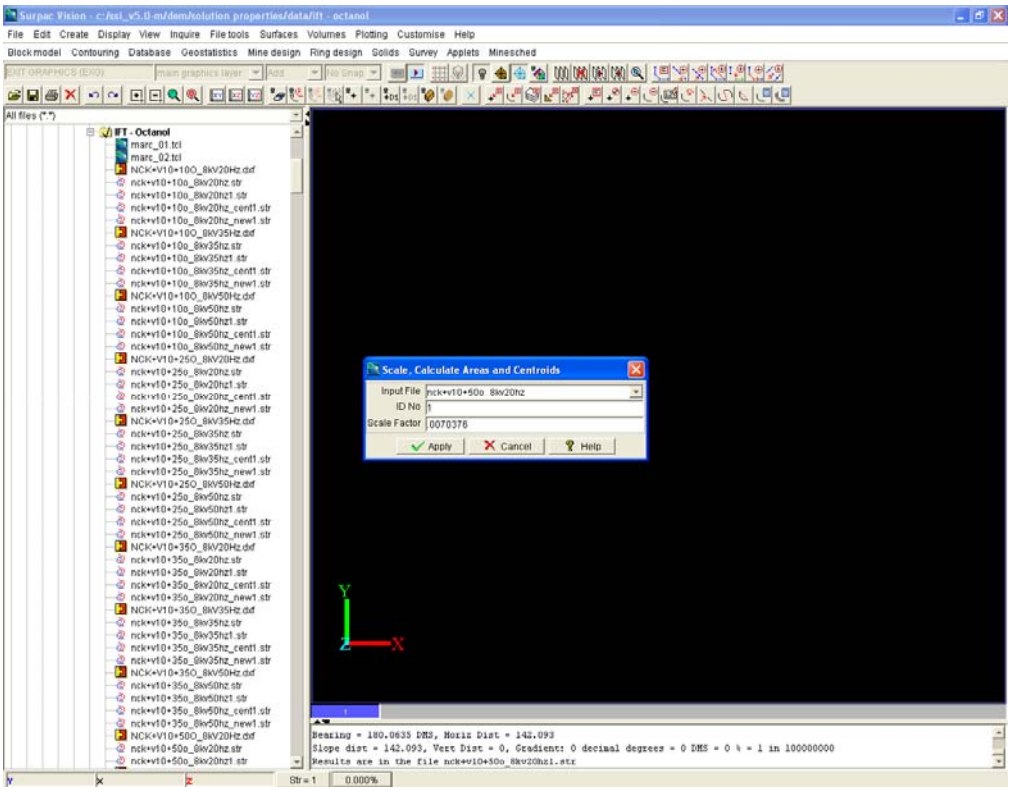


Figure 4. Spreadsheet where droplet diameters are calculated and tabulated.

| | | | | | | | | | | | | | | | | | |
|---|---|---|---|---|---|---|---|---|---|---|---|---|---|---|---|---|---|
| 1 | Aqueous Flowrate (mL/hr) | | 400 mL/hr | | | | | | | | | | | | | | |
| 2 | Cone Disperser | | | | | | | | | | | | | | | | |
| 3 | | | | | | | | | | | | | | | | | |
| 4 | Applied Voltage (kV) | | | | Applied Voltage (kV) | | | | Applied Voltage (kV) | | | | Applied Voltage (kV) | | | | |
| 5 | 0 | | | | 1 | | | | 1.5 | | | | 2 | | | | |
| 6 | Statistics | | | | Statistics | | | | Statistics | | | | Statistics | | | | |
| 7 | Average: | 0.910088 | | | Average: | 0.509937 | | | Average: | 0.305744 | | | Average: | 0.284412 | | | Average: |
| 8 | Standard Deviation: | 0.171608 | | | Standard Deviation: | 0.409873 | | | Standard Deviation: | 0.314486 | | | Standard Deviation: | 0.285222 | | | Standard |
| 9 | Maximum diameter: | 1.047082 | | | Maximum diameter: | 1.364907 | | | Maximum diameter: | 1.507837 | | | Maximum diameter: | 1.324481 | | | Maximum |
| 10 | Minimum diameter: | 0.207005 | | | Minimum diameter: | 0.139187 | | | Minimum diameter: | 0.130931 | | | Minimum diameter: | 0.066272 | | | Minimum |
| 11 | Population: | 26 | | | Population: | 71 | | | Population: | 276 | | | Population: | 321 | | | Populatio |
| 12 | | | | | | | | | | | | | | | | | |
| 13 | | | | | | | | | | | | | | | | | |
| 14 | | | | | | | | | | | | | | | | | |
| 15 | | | | | | | | | | | | | | | | | |
| 16 | | | | | | | | | | | | | | | | | |
| 17 | | | | | | | | | | | | | | | | | |
| 18 | | | | | | | | | | | | | | | | | |
| 19 | | | | | | | | | | | | | | | | | |
| 20 | | | | | | | | | | | | | | | | | |
| 21 | Raw Data | | | | Raw Data | | | | Raw Data | | | | Raw Data | | | | |
| 22 | 1.047082 | 3.44438 | | | 1.364907 | 5.852698 | | | 1.507837 | 7.14264 | | | 1.324481 | 5.511142 | | | 1.396818 |
| 23 | 1.001168 | 3.148934 | | | 1.279872 | 5.146154 | | | 1.309945 | 5.390838 | | | 1.258278 | 4.973966 | | | 1.30372 |
| 24 | 0.990344 | 3.081216 | | | 1.201796 | 4.537442 | | | 1.244527 | 4.865846 | | | 1.258263 | 4.973848 | | | 1.21759 |
| 25 | 0.990304 | 3.080964 | | | 1.189624 | 4.445998 | | | 1.223541 | 4.703132 | | | 1.193866 | 4.477766 | | | 1.193374 |
| 26 | 0.983852 | 3.040948 | | | 1.174805 | 4.335922 | | | 1.195244 | 4.488104 | | | 1.192103 | 4.464544 | | | 1.150654 |
| 27 | 0.981726 | 3.02782 | | | 1.158217 | 4.214342 | | | 1.180674 | 4.379352 | | | 1.192051 | 4.464156 | | | 1.140756 |
| 28 | 0.981705 | 3.027694 | | | 1.144821 | 4.117418 | | | 1.130638 | 4.016028 | | | 1.156581 | 4.202446 | | | 1.107855 |
| 29 | 0.981698 | 3.027652 | | | 1.108613 | 3.86109 | | | 1.121192 | 3.949208 | | | 1.125873 | 3.982252 | | | 1.089987 |
| 30 | 0.981646 | 3.027328 | | | 1.10157 | 3.812184 | | | 1.121141 | 3.94885 | | | 1.125832 | 3.981964 | | | 1.086548 |
| 31 | 0.981635 | 3.027262 | | | 1.079379 | 3.660142 | | | 1.121129 | 3.948762 | | | 1.05963 | 3.527432 | | | 1.065323 |
| 32 | 0.981627 | 3.02721 | | | 1.058523 | 3.520066 | | | 1.121089 | 3.948478 | | | 1.05963 | 3.527428 | | | 1.051101 |
| 33 | 0.981609 | 3.0271 | | | 1.057625 | 3.514094 | | | 1.115362 | 3.90824 | | | 1.059627 | 3.527412 | | | 1.046599 |
| 34 | 0.981606 | 3.027084 | | | 1.056727 | 3.50813 | | | 1.113466 | 3.89497 | | | 1.059614 | 3.527326 | | | 1.043023 |
| 35 | 0.981601 | 3.027054 | | | 1.0363 | 3.373814 | | | 1.113448 | 3.894842 | | | 1.059595 | 3.527198 | | | 1.008016 |
| 36 | 0.981601 | 3.02705 | | | 1.027873 | 3.319164 | | | 1.08027 | 3.666184 | | | 0.995531 | 3.113576 | | | 1.003418 |
| 37 | 0.966314 | 2.933504 | | | 1.013647 | 3.227926 | | | 1.056115 | 3.504066 | | | 0.993429 | 3.10044 | | | 0.999602 |
| 38 | 0.943842 | 2.798652 | | | 0.934 | 2.740588 | | | 1.05607 | 3.503766 | | | 0.993419 | 3.100382 | | | 0.999562 |
| 39 | 0.918599 | 2.650952 | | | 0.925684 | 2.692004 | | | 1.049954 | 3.463302 | | | 0.993382 | 3.100148 | | | 0.999526 |
| 40 | 0.918491 | 2.650328 | | | 0.898026 | 2.533542 | | | 1.047947 | 3.450072 | | | 0.993339 | 3.099882 | | | 0.960117 |
| 41 | 0.916229 | 2.637288 | | | 0.897989 | 2.533332 | | | 1.047932 | 3.449976 | | | 0.993325 | 3.099794 | | | 0.960098 |
| 42 | 0.916223 | 2.637258 | | | 0.846897 | 2.25326 | | | 1.001996 | 3.154144 | | | 0.948221 | 2.82468 | | | 0.960025 |
| 43 | 0.873154 | 2.395144 | | | 0.841166 | 2.222868 | | | 0.984701 | 3.046202 | | | 0.948221 | 2.82468 | | | 0.957102 |

CD - 130 mLhr summary | CD - 270 mLhr summary | CD - 400 mLhr summary

# APPENDIX B - DESIGN OF LAB-SCALE ESX EQUIPMENT

## Appendix B1: Diagrams of Lab-scale Test Cells and Columns

Small Lab-Scale Dispersion Cell –Aerial View

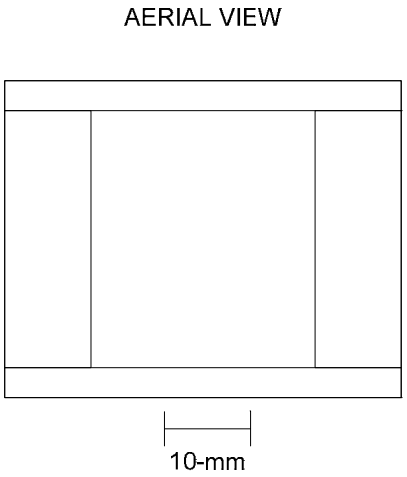

## Small Lab-Scale Dispersion Cell – Front and Side View

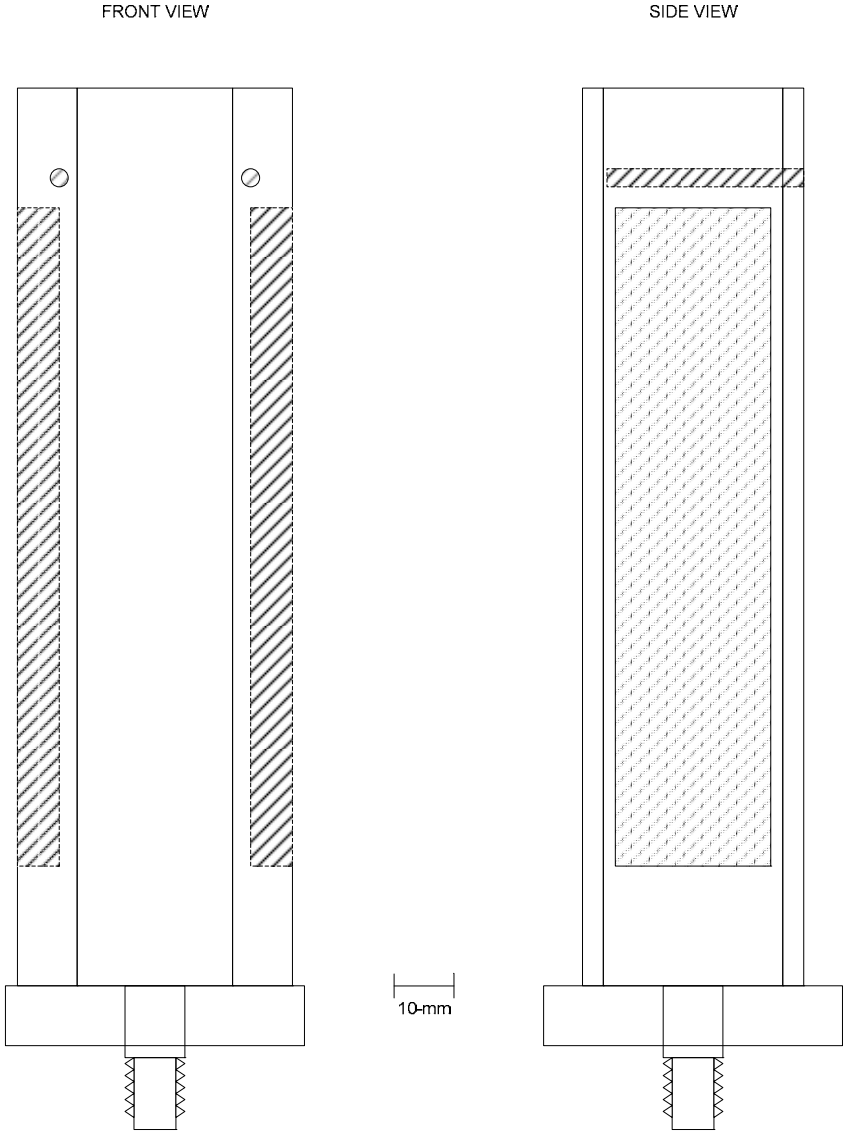

## Large Lab-Scale Dispersion Cell – Front Side and Aerial View

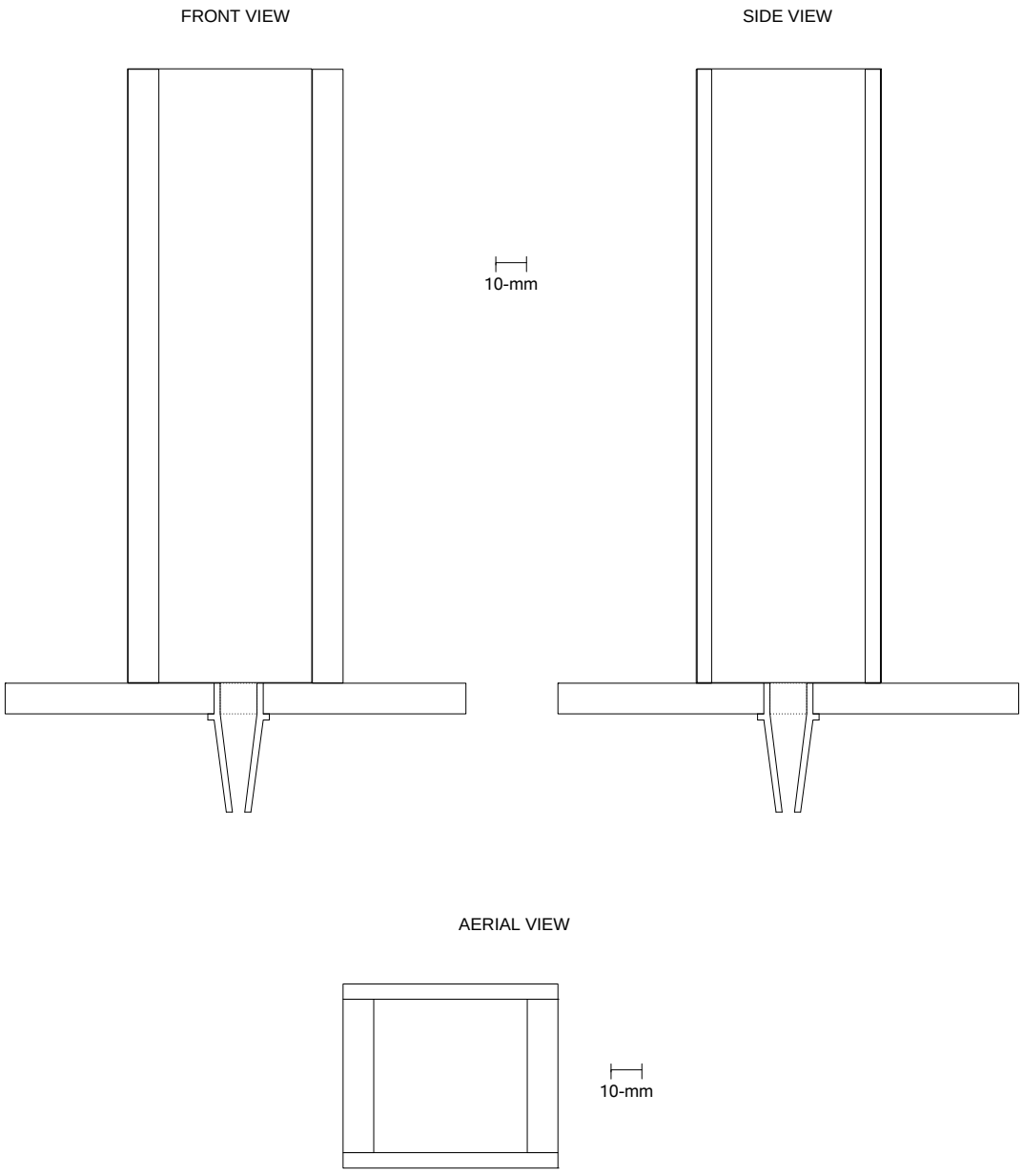

## Lab-Scale Counter-current ESX Column – Front and Side View

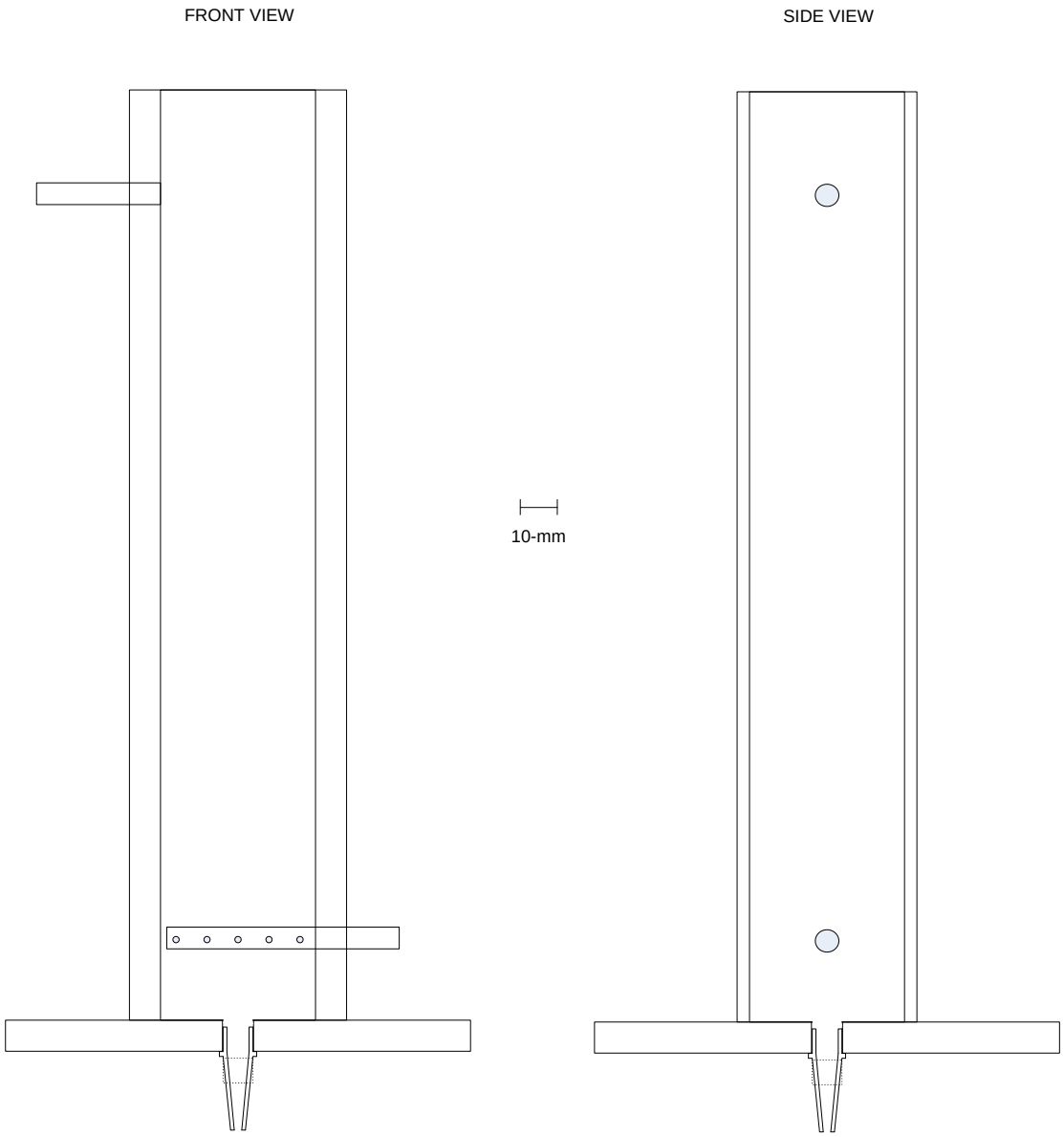

# Lab-Scale Counter-current ESX Column – Aerial View

AERIAL VIEW

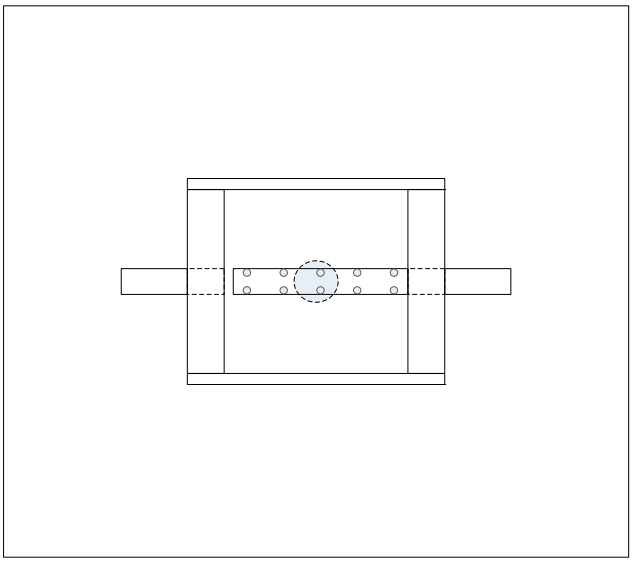

10-mm

## Appendix B2: Descriptions of DC Disperser Electrodes

### Needle-Point Electrode

The needle-point electrode was simply constructed from two hypodermic needles placed into a Perspex™ lid. The feed needle was a 20-gauge needle with a flat tip, and the point was a 22-gauge needle that had been bent around such that its end was directly below the feed needle. A short piece of 0.6-mm diameter steel wire was inserted into the end of the tip needle and glued with Epoxy.

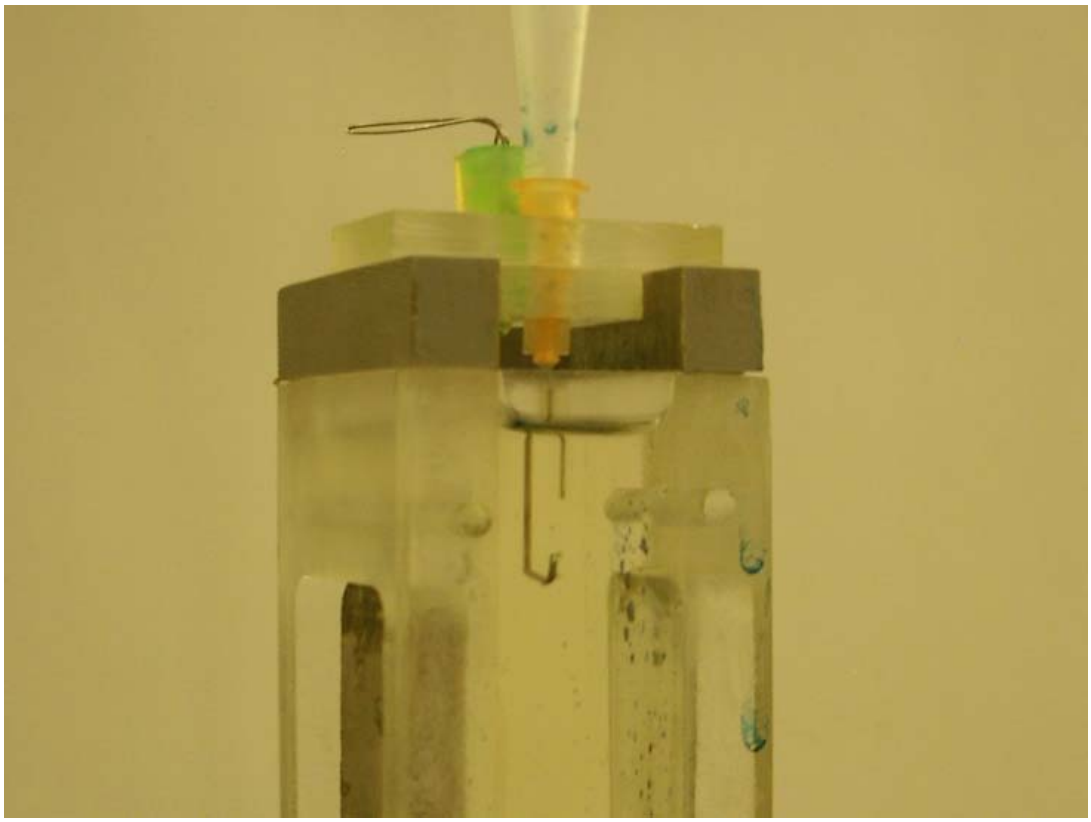

## Perspex™ Coated Rod Electrode

The Perspex™ coated rod electrode utilised the Perspex™ cell for electrode insulation. A pair of 4-mm diameter stainless steel rods were connected by copper wire and inserted into holes that were drilled into the side of the small Perspex™ cell, which allowed a 2-mm layer of Perspex™ between the rod and the inside of the cell.

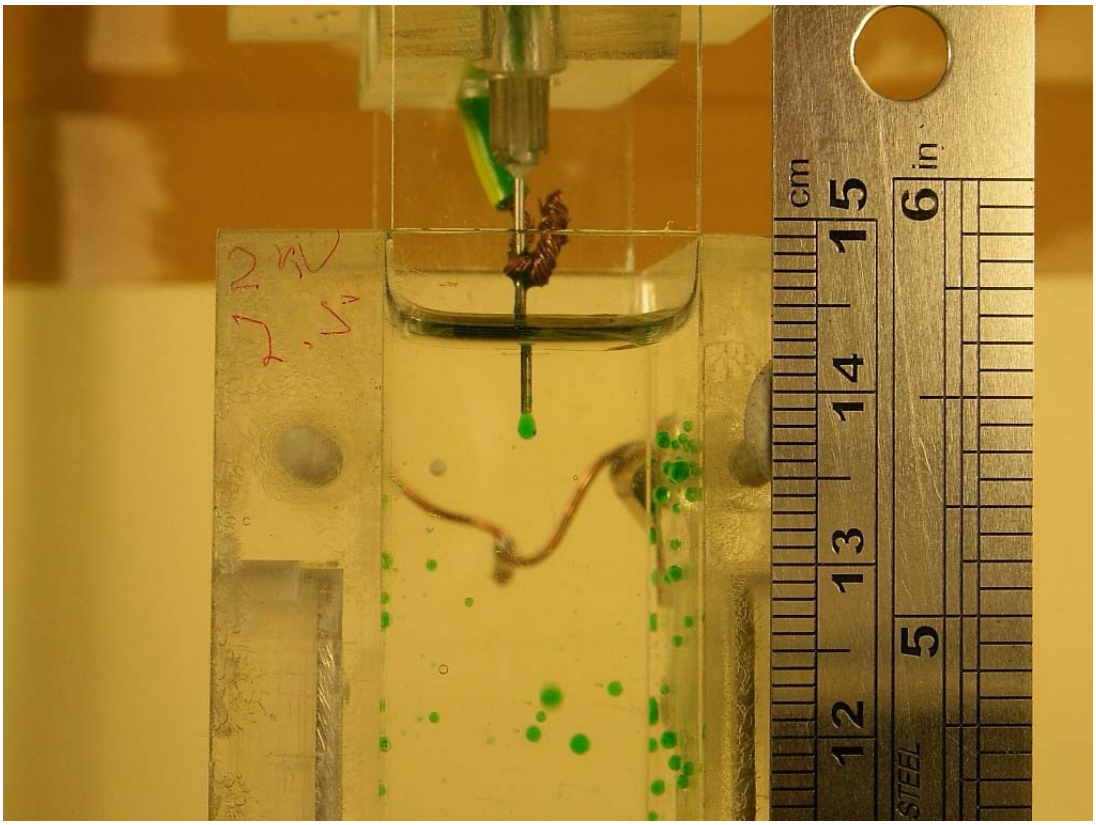

## Heat Shrink Teflon® Coated Electrode

The heat-shrink Teflon® coated electrode was constructed from a 22-cm length of 3-mm diameter soft-iron rod covered with heat shrink Teflon®. The rod was bent into a "U" shape with an 18-mm diameter. The electrode was then fitted into the cell lid that held the electrode in place.

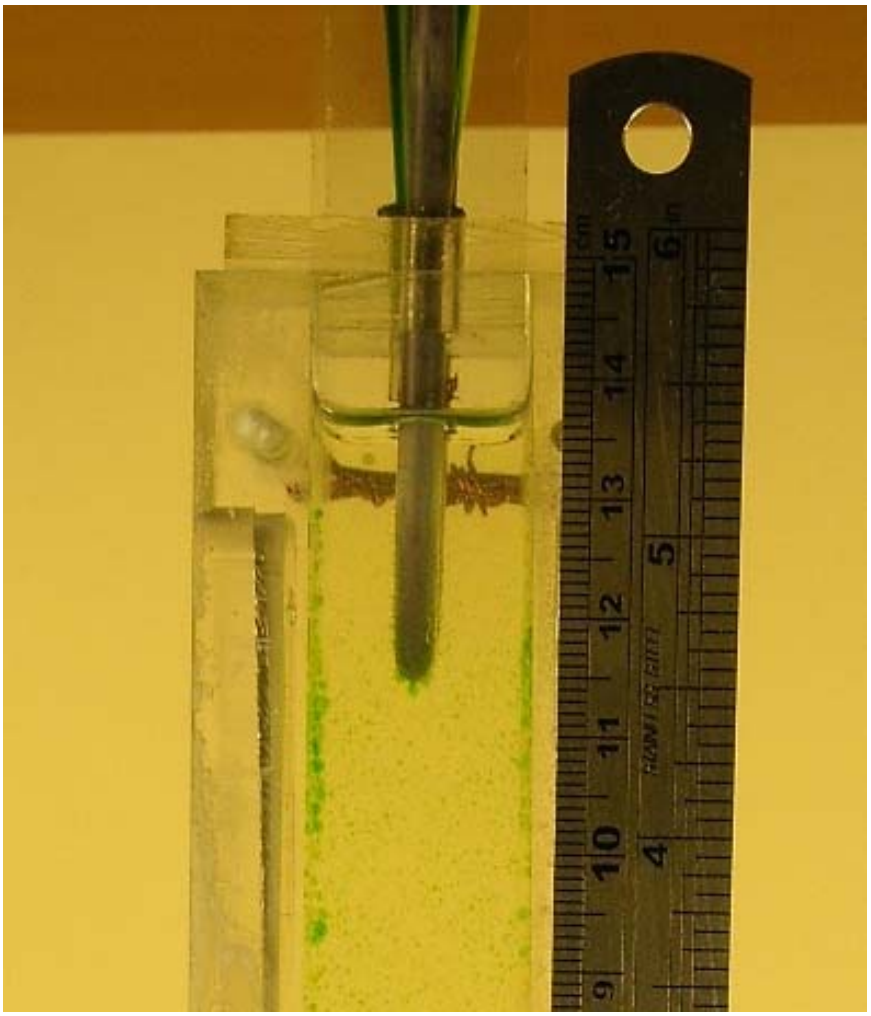

## Copper Ring Electrode

The copper ring electrode is constructed from 1-mm thick copper wire. The wire was worked into a 15-mm diameter ring, with a 35-mm length of wire coming directly upward to allow connection to a power supply. The 35-mm length was covered with 0.8-mm Viton® tubing in later tests to prevent arcing.

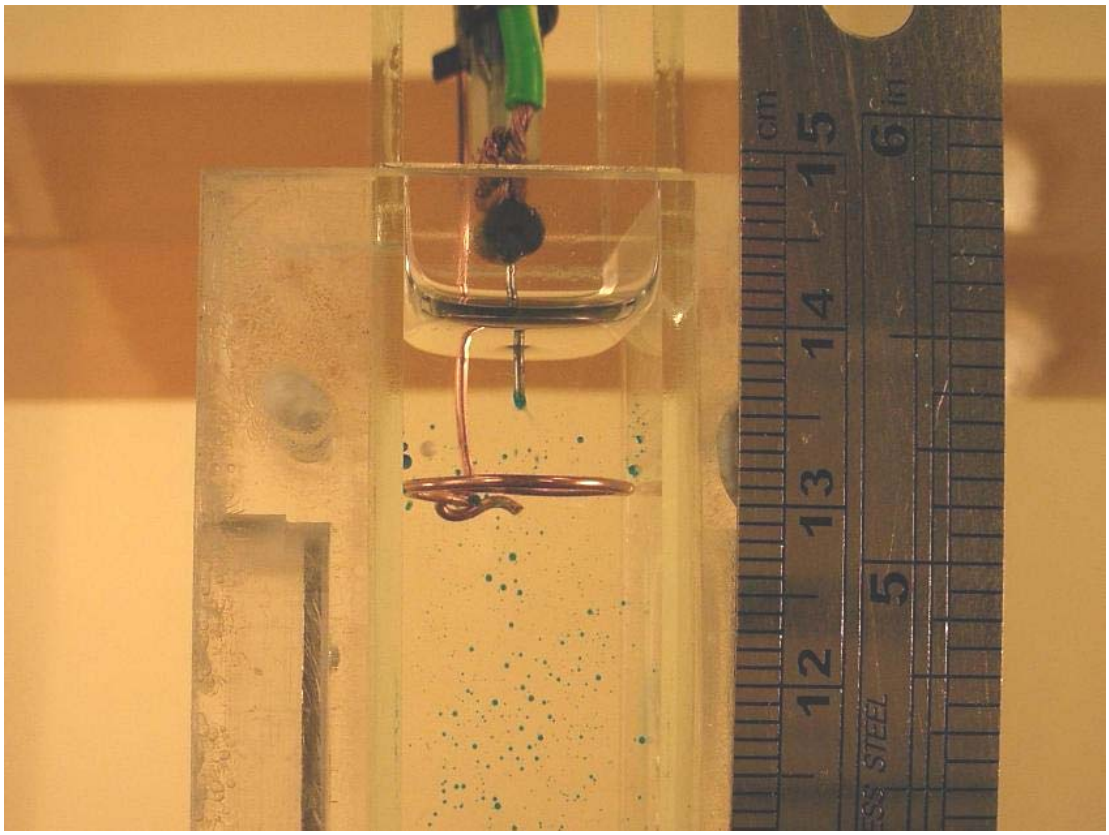

## Mesh Electrode

The mesh electrode was constructed of stainless steel mesh with 1-mm apertures. The mesh was cut into a dumbbell shape, with 14 x 14 mm bells and a 4 x 40 mm connection. A 90° bend was made 8-mm along the bar, and a length of 3-mm diameter insulated wire was soldered to one of the bells for connection to a power supply.

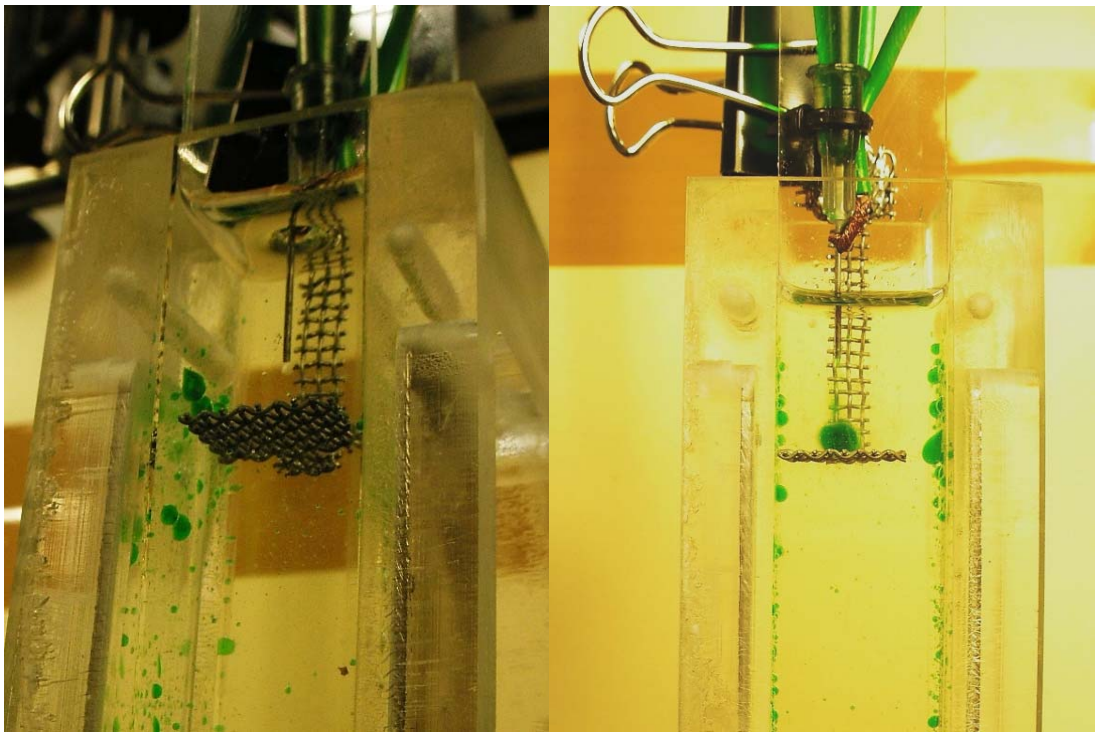

## Glass Plate Electrode

The glass plate electrode was constructed of: (1) 2 sections of 21 x 100 x 2 mm glass, (2) 2 sections of 75 x 21x 1 mm glass, (3) 2 pieces of 17 x 80 mm aluminium tape in which a 15 x 45 mm section was removed from one side of each piece, and (4) 1 section of 25 x 40 x 1mm glass. The electrode was constructed as follows: (1) the aluminium tape was stuck centrally on each of the 2-mm thick glass pieces, (2) the surface on which the aluminium tape is stuck is then covered with epoxy and the 1-mm thick sections placed on top such that a section of aluminium foil remained exposed for attachment of high-voltage leads, and (3) the two individual electrodes were placed parallel to each other with a 12-mm gap between them and (5) the 25 x 40 x 1 mm section of glass glued to the edges to set the distance between the individual electrodes.

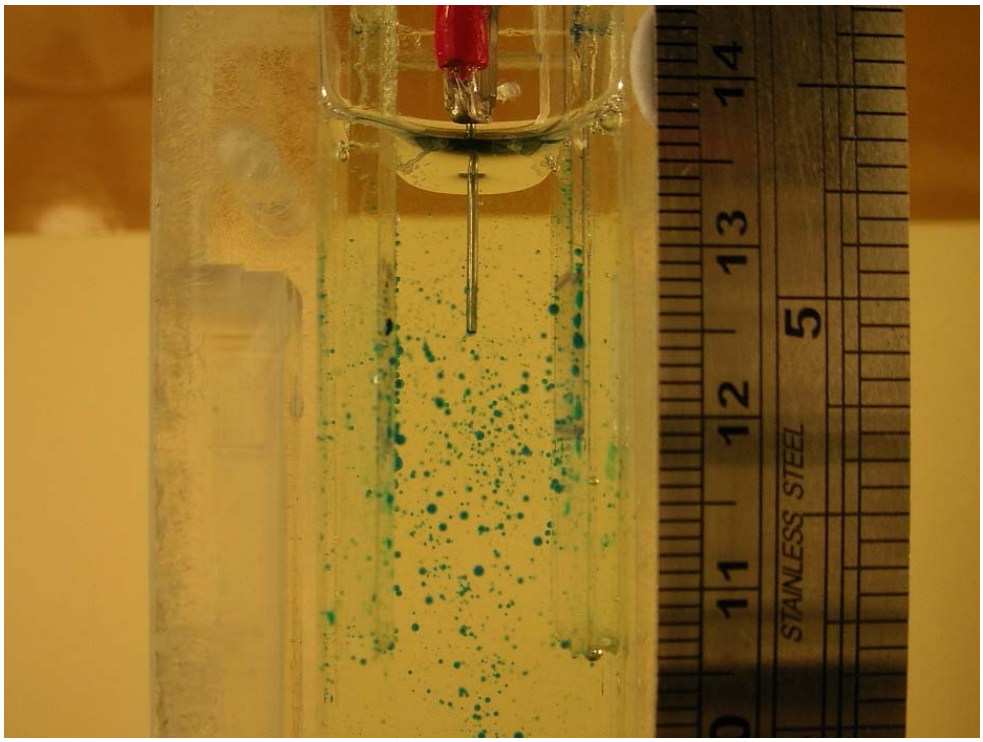

## Glass Cone Electrode

The glass cone electrode was constructed of: (1) a 55 mm tall glass cone with an upper diameter of 13-mm and lower diameter of 38-mm, (2) 2 x triangular Perspex™ lugs in which 3-mm diameter holes were drilled, (3) 0.9-mm diameter copper wire, and (4) 2 x 3-mm diameter Perspex™ rods. The electrode was constructed as follows: (1) the Perspex™ lugs were glued on opposite sides of the cone, (2) a ring of copper wire was glued onto the lower section of the cone, (3) an insulated copper wire was attached to the copper ring for connection to a power supply (4) the ring and connection to the copper wire was completely covered with glue, and (5) the Perspex™ rods were inserted into the holes in the lugs to allow the disperser to be suspended from the top of the column.

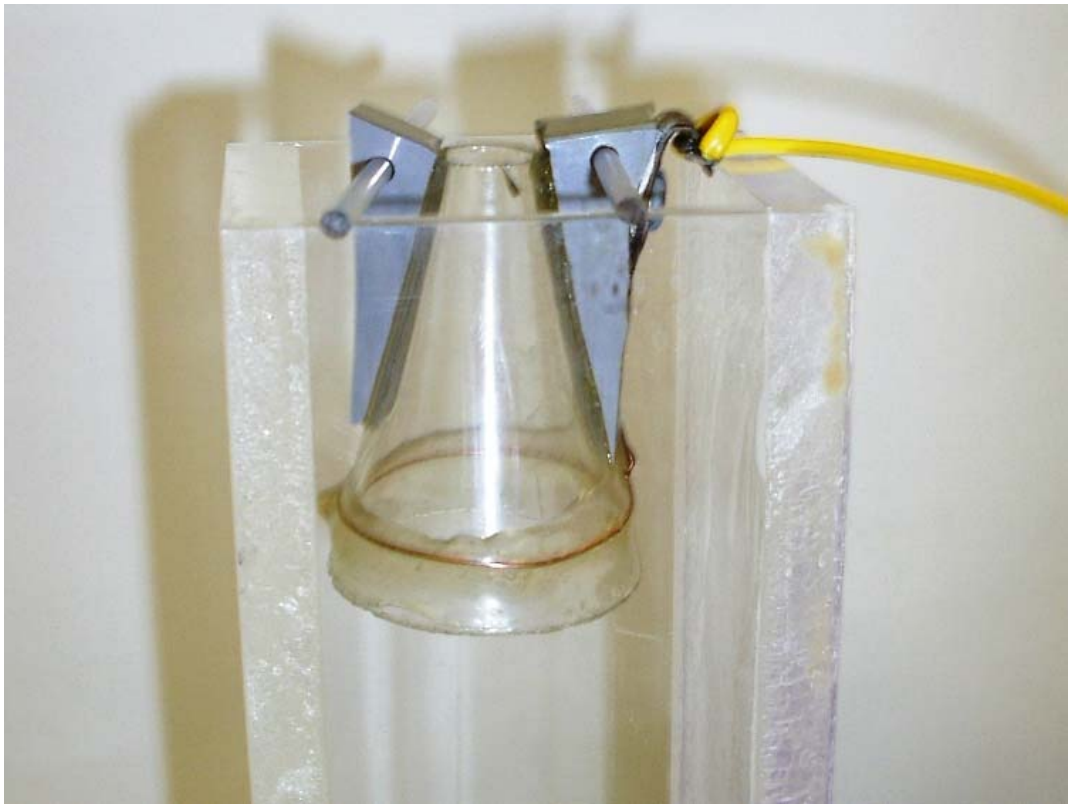

## Appendix B3: Descriptions of AC Disperser Electrodes

### Glass Plate Dispersion (AC) Electrode

The glass plate AC electrode was constructed similarly to the glass plate electrode used for DC dispersion except larger. The glass plate AC disperser consisted of (1) 2 sections of 45 x 120 x 2 mm glass, (2) 2 sections of 45 x 100 x 2 mm glass, (3) 2 sections of 25 x 75 x 1 mm glass, (4) 2 sections of aluminium tape 33 x 60 mm in size, with a 2 x 45 mm strip leading off a corner, (5) 2 'L' shaped aluminium lugs with 5-mm diameter holes drilled in each and (6) 2 lengths of 4-mm diameter copper wire. The electrode was constructed as follows: (1) the sections of aluminium tape were applied to the larger sections of glass, (2) one side of the smaller sections of glass were coated with epoxy glue, and glued over the larger section of glass with aluminium tape, ensuring a section of aluminium tape remained exposed, (3) the aluminium lugs were then glued over the remaining exposed section of tape, (4) the copper wire was connected to the aluminium lugs, and (5) the two electrodes were aligned parallel – 20 mm apart – and glued the 1-mm sections of glass.

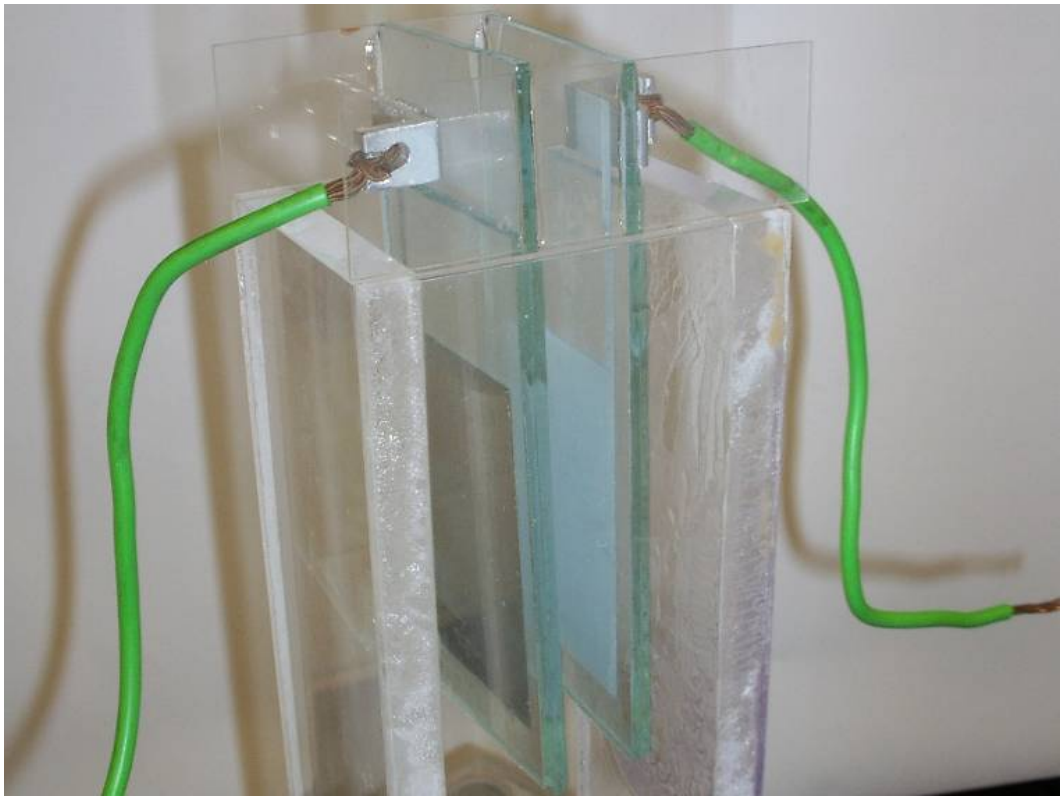

## Teflon®-Coated Plate Dispersion (AC) Electrode

The Teflon® coated AC electrode were constructed of: (1) two sections of 1-mm thick stainless steel sections of dimensions 45 x 85 mm, with a 12 x 3 mm rectangular hole being cut in the centre of the sheet and 8 mm from the top, (2) 2 sections of 7 mm diameter copper wiring with the ends stripped and (3) 2 sections of 150-mm long heat-shrink Teflon® tubing. The electrode was constructed as follows: (1) the stainless steel sheet was bent at a 45 degree angle 25-mm from the top, (2) the copper wire was attached to the stainless steel sections fastened through the rectangular holes, (3) the heat shrink Teflon® tubing was shrunk over the stainless steel sections and the ends welded shut. During use, the electrodes were held apart by 2 small Perspex™ sections that wedged on the bottom of the electrodes.

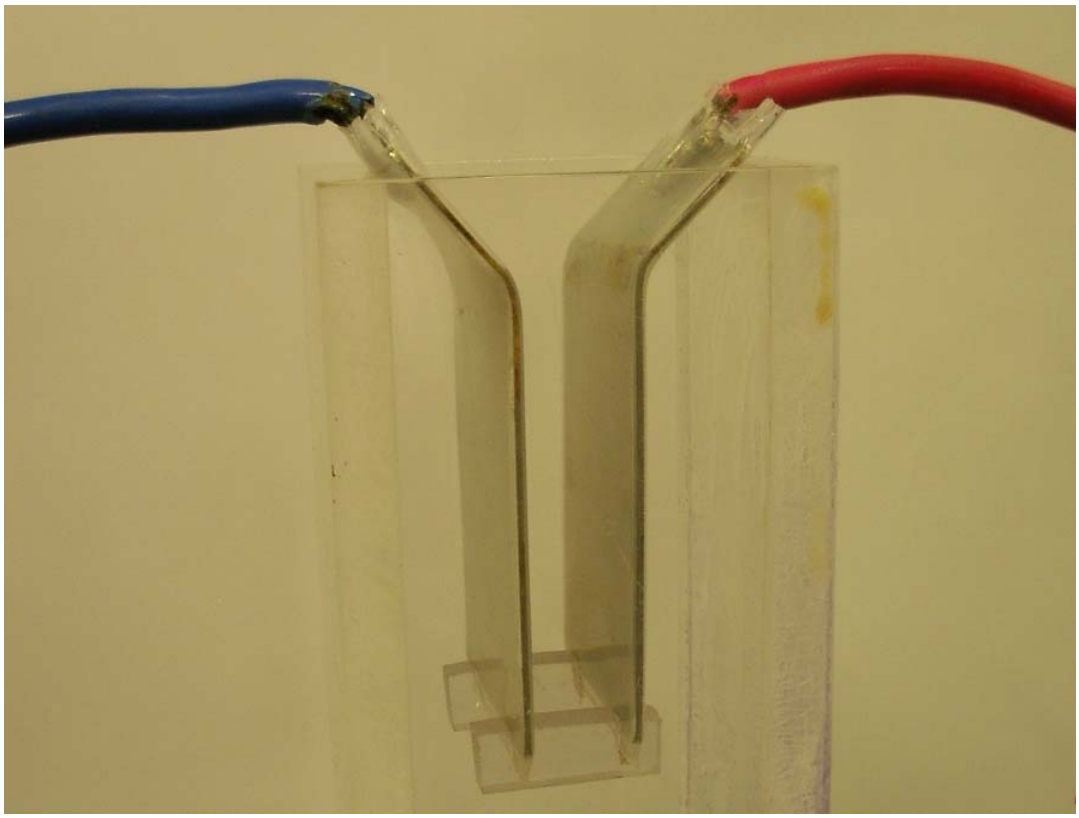

## Appendix B4: Descriptions of AC Agitation Electrodes

### Teflon®-Coated Plate Agitation Electrode

The Teflon®-coated plate agitation electrode is similar to the Teflon® coated dispersion electrode, except larger. The electrode was constructed using the following parts: (1) 4 sections of stainless steel, each being 95 x 44 mm with a 4 x 2 mm tab remaining on a corner, (2) 0.9-mm diameter copper wire, (3) heat-shrink Teflon® tubing, and (4) 1-mm thick and 5-mm thick sections of Perspex™, each 230 x 48 mm. The electrode was constructed as follows: (1) a 1-mm diameter hole was drilled in the tab of each electrode and a 20-mm long strand of copper wire attached, (2) heat-shrink Teflon® was shrunk over the stainless steel and the ends welded together, leaving a small gap for the copper wire to exit, (3) to the 5-mm thick section of Perspex™, 4 parallel slots, each 2.75 x 108 mm in size, were cut equidistantly apart and 40 mm from the bottom, (4) on one side of the 5-mm thick section and above each slot, 2-mm deep grooves were cut from the slot to the top of the section, (5) the electrodes were then placed into the slots, and the copper wire was fitted into the grooves and the 1-mm Perspex™ section glued over the grooved side, and (6) every second electrode was connected together.

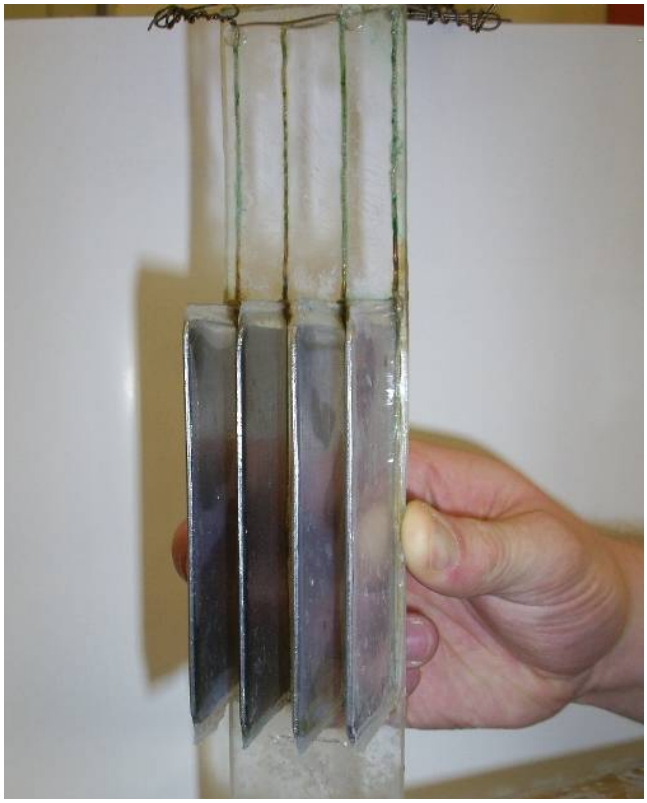

## Teflon®-Coated Rod Agitation Electrode

The Teflon® coated rod electrode was constructed similar to the Teflon® coated plate electrode with the rods being fitted instead of plates. The electrode was constructed using the following parts: (1) 28 x 3-mm diameter stainless steel rods with heat-shrink Teflon® applied, (2) 230 x 48 x 5-mm Perspex™ sheet with 3.1-mm diameter holes drilled 11 mm apart and on a triangular pitch, (3) 230 x 48 x 2-mm Perspex™ sheet and (4) 0.9-mm diameter copper wire. The electrode was constructed as follows: (1) the stainless steel rods with insulation applied were inserted into the pre-drilled holes, (2) grooves were cut into the rear of the 5-mm thick piece of Perspex™ between rods (3) copper wire was inserted into grooves to connect rows of electrodes, (4) the 2-mm thick Perspex™ section was glued onto the back of the 5-mm thick Perspex™ section to encase the copper wiring and (5) the protruding end of the electrodes were sealed with epoxy.

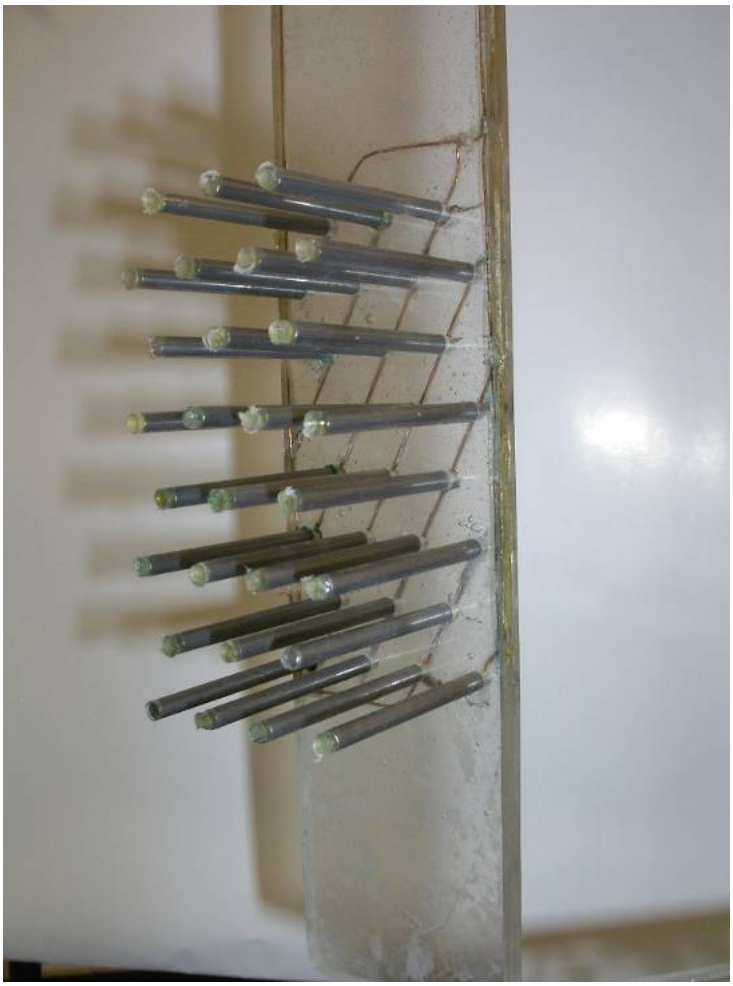

## Tefzel®-Coated Wire Agitation Electrode

The Tefzel® coated wire electrode consists of a Perspex™ frame through which Tefzel® wires are woven. The frame was constructed using the following parts: (1) two 5-mm thick Perspex™ sections, one 165 x 48 and the other 250 x 48 mm, and (2) two 10-mm thick Perspex™ sections that are 37 x 48 mm in the middle of which are 35-mm diameter holes. The electrode was constructed as follows: (1) 72 x 2-mm diameter holes drilled 11 mm apart on a triangular pitch into the 5-mm thick Perspex™ sections, (2) the 5-mm sections were placed upright and aligned parallel, (3) the 10-mm Perspex™ sections glued in between and at either end of the 5-mm thick sections to maintain a 37 mm separation and (4) Tefzel® wire was woven through the 2-mm diameter holes in the selected electrode configuration.

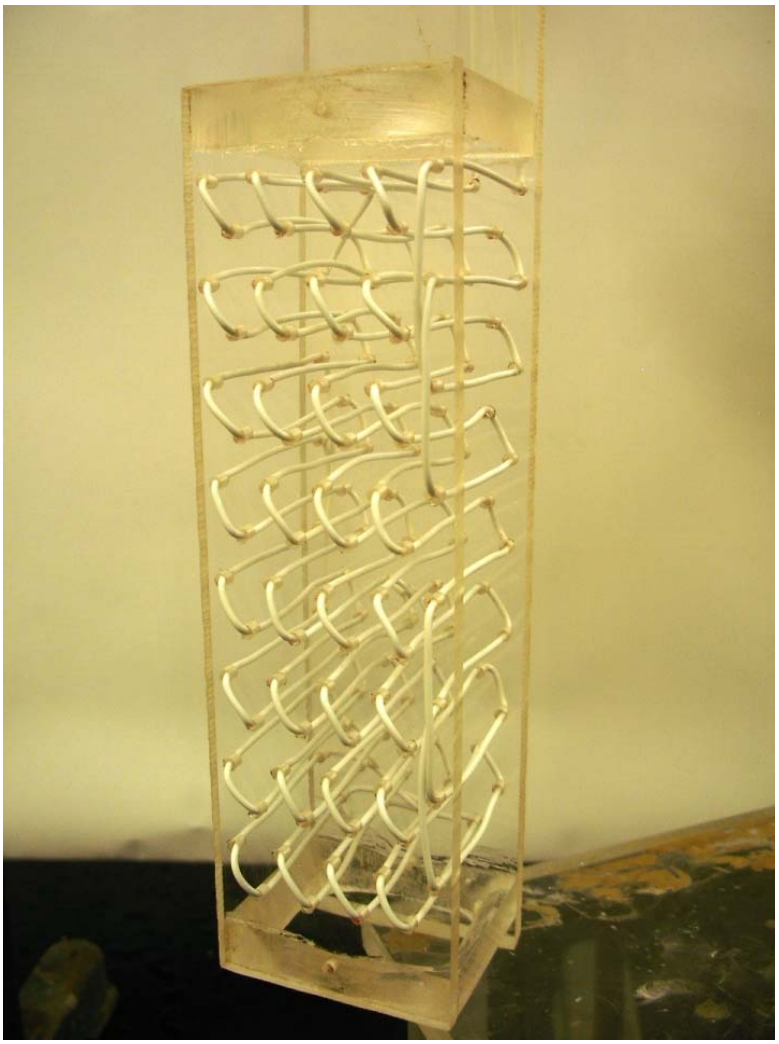

# APPENDIX C - DESIGN OF PILOT-SCALE ESX COLUMN

Appendix C1: Diagrams and Photographs of the Column Body Sections

Column Body – Cross Section

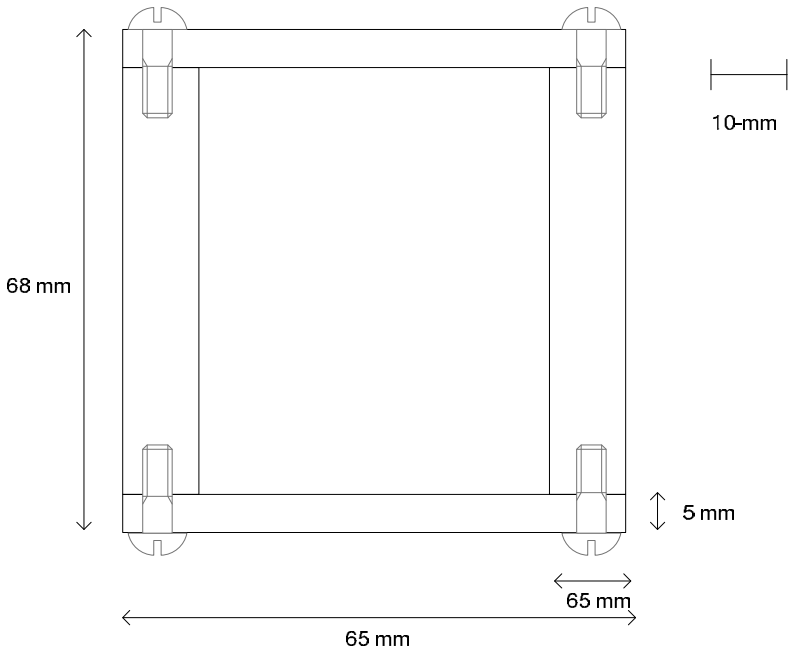

## Column Body – Cross Section – with Electrode Frame

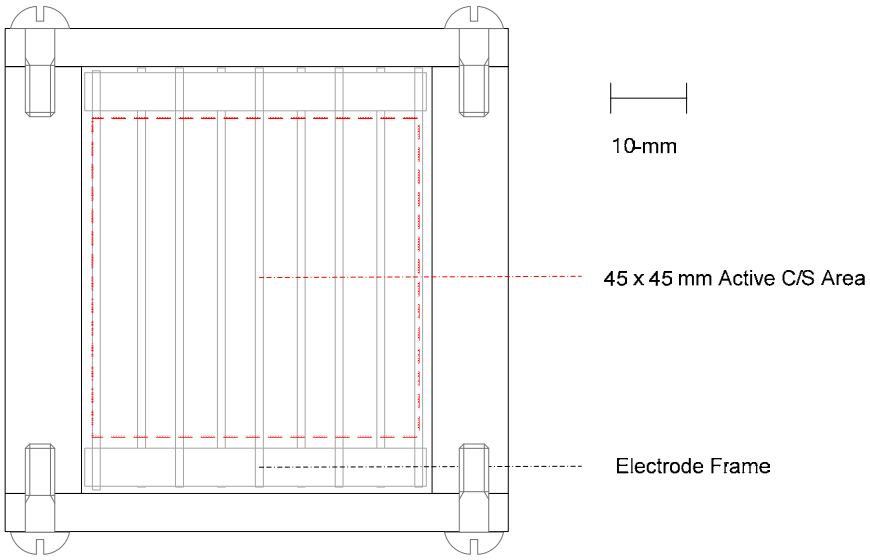


## Flanges – Aerial View

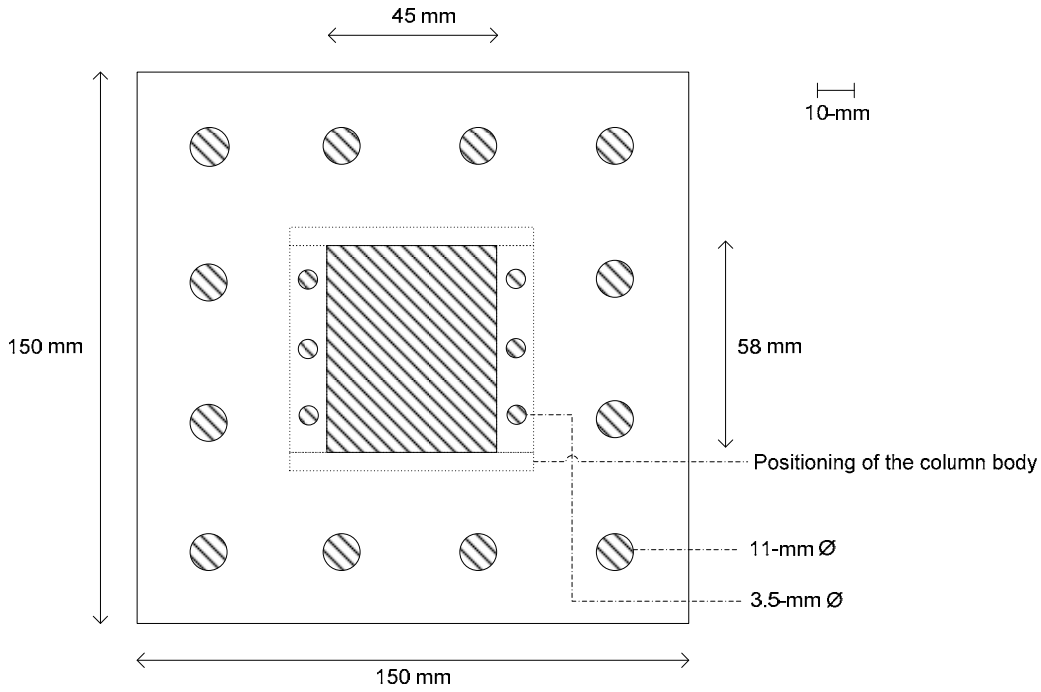

Flange Connections – Front and Side View

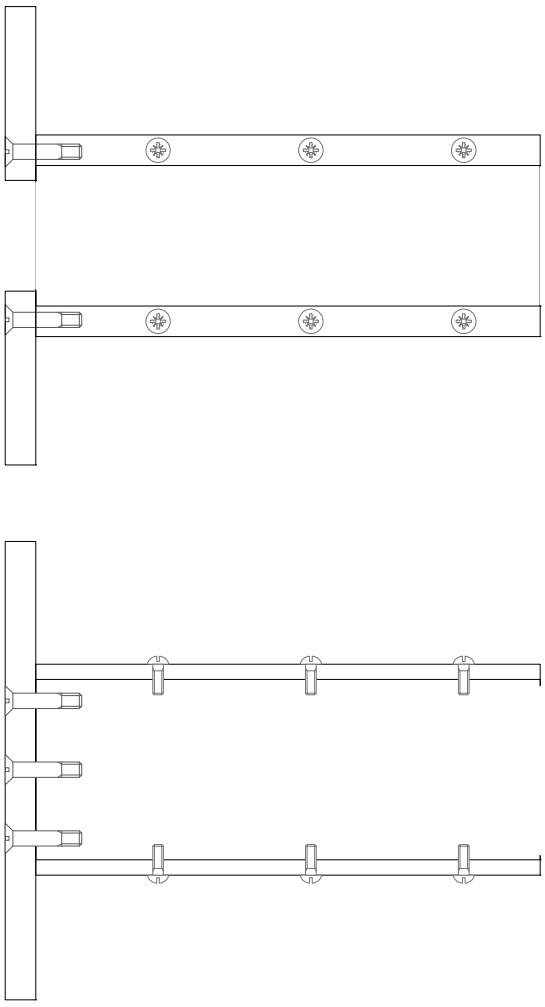

Column Body Sections – Front and Side View

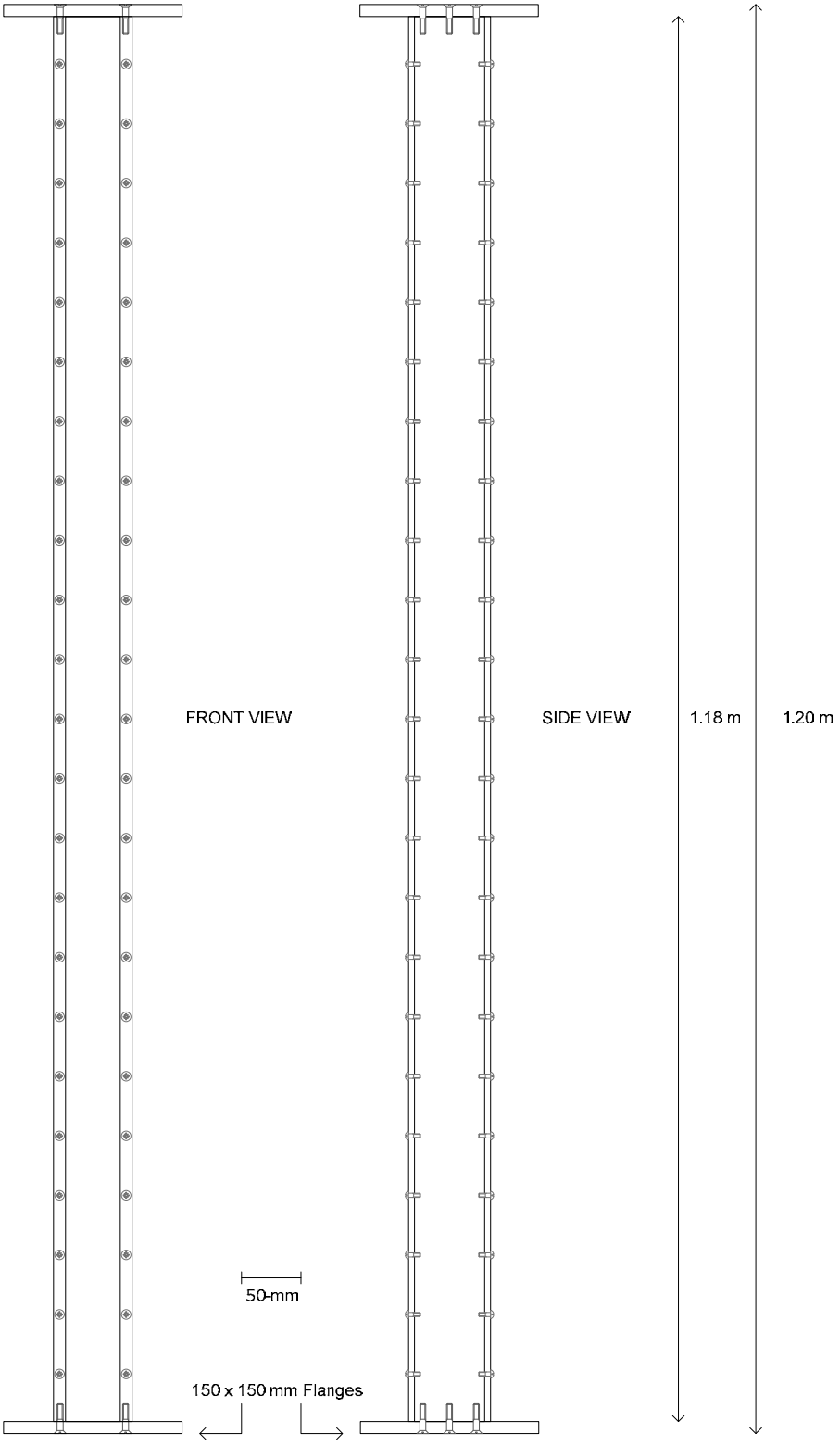

# Flange Connections – Front and Side View

FRONT VIEW

SIDE VIEW

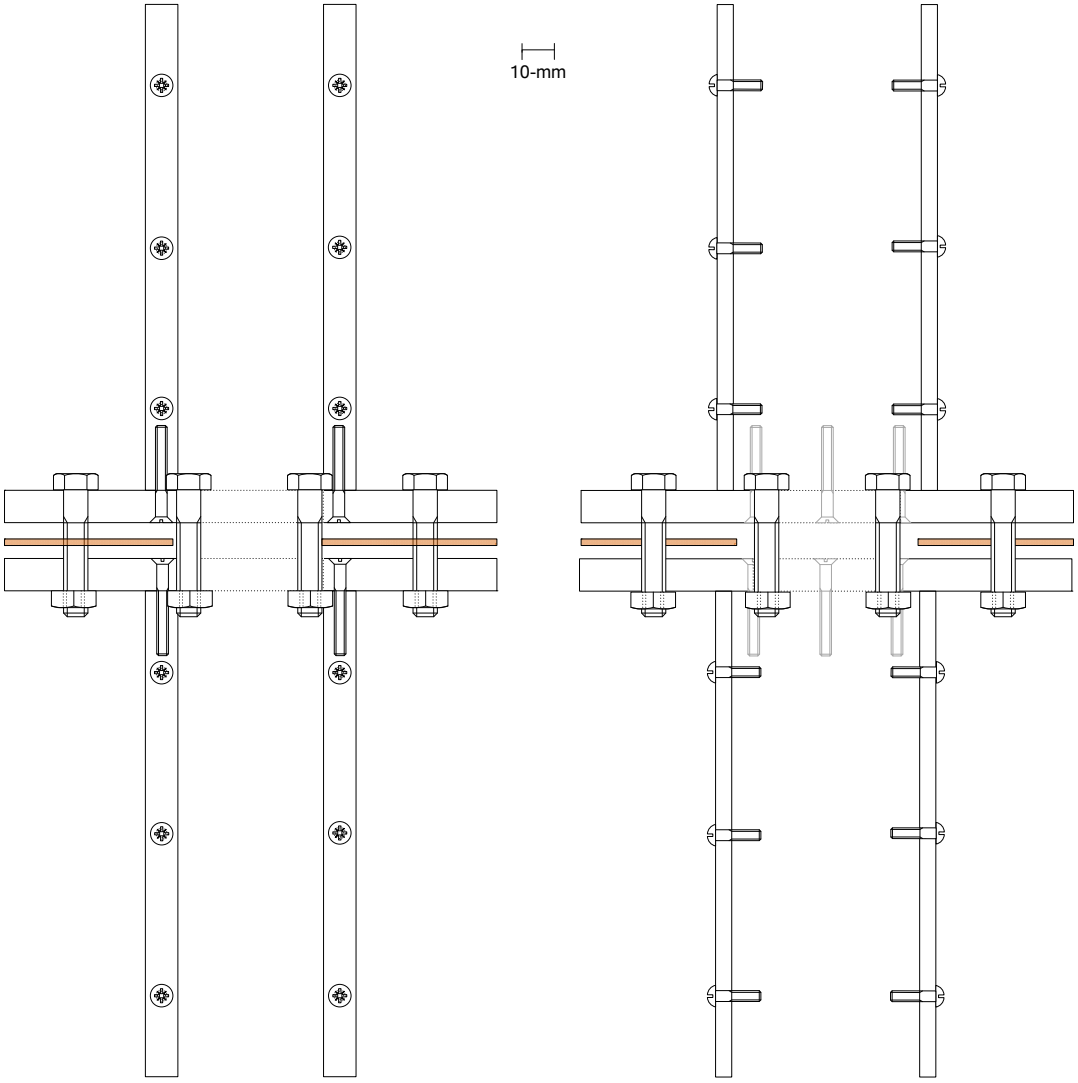

Column Body – Photograph

## Appendix C2: Diagrams and Photographs of Upper and Lower Settlers

### Upper Settler – Front and Side Views

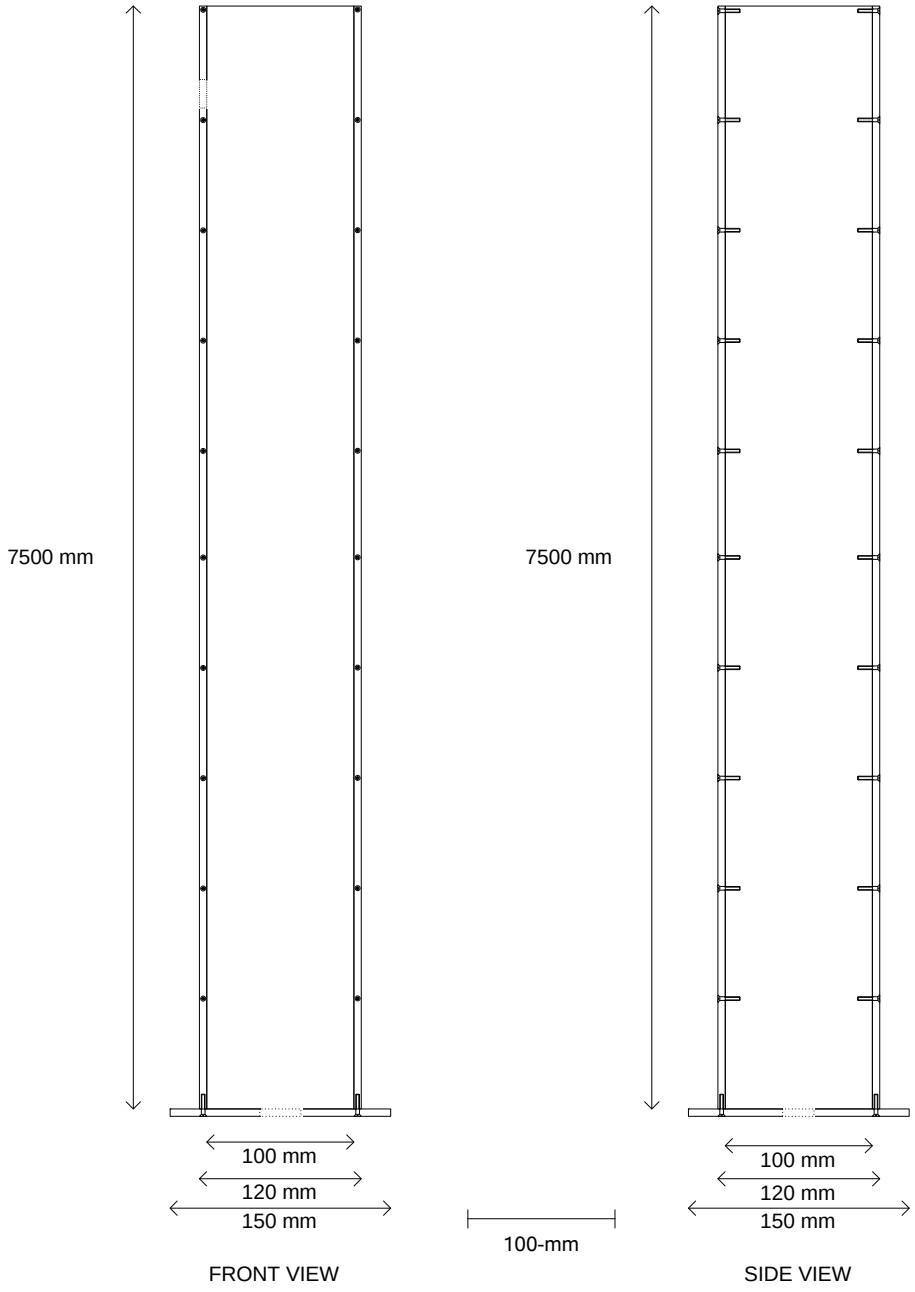

Upper Settler Body – Cross Section

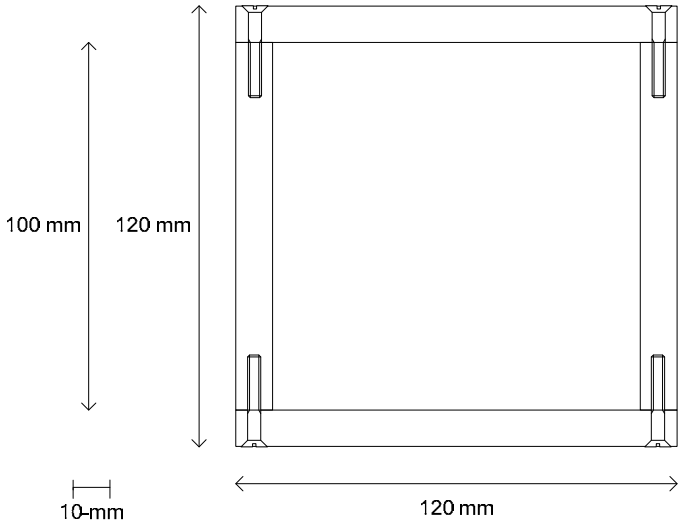


Upper Settler – Photograph

# Lower Settler – Front View

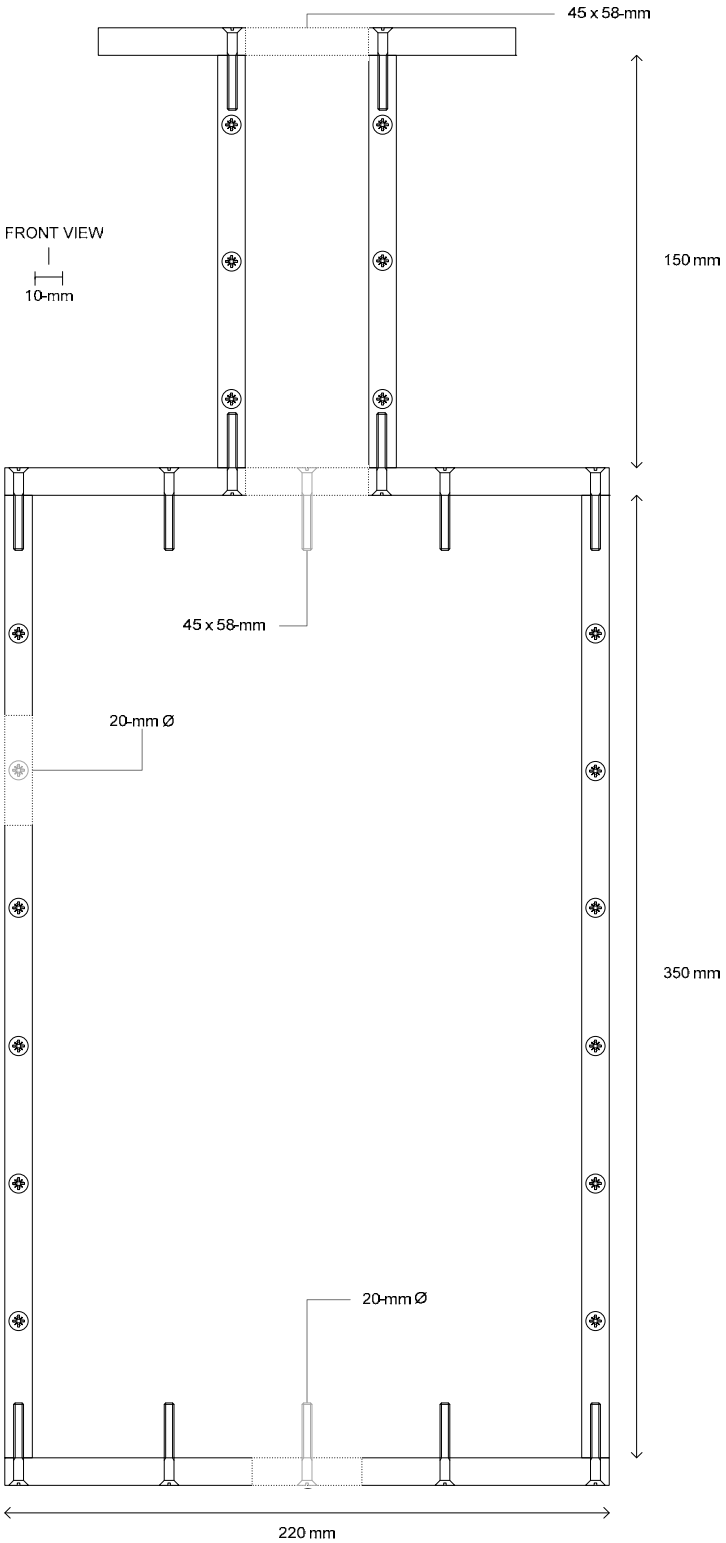

# Lower Settler – Side View

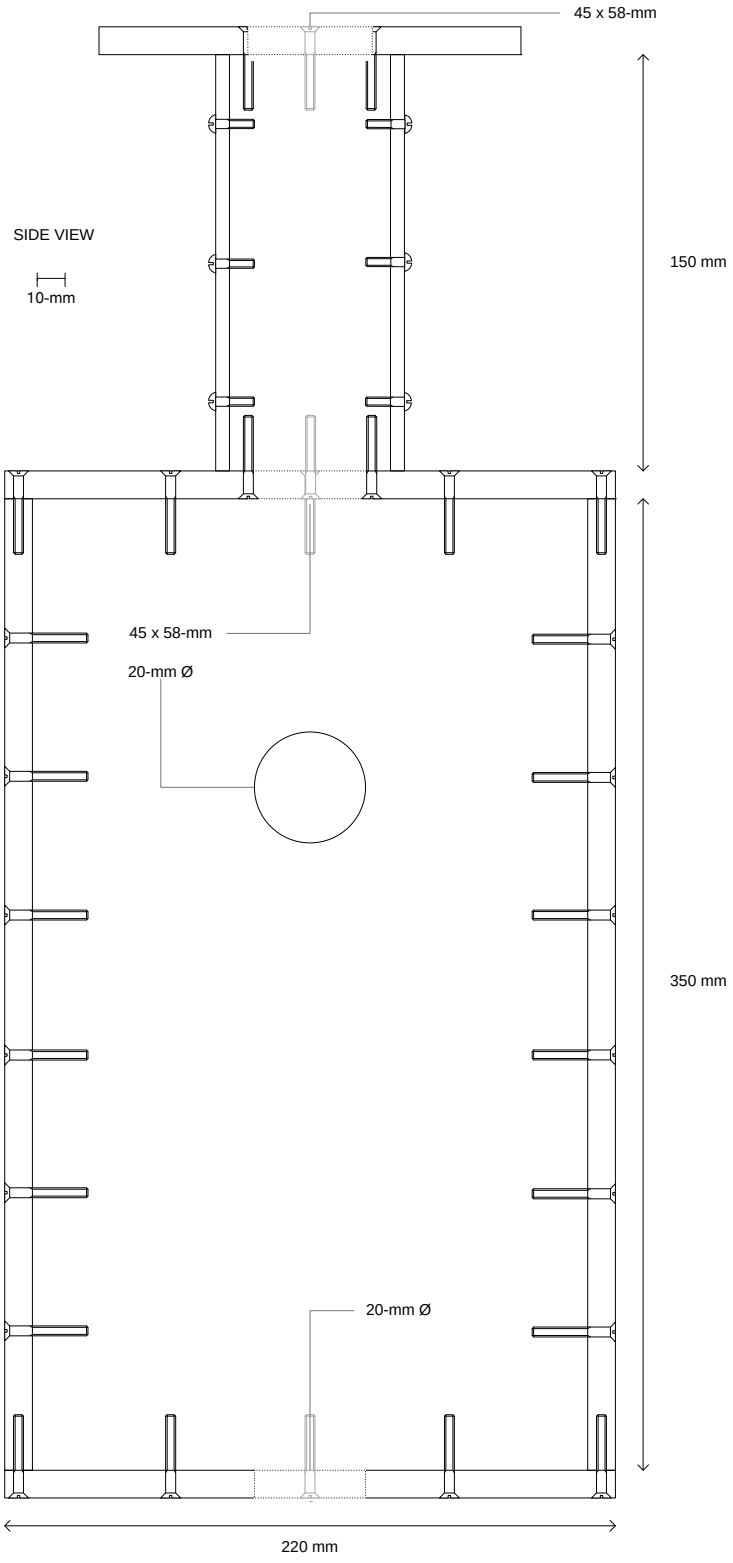

## Lower Settler – Lower Compartment Cross-Section

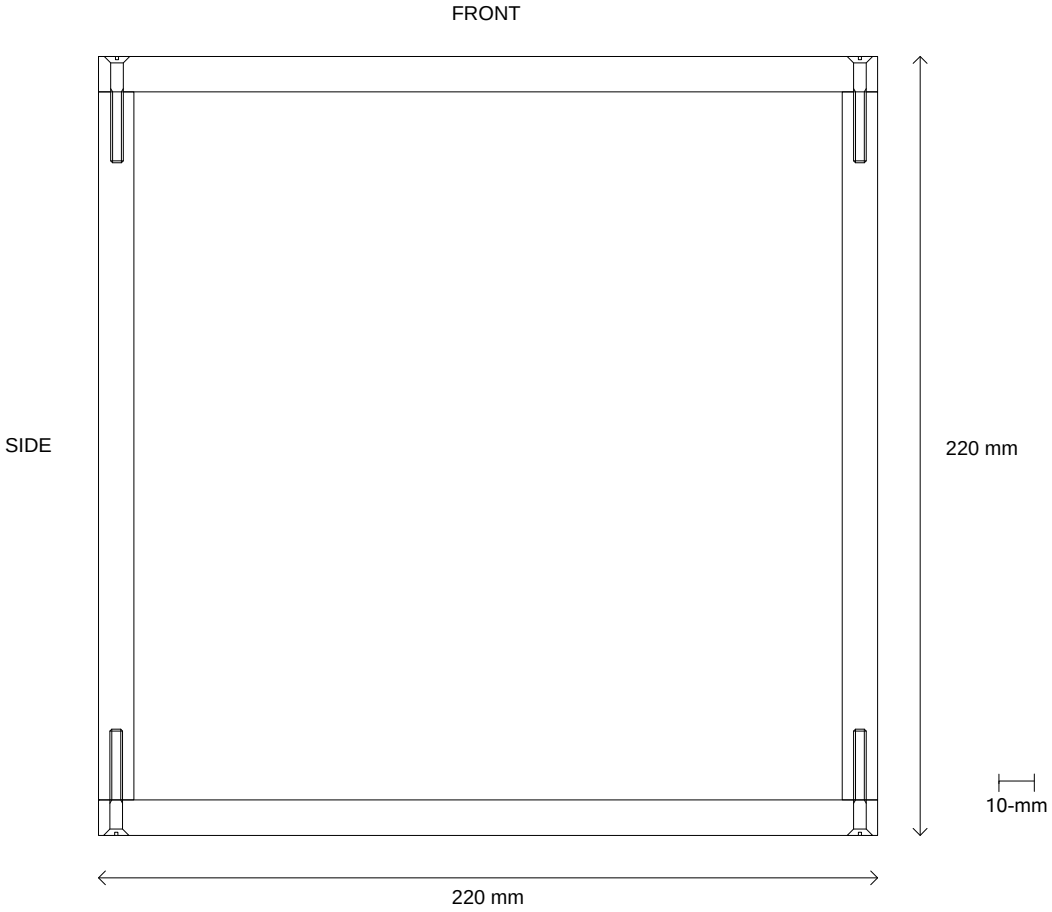


## Lower Settler – Upper Compartment Cross-Section

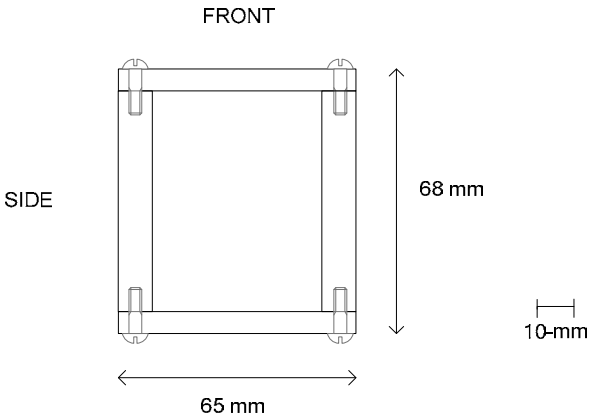

Lower Settler – Photograph

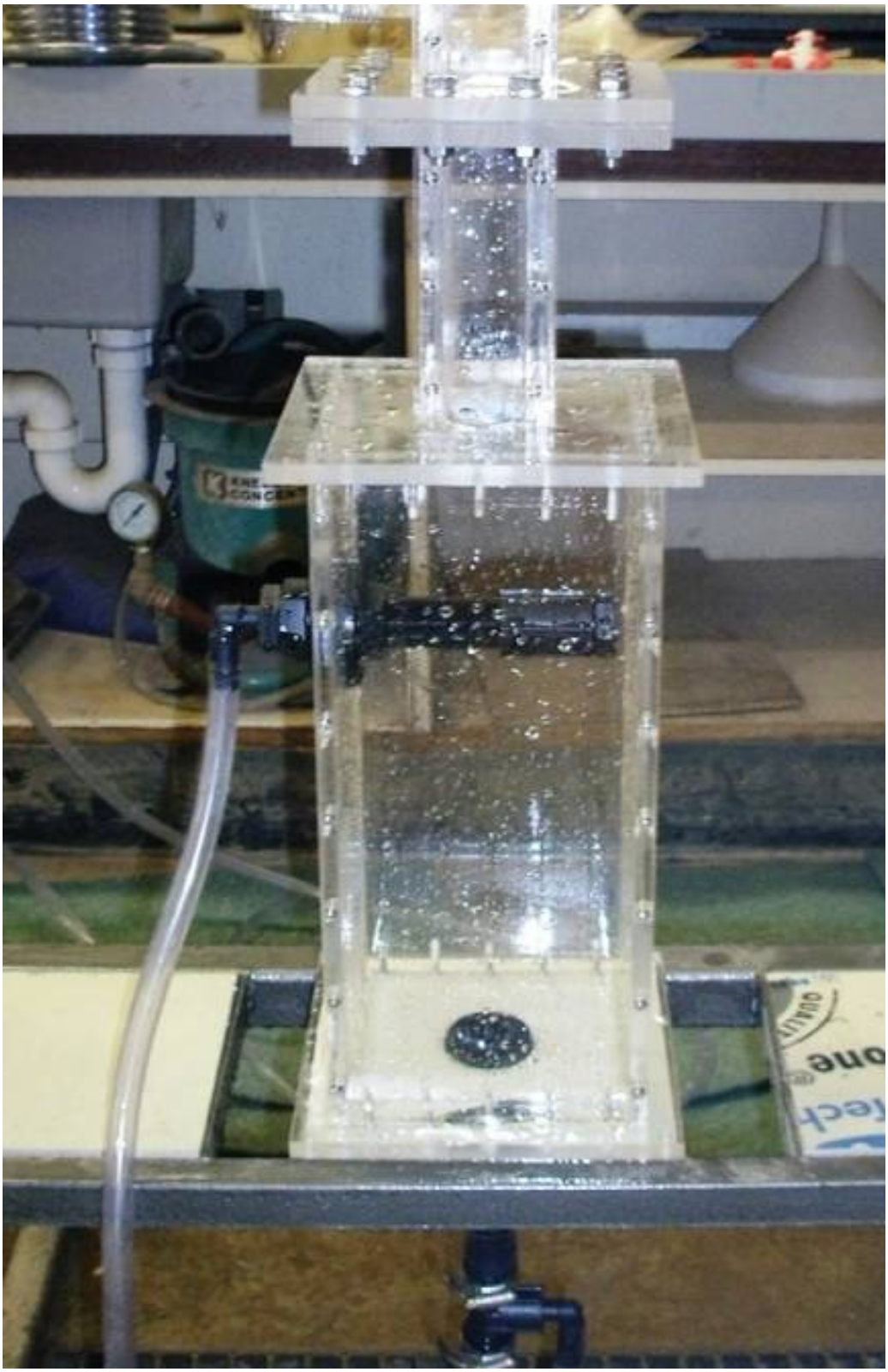

## Appendix C3: Diagrams and Photographs of the Electrodes

### Electrodes – Aerial View – Without Wires

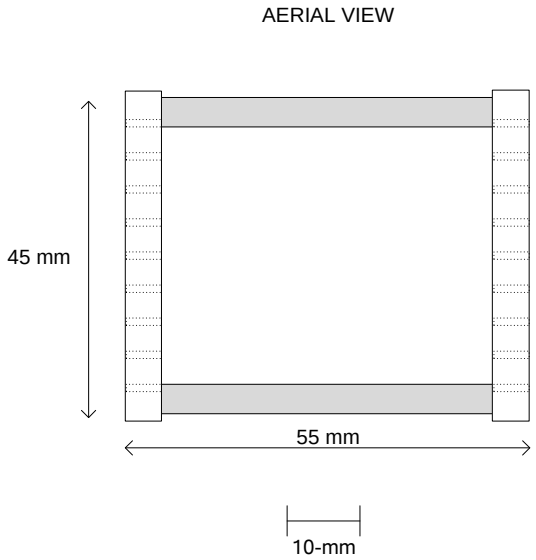


### Electrodes – Aerial View – With Wires

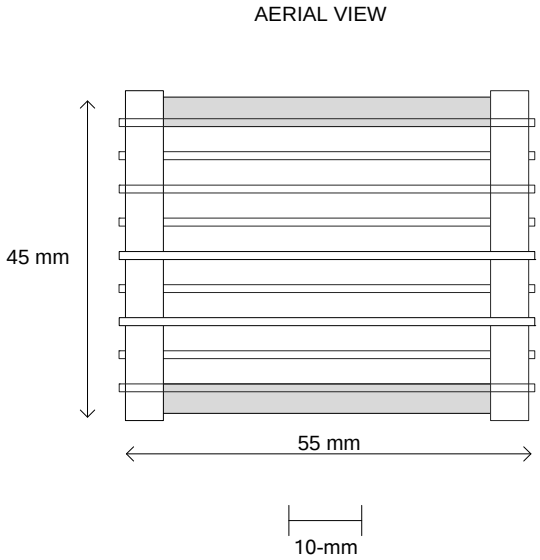

Electrodes - Front and Side View – Without Wires

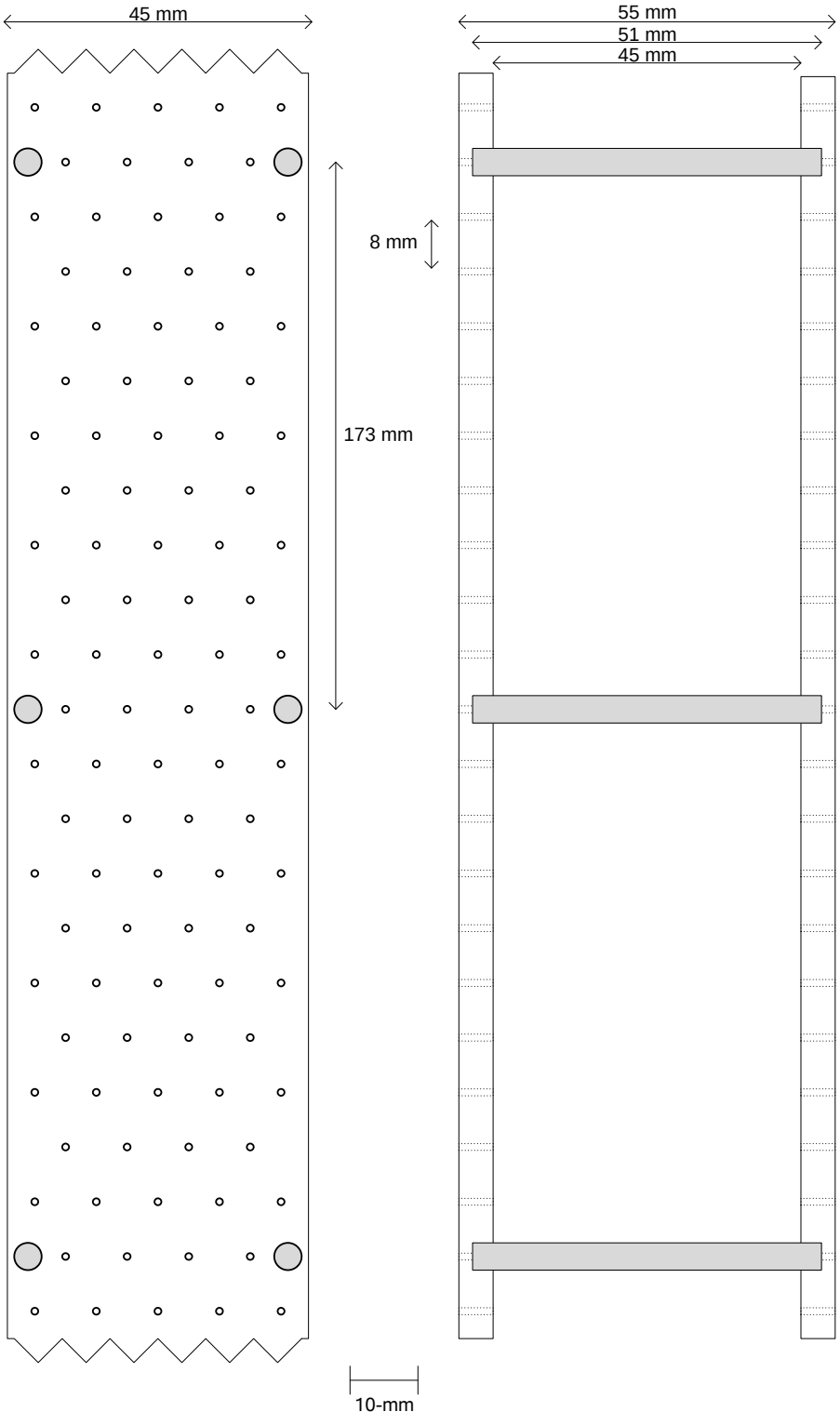

Electrodes - Front and Side View – With Wires

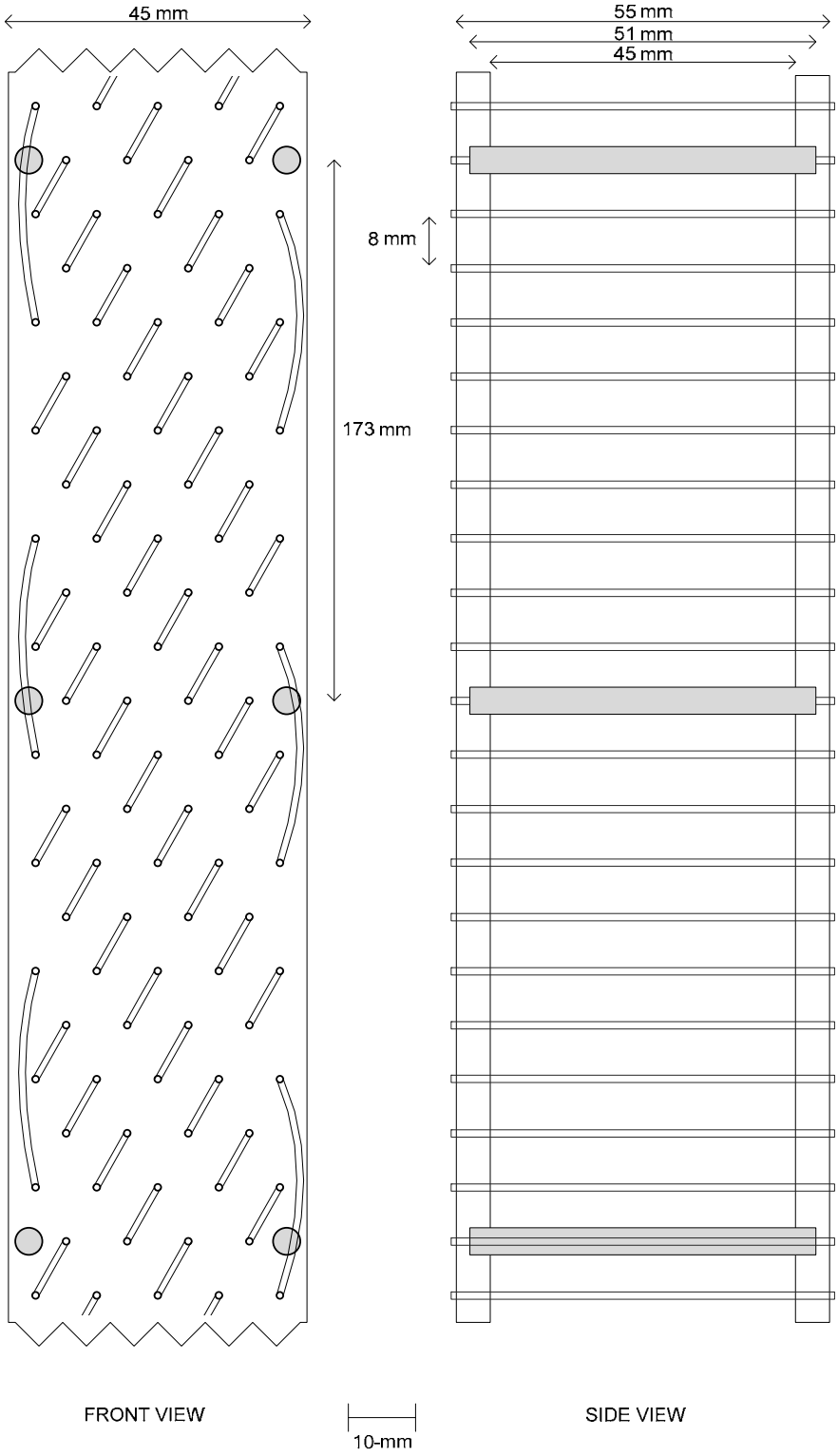

Electrodes – Photograph During Weaving and Tightening of Electrode Wire

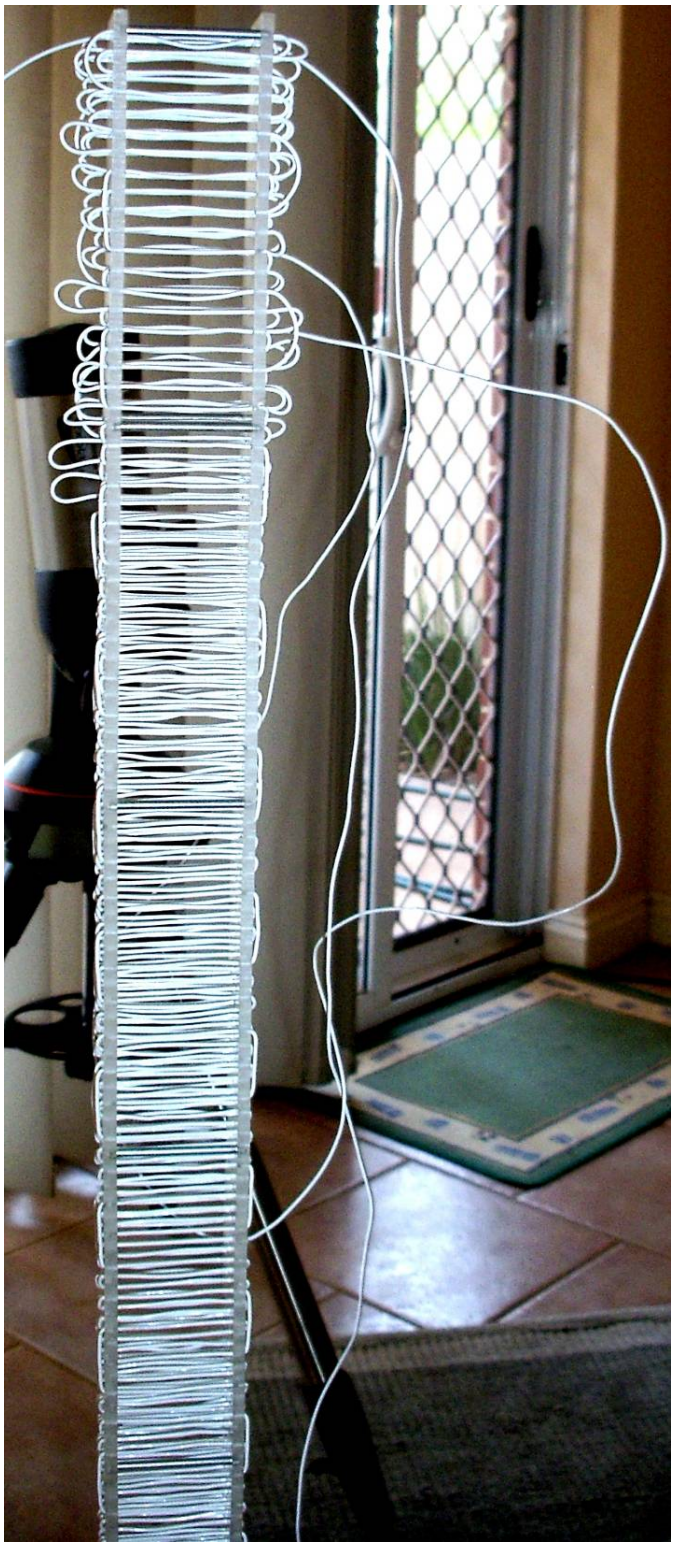

Electrodes – Photograph of Electrode Connection and Fitting into Column

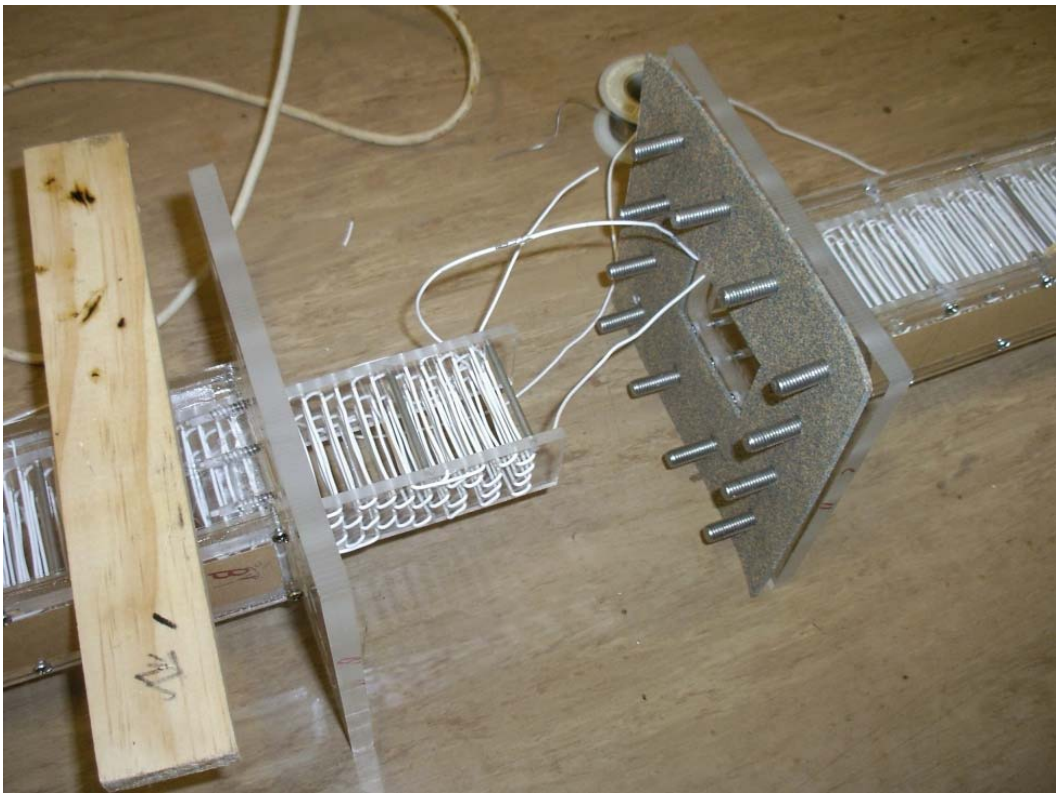

## Appendix C4: Photographs of the Injection Ports

PLS Injection Port

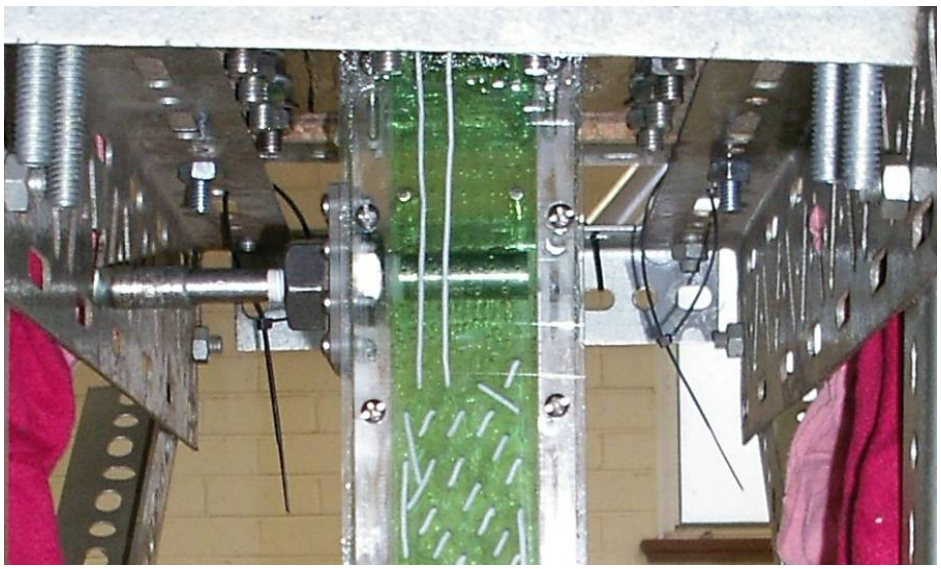

Solvent Injection Port

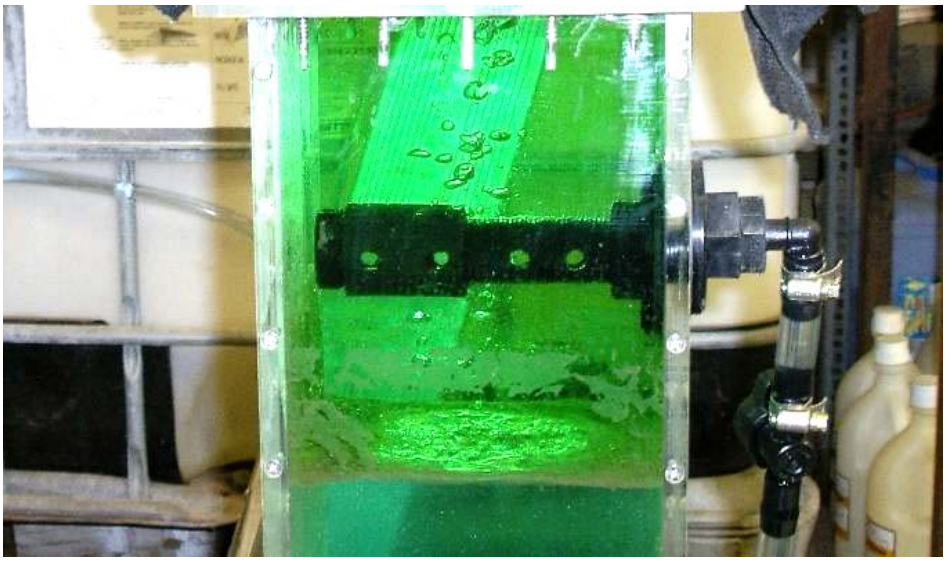

# APPENDIX D - PILOT PLANT OPERATIONS

## Appendix D1: Photographs of the Pilot Plant

Simultaneous Operation of the ESX and Sieve-Plate Pulse Columns

Stripping Mixer-Settler

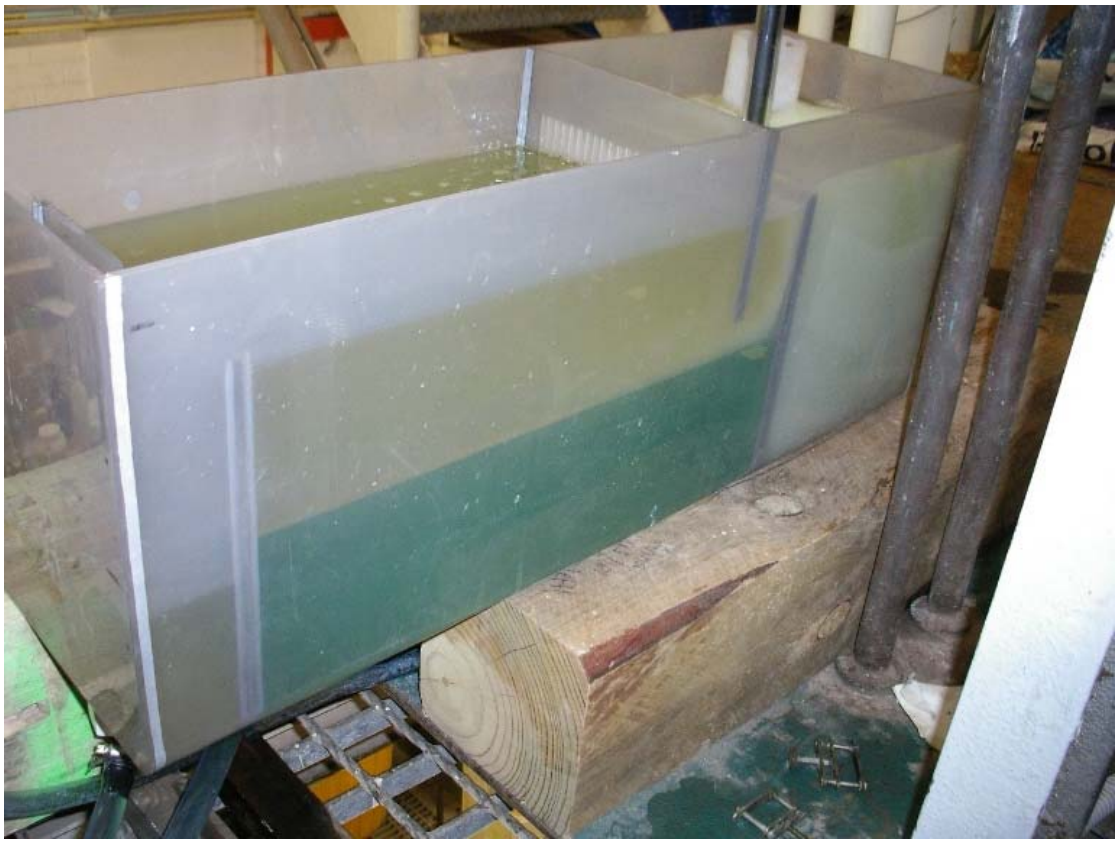

Pulse Column Pulsing Mechanism During Testing

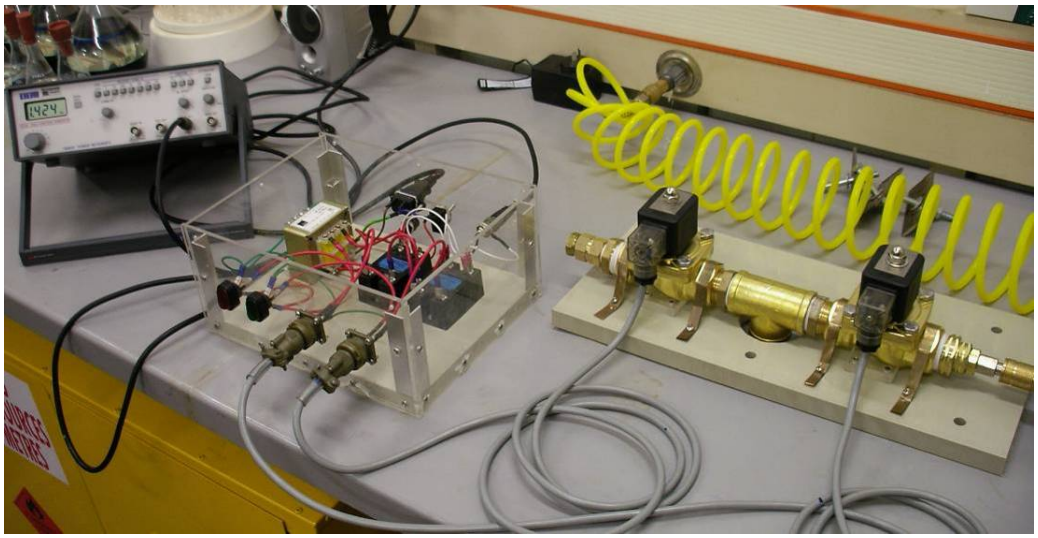

Pulse Column Pulsing Mechanism During Operation